The University of Manchester

Dissertation

Characterisation of Structural Response Signals produced by Hypervelocity Impact

Dominic Kloecker

ID: 10341231

Department of Mechanical, Aerospace and Civil Engineering

2020-21

Abstract

As a spacecraft experiences a Hypervelocity Impact (HVI), structural response signals such as shock waves are produced through the dynamic mechanical loading on the spacecraft structure. The induced shock loads propagate towards the spacecraft payloads where they can apply potentially dangerous shock loads, jeopardising the functionality of system critical components and instruments. These signals are rich with information of the HVI event and can be used for critical tasks such as damage assessment and localization.

The successful and quick characterisation of structural response signals is of vital importance to satellite operators and human personal on satellites to ensure safe on board operations and the safety of the space environment as a whole. This project will attempt to characterise the structural response signals generated in previously conducted HVI experiments as well as studying the wave dispersion and propagation features present in these signals. Additionally to this, the structural response signals generated by Hypervelocity impact from previous literature will be collected and compared to investigate whether there are common signal features present. This collection of the structural response signals generated by Hypervelocity impact is intended to aid in the future research of the field and to provide a adequate starting point for new research.

Acknowledgements

I would like to thank my project supervisor, Prof. Qingming Li as well as my PhD advisor Xianglin Huang for their invaluable guidance and help throughout this project.

While their have been many guiding lights throughout my time at university, I would like to extend my special acknowledgements to my closest friends, without whom this year would have been so much more challenging. I want to say an immense thank you to Stefan Strat `https://www.linkedin.com/in/stefan-strat/` who has not only been a constant source of motivation and inspiration but has always been a pillar of support to me when I needed it the most. I would also like to extend my deepest gratitude to May Ling Har and Francis Brankin, who have been exceptional peers throughout my time at university and have helped make this time of learning into a time of joy. Additionally I would like to thank some of my oldest friends that have been supporting me in all endeavours. A special thank you to Kathy Li, Leo Lutz and Tobias Klaus for their years of companionship.

Contents

1 Introduction **3**
1.1 Hyper velocity Impacts . . . 3
1.2 Structural Response Signals . . . 3
1.3 Simulation of Hypervelocity Impact . . . 4

2 Background Theory **6**
2.1 Acoustic Emission Signals . . . 6
2.2 Wave Propagation in Elastic Solids . . . 6
2.2.1 Longitudinal and Transverse Waves . . . 7
2.2.2 Surface Waves . . . 8
2.2.3 Lamb Waves . . . 8
2.3 Signal Analysis . . . 9
2.3.1 Frequency Analysis . . . 11

3 Literature Review **15**
3.1 HVI induced signals . . . 15
3.2 Analysis of HVI induced Signals . . . 19
3.3 HVI induced damage . . . 20
3.4 Acoustic Emission Signal Analysis . . . 23

4 Methodology **28**
4.1 Collection of HVI signals . . . 29
4.2 Selection of Input Signal . . . 35
4.3 ABAQUS Simulation . . . 36
4.3.1 Simulation Inputs . . . 38
4.4 Calculation of Arrival Times . . . 40
4.5 Source Localisation . . . 41
4.5.1 TOA Triangulation . . . 41

5 Results and Discussion **44**
5.1 Wave Propagation Characteristics . . . 44
5.1.1 S0 Wave Input . . . 44
5.1.2 A0 Wave Input . . . 46
5.1.3 Combined Input . . . 48
5.1.4 HVI induced amplitude characteristics . . . 49
5.1.5 HVI induced frequency characteristics . . . 55
5.2 Source Localisation . . . 59
5.2.1 S0 Wave input . . . 59
5.2.2 A0 Wave input . . . 60
5.2.3 Complete Wave input . . . 61

6 Conclusion & Future Work **63**
6.1 Common Features of HVI induced AE signals . . . 63
6.2 A novel method to study HVI induced AE signal features . . . 63
6.3 HVI induced signal propagation characteristics . . . 64
6.3.1 Amplitude Characteristics . . . 64
6.3.2 Frequency Characteristics . . . 65

6.4 Source Localisation 66

7 Appendix 1 **68**
7.1 Project Plan Management 68

8 Appendix 2 **78**

List of Figures

1 Illustration of Acoustic Emission signal acquisition 6
2 Illustration of longitudinal wave propagation (left) and transverse wave propagation (right) [1]. 7
3 Illustration of surface wave propagation [2]. 8
4 Illustration of lamb wave propagation [2]. 8
5 Illustration of parameter based approach and some of the signal features that are obtained from it [3]. 9
6 Arbitrary signal $g(t)$ and its corresponding Fast Fourier Transform $G(f)$. 11
7 Illustration of the addition of the individual waveforms to recreate the original signal (top) and recreation of the original signal after filtering out its highest frequency component (lower). 12
8 Arbitrary signal $g(t)$ and its corresponding Fast Fourier Transform $G(f)$ 13
9 Illustration of Fourier transform over discrete time windows. Shorter time windows with no overlap at the top and Longer time windows with overlap at the bottom. . . 14
10 STFT of the arbitrary signal $g(t)$. Left: Narrow-Band Spectrogram; Right: Wide-Band Spectrogram. 14
11 Comparison of filtered signals from simulated and experimental results captured a PTZ wafer (EXP - experimental, SIM - simulated) [4]. 15
12 Restult of delay and sum imaging algorithm using , noise filtered and reflection screened AE singnals obtained from case 3 (oblique direction HVI and punctured) [4]. 16
13 Typical HVI induced acoustic emission signals (a) Raw signal, (b) Processed signal fit by an exponential decay function [5]. 17
14 signals recorded by sensor on (left) the 2 mm thick Al-alloy plate, (right) the Al-H/C SP 18
15 Experimentally acquired AE signals, FIL denotes signals after second order Butterworth filter was applied. Left: Case 1 (no penetration), Middle: Case 2 (penetration) , Right: Case 3 (penetration) [6]. 19
16 Energy ratio vs Frequency (15 kHz - 145 kHz) from HVI induced AE signals [6]. . . 20
17 Left: Prediction of HVI induced damage by baseline model, Right: High-speed shadowgraphs (28 s, 55 s; exposure 100 ns) of HVI induced debris cloud impacting a composite plate [7]. 21
18 shadow graph of of CFRP plates under HVI. Upper: None penetration case, Lower: Penetration case [8]. 22
19 Left: Relationship between damage area vs impact energy and plate thickness (log-log), Right: Relationship vs residual strength vs impact energy and plate thickness [8]. . . 22
20 Damage prediction by the neural network. Left: crater mode, right: penetration mode [9] 23
21 Original vs reconstructed input signal from the enhanced time reversal method. Left: Intact target plate, Right: Target plate with internal delamination[10]. 24

22 Displacement field snapshots throughout plate due to 2 Mhz excitation pulse [11]. . . 25
23 Dispersion trends for pulse excitation of various frequencies. (a): Rise time vs Distance; (b) RA vs Distance; (c) Signals at various sensors due to 2 MHz excitation. pulse [11] 26
24 AE signal received and corresponding Fourier Transform, at the same distance from the source for a) Ultrasonic Broadband transducer; b) Point like transducer. [12] . . 27
25 Flow chart of main project activities 28
26 Experimentally acquired AE signal recorded (left) corresponding FFT (right) [5]. . . 29
27 Experimentally acquired AE signals recorded. Penetration Case (left) Non Penetration Case (right) [9] 30
28 Experimentally acquired AE signals recorded (top left), detailed view of the first arriving waves (top right), FFT of the aquired signal (bottom) [4]. 31
29 Experimentally acquired AE signals recorded (left), detailed view of the first arriving waves (right) [4]. 32
30 Experimentally acquired AE signals recorded (left), detailed view of the first arriving waves (right) [4]. 32
31 Experimentally acquired AE signal recorded. Penetrated (top), Not Penetrated (bottom) corresponding [5]. 33
32 Experimentally acquired AE signal[13] 34
33 Final chosen input signal [4]. 35
34 Visualisation of the normalised displacement at a propagation distance of 50 mm for various mesh element sizes. 37
35 Left: Visualisation of the simulated plate and it's support condition as well the partitions used at the points of interest; Right: Visualisation of the uniform 0.5 mm element mesh grid. 37
36 Visualisation the three inputs investigated in this study. Left: Complete wave mode input; Middle: S0 wave mode input; Right: A0 wave mode input. 38
37 Visualisation of the application of the original experimental sensor reading as input in the ABAQUS model. 39
38 Schematic diagram of the energy based triangulation method developed for source localisation by Nivesrangsan et al. [14]. 41
39 Left: Normalised out of plane displacement signals due to S0 Wave mode input; Right: FFT spectra due to the S0 wave mode input. 44
40 S0 input induced wave forms at various distances from the signal source. 45
41 Left: Normalised out of plane displacement signals due to A0 wave mode input; Right: FFT spectra due to the A0 wave mode input. 46
42 A0 input induced wave forms at various distances from the signal source. 47
43 Left: Normalised out of plane displacement signals due to complete wave input; Right: FFT spectra due to the complete wave input. 48
44 Complete wave input induced wave forms at various distances from the signal source. 48
45 Maximum displacement at various distances from source input 49
46 Maximum displacement at various distances from source input, fitted with a double exponential decay function for the S0 mode, A0 mode and combined input. 51
47 Rise Time of the three inputs as a function versus the distance from the signal source. 52
48 RA ratio versus propagation distance from the input source. Left: Max. displacement/rise time., Right: Absolute max. displacement/rise time 52
49 Signal total proportionally equivalent energy content versus propagation distance. Left: Including the energy of the source input, Right: Excluding the energy if the source input. 54

50 Left: Dominant frequency versus propagation distance; Right: Mean frequency versus propagation distance. 55
51 STFT of signals received due to combined input at various distances from the source. 56
52 STFT of signals received due to S0 input at various distances from the source. . . . 57
53 STFT of signals received due to A0 input at various distances from the source. . . . 57
54 Visualisation of the source predictions made by the TOA triangulation algorithm, based on the S0 wave input. Left: Source prediction visualised on the entire target plate; Right: Close up of the source prediction. 59
55 Comparison of the errors through the use of the extensional wave velocity C_E, the longitudinal wave velocity C_L and the transverse wave velocity C_T. 60
56 Visualisation of the source predictions made by the TOA triangulation algorithm, based on the A0 wave input. Left: Source prediction visualised on the entire target plate; Right: Close up of the source prediction. 61
57 Comparison of the errors through the use of the extensional wave velocity C_E, the Longitudinal wave velocity C_L and the Transverse wave velocity C_T. 61
58 Visualisation of the source predictions made by the TOA triangulation algorithm, based on the complete wave input. Left: Source prediction visualised on the entire target plate; Right: Close up of the source prediction. 62
59 Comparison of the errors through the use of the extensional wave velocity C_E, the Longitudinal wave velocity C_L and the Transverse wave velocity C_T. 62

List of Tables

1 Schafer and Janovsky [5], penetration case. 29
2 Zhang et al. [9], penetration case 30
3 Zhang et al. [9], non penetration case 30
4 Liu et al. [4], normal penetration case. 31
5 Liu et al. [4], oblique penetration case. 32
6 Liu et al. [4], non penetration case. 32
7 Iliescu et al. [15], penetration case. 33
8 Iliescu et al. [15], non penetration case. 33
9 Burchell et al. [13] penetration case. 34
10 Material and model properties used for ABAQUS simulation. 37
11 Locations of sensors on the surface of the model. 39
12 Theoretical mode velocities. 40

Declaration

I Dominic Kloecker, declare that this thesis was composed by myself, that the work contained herein is my own except where explicitly stated otherwise in the text, and that this work has not been submitted for any other degree or processional qualification except as specified.

Intellectual Property Statement

I The author of this dissertation (including any appendices and/or schedules to this dissertation) owns certain copyright or related rights in it (the "Copyright") and s/he has given The University of Manchester certain rights to use such Copyright, including for administrative purposes.

II Copies of this dissertation, either in full or in extracts and whether in hard or electronic copy, may be made only in accordance with the Copyright, Designs and Patents Act 1988 (as amended) and regulations issued under it or, where appropriate, in accordance with licensing agreements which the University has entered into. This page must form part of any such copies made.

III The ownership of certain Copyright, patents, designs, trademarks and other intellectual property (the "Intellectual Property") and any reproductions of copyright works in the dissertation, for example graph sand tables ("Reproductions"), which may be described in this dissertation,may not be owned by the author and may be owned by third parties.Such Intellectual Property and Reproductions cannot and must not be made available for use without the prior written permission of the owner(s) of the relevant Intellectual Property and/or Reproductions.

IV Further information on the conditions under which disclosure, publication and commercialisation of this dissertation, the Copyright and any Intellectual Property and/or Reproductions described in it may take place is available in the University IP Policy, in any relevant Dissertation restriction declarations deposited in the University Library, and The University Library's regulations.

1 Introduction

1.1 Hyper velocity Impacts

Hyper velocity Impacts, are impacts of particles traveling at a speeds exceeding 1 km/s [4] with the typical impact velocity of space debris impacting space craft being around 10 km/s [16]. Due to their extreme velocities, these particles have large amounts of kinetic energy and thus even small particles can cause significant damage.

The severity of the damage caused by HVI depends on a number of factors, such as but not limited to the particle velocity, size and density but also on the structure of the spacecraft experiencing the HVI and its shielding. Small particles may only lead to minor defects through small punctures in the spacecraft structure while larger particles can result in the complete destruction of the spacecraft, such as the first recorded orbital collision of the American satellite Iridium-33 and the Russian satellite Kosmos2251 in 2009 [17]. This collision resulted in the complete destruction of both satellites and produced over 2300 trackable fragments in orbit.

As the velocities required for a impact to be considered a HVI are very large, these events typically do not naturally occur outside of the space environment. This means that to gather data regarding these events and their subsequent effects, costly and complex experiments including specialised equipment such as a two stage light gas canon are required to accelerate the impacting particles to the sufficient velocities [18]. This requirement for specialised and high precision equipment results in the fact that the data available for certain HVI impact conditions and resulting factors is still relatively scares.

1.2 Structural Response Signals

During hyper velocity impact, the area in close vicinity of the impact, experiences extreme material deformation and compression which the structure is not able to absorb and thus shock waves are created and propagate elastically through the structure [4]. As these waves propagate through the structure, they lead to strains and corresponding

displacements within the structure which can be measured by sensors. The signals recorded by these sensors can carry large amounts of information about the HVI such as location of the impact and severity of the damage caused. Previous literature has found that structural response signals generated in structures subjected due HVI vary significantly from signals generated by low velocity impacts. For instance it has been found that extensional waves dominate flexible waves in HVI scenarios while the opposite holds true for low velocity impacts [19] As such the characterisation of the structural response signals generated by hypervelocity impact needs to be based on different criteria than the previously established criteria for low velocity impact.

This project will attempt to collect the structural response signals generated under HVI conditions from previous literature and characterise those signals with regards to common signal features to obtain useful information on the original source event such as whether or not the target structure was penetrated as a result of the impact.

1.3 Simulation of Hypervelocity Impact

The above-mentioned extreme material conditions that are present under HVI, make the accurate modelling and simulation of HVI events infeasible through the use of traditional and simplified Finite Element (FE) or Finite difference (FD) approaches. This is caused by the fact that unlike low or high velocity impacts, HVI features a adiabatic loading process due to its extreme and as such, material in close vicinity to the impact location, exhibits material traits that resemble its liquid and vapour states [4]. These extreme conditions can cause errors in FD modelling due to the extreme gradients associated with the material deformation close to the impact centre, while an FE approach, which is dependent on its spatial grid, can suffer from extremely distorted elements, resulting in erroneous results [4]. After the initial extreme material conditions that are present in the close vicinity to the impact location, the induced shock waves will quickly convert to propagate elastically throughout the target structure, the effects of which can be modelled by the traditional methods. As such direct modelling of HVI, involves significant complexity and requires special modelling methods such as the coupling of a

dedicated smooth particle hydrodynamics (SPH) modelling approach with the traditional FE approach [4].

This project will investigate a novel method to replicate the structural response signal features induced by HVI by applying the elastically propagating signals recorded in previous literature as a out of plane displacement inputs in a traditional FE model. The thus generated out of plane displacements along the target structure will then be investigated to identify whether the induced structural response signals features resemble those that are found in the actual HVI event. This method will then be used to investigate the specific wave propagation and dispersion characteristics that are present in HVI induced signals to identify relationships that allow for the successful and quick characterisation of such features. Additionally, the project will attempt to localize the signal source from the received signals based on a time of arrival triangulation algorithm.

2 Background Theory

2.1 Acoustic Emission Signals

Acoustic Emission (AE) waves are stress waves that are generated in a solid due to the rapid release of energy caused by a permanent change in its internal structure, such as crack initiation/growth or yielding [20] caused by external loads. Through the application of sensors on the surface of a structure, it is possible to measure and record ultrasonic signals corresponding to the deformations caused by the stress waves following a external loading event.

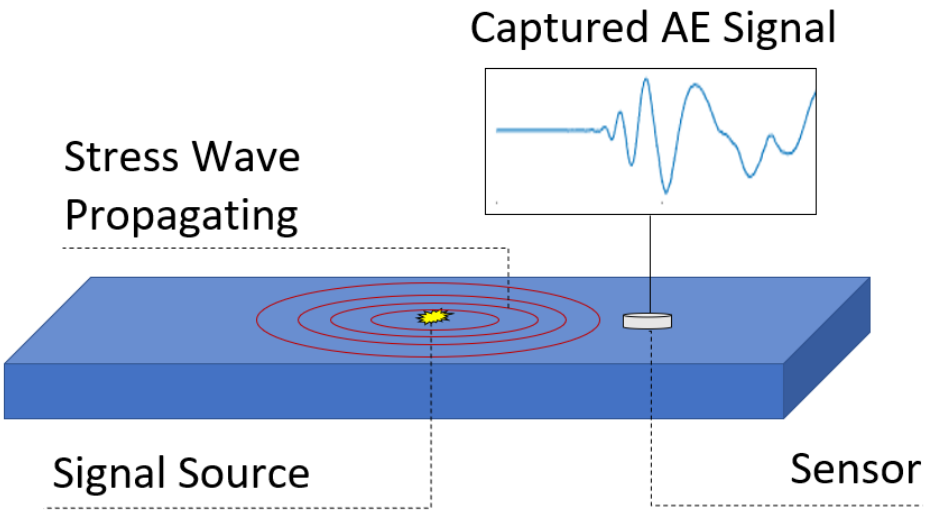

Figure 1: Illustration of Acoustic Emission signal acquisition

2.2 Wave Propagation in Elastic Solids

While the propagation of ultrasonic stress signals in elastic solids is hihgly complex [21], the wave propagation can be analysed through its four main modes of propagation i.e., longitudinal, transverse, surface and lamb waves. A brief introduction into the various wave modes will be presented in the following section. However as HVI often occurs on thin plate like structures the resulting effects are dominated by lamb waves and as such, these will be the focus of this project.

2.2.1 Longitudinal and Transverse Waves

Longitudinal waves are referred to as primary or P waves. They are compression waves and oscillate along the direction of wave propagation. Unlike longitudinal waves, transverse waves, also referred to as S or shear waves, oscillate normal to the direction of wave propagation. Both longitudinal and transverse waves are referred to as body or bulk waves [2].

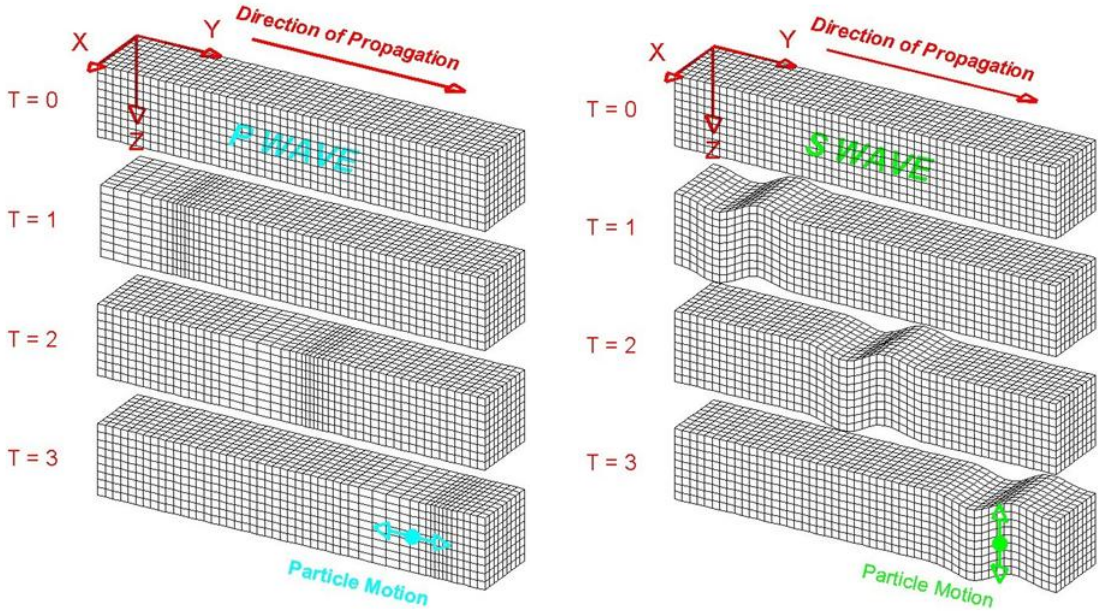

Figure 2: Illustration of longitudinal wave propagation (left) and transverse wave propagation (right) [1].

The two wave modes propagate at different velocities throughout the solid and as such a phenomenon referred to as mode separation can be observed. The longitudinal wave velocity C_L and transverse wave velocity C_T are dependent on the young's modulus E, the density ρ and the poisson's ratio v [20]. It is noteworthy that due to this, the longitudinal wave velocity is always greater than the transverse wave velocity.

$$C_L = \sqrt{E/\rho} \tag{1}$$

$$C_T = \sqrt{E/2\rho(1+v)} \tag{2}$$

2.2.2 Surface Waves

Surface waves, also referred to as Rayleigh waves, are caused by the interaction of the longitudinal and transverse wave modes when they strike a boundary. These waves will start to dominate the waveform at the surface of a plate as the distance from the source increases [21].

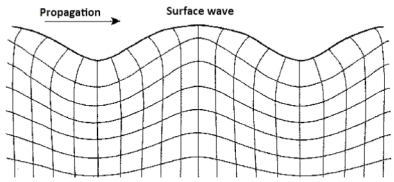

Figure 3: Illustration of surface wave propagation [2].

2.2.3 Lamb Waves

Lamb waves, also referred to as plate waves, are commonly present in thin plate like structures. Lamb waves consist of two fundamental modes, the symmetric, extensional (S0) wave mode and the asymmetric, flexural (A0) wave mode [2]. Higher order wave modes such as A1 and S1 can exist but are not considered in the scope of this research.

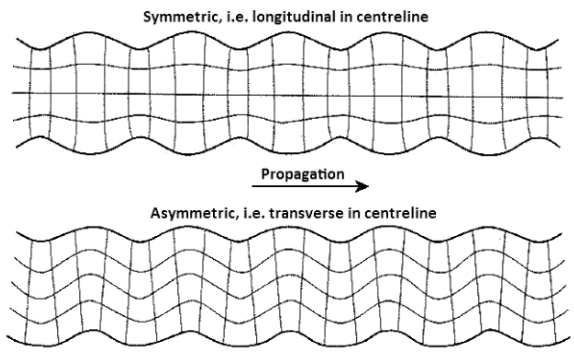

Figure 4: Illustration of lamb wave propagation [2].

The extensional wave mode velocity C_E and flexural wave mode velocity C_F are factors of the plate thickness t and the angular frequency of the signal ω [20].

$$C_E = \sqrt{E/\rho(1 - v^2)} \tag{3}$$

$$C_F = \sqrt[4]{Et^2/12\rho(1 - v^2)}\sqrt{\omega} \tag{4}$$

2.3 Signal Analysis

The analysis of AE signals can provide valuable data on the original source event. The two main methods used for AE signal analysis are parameter based analysis and waveform based analysis. Parameter based analysis is focused on recording certain features of the signal without recording the signal itself. This has the advantage of reducing the amount of data that needs to be stored [2] and as such, reduces the complexity of the data acquisition equipment required for the analysis.

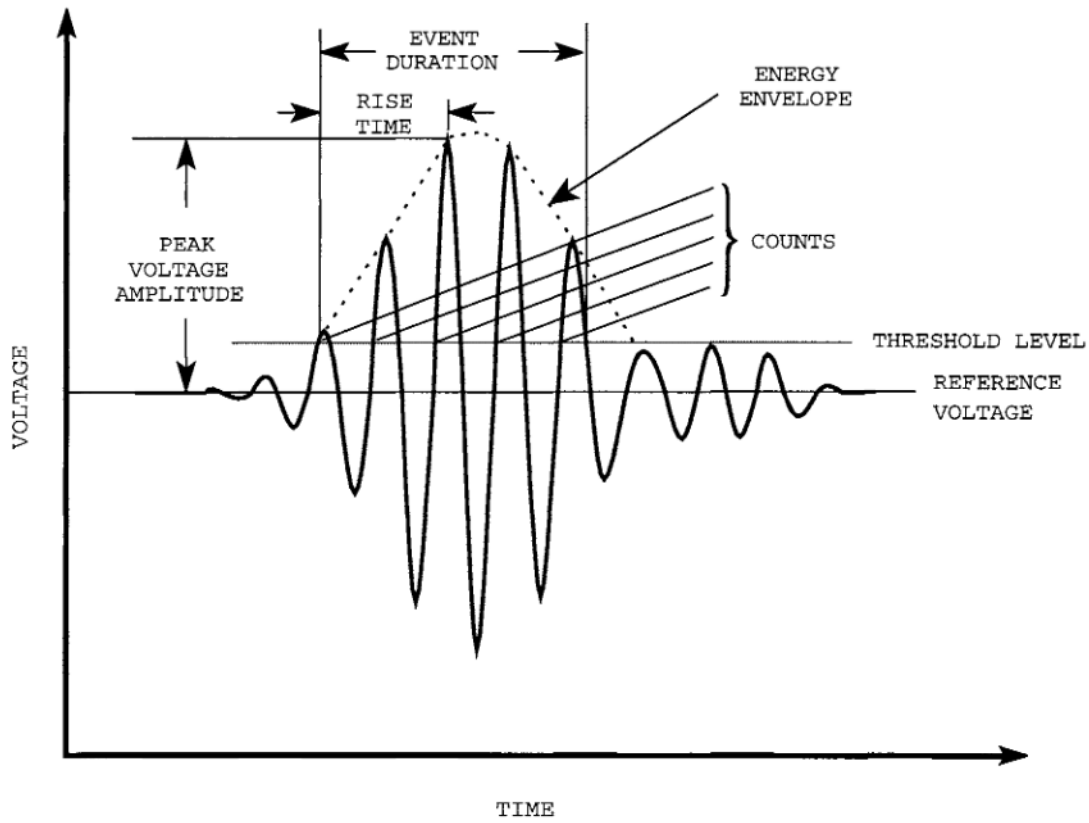

Figure 5: Illustration of parameter based approach and some of the signal features that are obtained from it [3].

Parameters used for parameter based signal analysis	
Parameter	Description
Threshold	The threshold value describes the minimum voltage that has to be reached before the signal recording is started. This value has to be chosen carefully to ensure that it does not miss out on weak signals but is not triggered by background noise [2].
Peak Amplitude	Describes the maximum recorded voltage during the event duration [2].
Rise Time	Describes the time interval between the triggering of the threshold value and the time at which the signal reaches its peak amplitude [2].
Event Duration	Describes the duration of the event which is defined as the time in between the signal is triggered and the time at which it decreases below the threshold value [2].
Energy Envelope	Describes the energy transferred to the system within the event duration. It effectively describes the area under the voltage time diagram [2].
Hit	A hit occurs when a signal is recorded whose value exceeds the threshold value [2].
Counts	Counts are the number of hits recorded within the event duration time [2].

The waveform based analysis is a newer method that records the entire signal. This allows for the extraction of important signal features such the frequency contents of the signal and its time-frequency spectrum. This method however requires much more data to be stored and as such it is only possible due to the improvements in signal acquisition methods and data storage. Waveform based analysis of AE signals is usually achieved through application of the Fast Fourier Transform (FFT) to obtain the captured frequency components of the entire signal or through the application of wavelet or Short Time Fourier Transforms (STFT) to obtain the time-frequency spectrum of the signal [2].

2.3.1 Frequency Analysis

In the analysis of structural response signals, it is important to know what frequencies were present in the analysed signal, therefore a brief overview of the methods used for frequency analysis will be given in this section. Frequency components can be relevant for purposes such as the filtering of background noise that was captured such as background vibrations. Through learning what frequency components were present in a captured signal, it is however also possible to obtain important information about the source of the signal, i.e. whether a target was punctured in the case of HVI induced AE signal.

Fast Fourier Transform

The Fast Fourier Transform (FFT), is a commonly used method for signal frequency analysis. The FFT effectively takes the signal $g(t)$ and returns the function $G(f)$ that states how much power $g(t)$ has at specific at the frequency f [22]. This is made possible by the assumption that the signal $g(t)$ can be replicated perfectly by the sum of individual sin waves.

$$G(f) = \int_{-\infty}^{\infty} g(t)e^{-2\pi i f t}dt \tag{5}$$

To illustrate, consider the arbitrary signal $g(t)$ and its corresponding FFT $G(f)$.

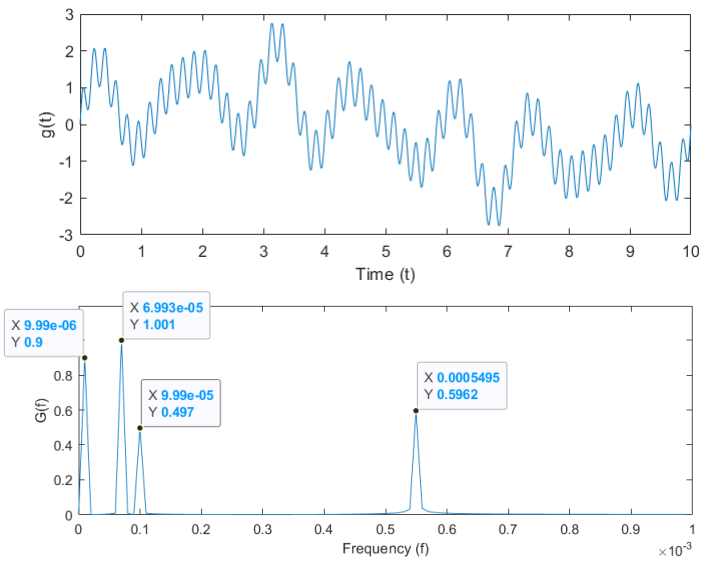

Figure 6: Arbitrary signal $g(t)$ and its corresponding Fast Fourier Transform $G(f)$.

The FFT, shows that the signal can be replicated through the 4 separate sinusoidal waves at their corresponding frequencies and amplitudes. These 4 individual sinusoidal wave forms can be added to another to replicate the original signal. They can however also be subsequently processed for purposes such as noise filtering by eliminating the waveform in certain frequency ranges.

The FFT does however suffer under the limitation that while it accurately represents the frequency spectrum in signal $g(t)$, during the FFT, the phase information of the individual frequency components is lost. For example, if a signal has experiences the addition of a new frequency component after an arbitrary time such as $t > 5$ s, the corresponding FFT does not show that while $t < 5$ s, this frequency component was not included in the signal. As such, it is only possible to reconstruct a signal from the FFT, if all of its corresponding frequency components have the same phase.

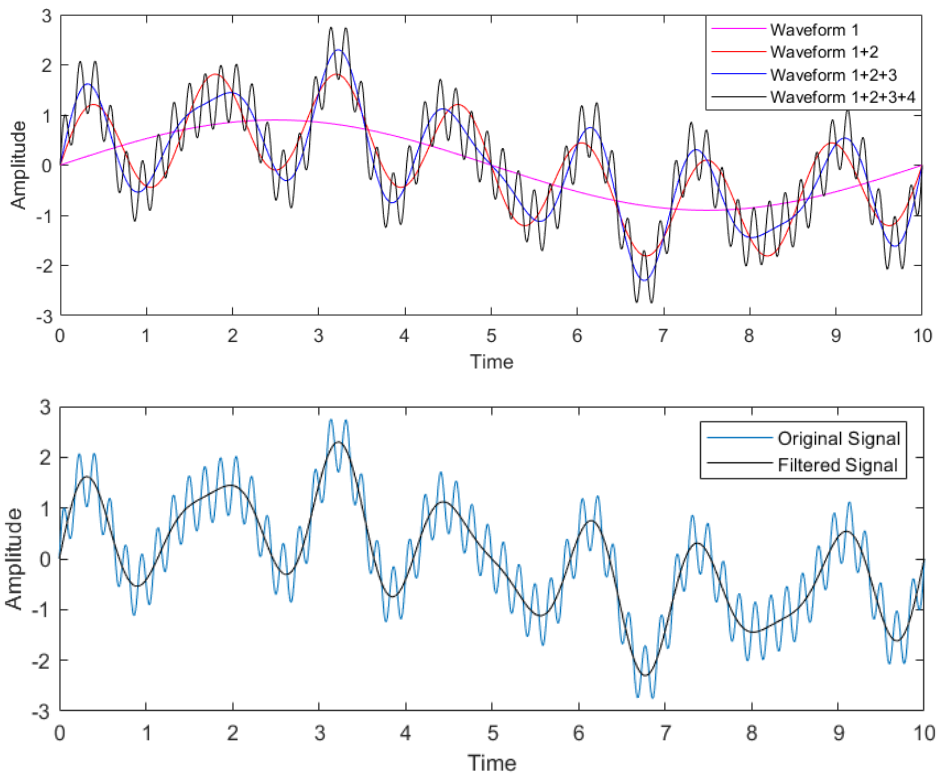

Figure 7: Illustration of the addition of the individual waveforms to recreate the original signal (top) and recreation of the original signal after filtering out its highest frequency component (lower).

Short Time Fourier Transform

Another method used in the analysis of the frequency domain, is the Short Time Fourier Transform (STFT). STFT, essentially is an applied form of the standard Fourier transform but instead of analysing the frequency contents of the entire signal, it evaluates the frequency contents in the signal over time.

To illustrate the necessity for this frequency vs time spectrum, consider the following arbitrary signal $g(t)$ and it's corresponding FFT $G(f)$. It can be observed that the signal is subject to varying frequency components throughout time, thus while the Fourier transform of the signal still provides us with the right frequency components of the signal, it provides no information with regards to how these frequency components change throughout the duration of the signal.

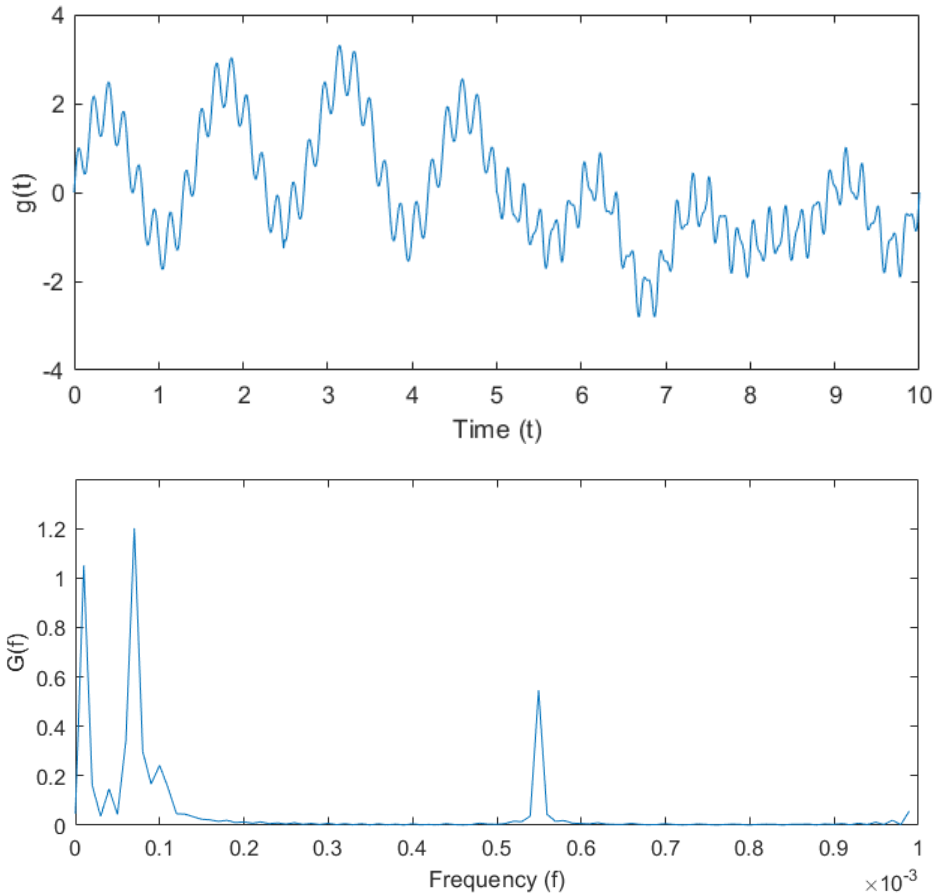

Figure 8: Arbitrary signal $g(t)$ and its corresponding Fast Fourier Transform $G(f)$

The Short Time Fourier Transform, analyses the signal in discrete windows to obtain a measure of the frequency components in the signal over time. The choice of window

length and whether these windows overlap one another has significant impact on the final results of the STFT. Specifically speaking, longer windows provide narrow-band spectrograms, offering better frequency resolution while shorter windows provide wide-band spectrograms which provide better resolution in the time domain.

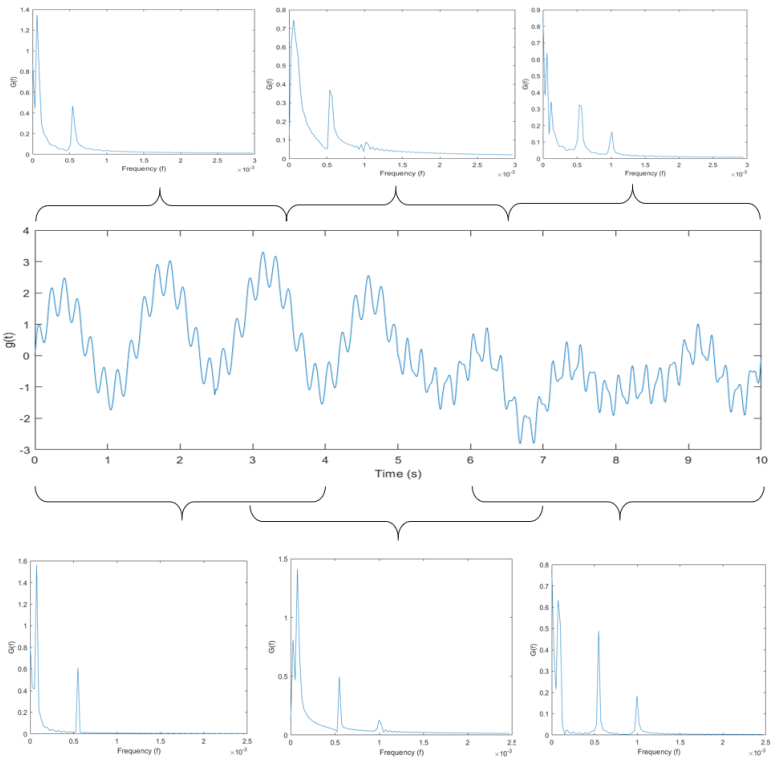

Figure 9: Illustration of Fourier transform over discrete time windows. Shorter time windows with no overlap at the top and Longer time windows with overlap at the bottom.

Through obtaining the FFT for all discrete windows over a signal, these windows can be added to another to obtain the STFT of the signal.

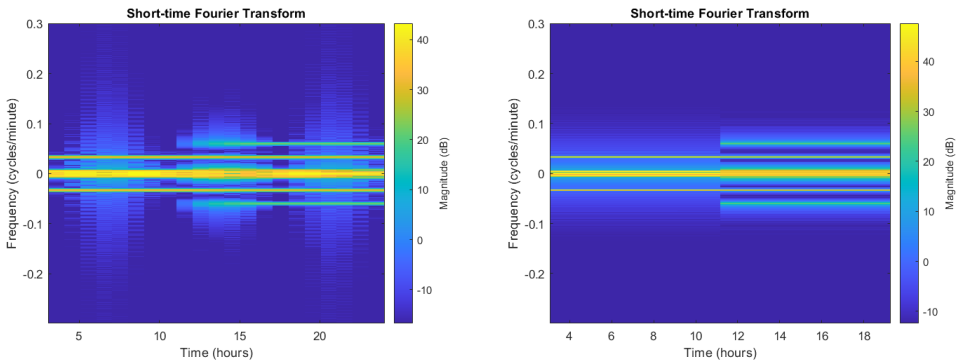

Figure 10: STFT of the arbitrary signal $g(t)$. Left: Narrow-Band Spectrogram; Right: Wide-Band Spectrogram.

3 Literature Review

3.1 HVI induced signals

Liu et al. [4] developed a smooth particle hydrodynamics (SPH) and finite element (FE) hybrid model to evaluate and analyze acoustic emission (AE) produced by HVI. Experimental signal acquisition was achieved through a series of three HVI on double layered aluminum plates to resemble a typical space shielding structure. A network of 7 PTZ wafers at varying distances from the impact spot was attached to the outer plate to measure the HVI induced AE signals.

The three HVI experiments were conducted at aluminum 2024-T4 plates with outer plate thickness of 8 mm, 2 mm and 2 mm respectively, while the thickness of the inner shield plate was held constant at 5 mm. The first impact was produced normally with a Φ3 mm projectile at 2.5km/s, resulting in a non penetration case. The second and third impacts were produced using Φ5 mm projectiles at 4 km/s in normal and oblique directions, both of which resulted in penetration of the outer plate.

The hybrid model was then applied to simulate the HVI cases and results were compared to the experimentally obtained data. It was concluded that after applying a high pass filter of 5 kHz, the simulated results were in good accordance to the experimentally obtained results.

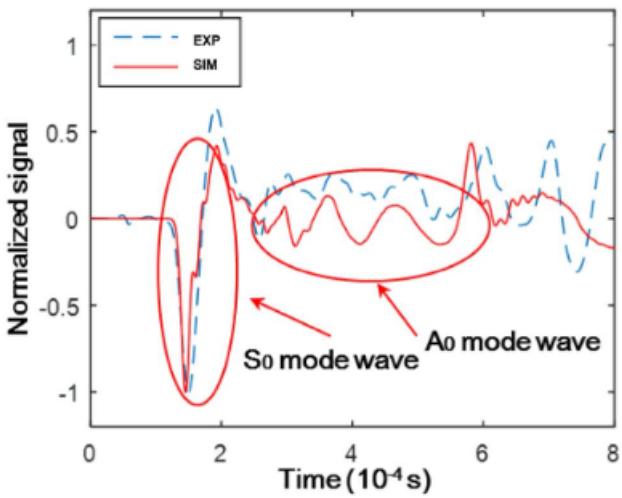

Figure 11: Comparison of filtered signals from simulated and experimental results captured a PTZ wafer (EXP - experimental, SIM - simulated) [4].

The paper concludes that along elastically guided waves, the fundamental symmetric Lamb wave retains most of the energy from the HVI induced shock wave, as well as dominating the signal energy over the fundamental anti symmetric Lamb wave . It is noted that the mode is able to facilitate the characterization of the damage caused by HVI. From the obtained simulation and experimental data, a delay and sum based imaging algorithm was developed which was successfully able to pinpoint the location of HVI spots from the AE signals obtained by the sensors on the shielding assembly.

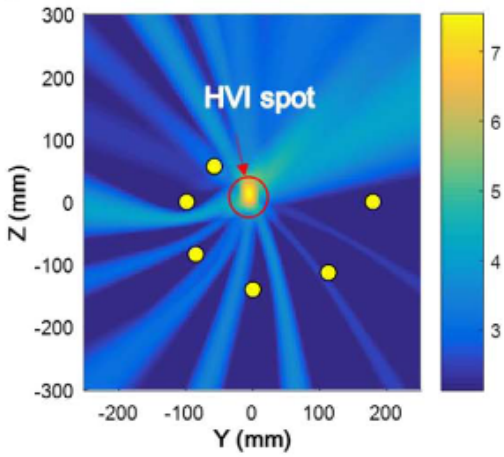

Figure 12: Restult of delay and sum imaging algorithm using , noise filtered and reflection screened AE singnals obtained from case 3 (oblique direction HVI and punctured) [4].

Burchell et al. [13] investigated the Acoustic response signals produced by HVI on aluminium and Duroid plates. A series of HVI were conducted on a set of 1.54mm thick aluminium plates as well as 0.788mm thick Duroid 6001 and 0.763mm thick Duroid 6002 plates. Impacts were produced for a range of impact velocities (1.1-6.4 km/s) using glass and stainless steel projectiles varying in sizes (0.3-3.0mm) over a range of incidence angles (0°- 75°).

A set of acoustic sensors made of poly-vinylidene fluoride (a piezo electric material that produces electric signals proportional to measured strain) were attached to the target plates and measured the acoustic emission signals produced by the HVI. The signals recorded by the sensor network show a large initial peak to peak amplitude of several volts which decays exponentially. An additional lower frequency signal was measured, that complicated analysis as it carries no information about the impact dynamics but is a function of vibrational modes of the plate and supporting structure. This signal could

be removed either through a digital high pass filter during analysis or the addition of a 30 kHz high pass filter in the data acquisition system.

The paper found that a close approximate to the original signal envelope could be found without use of a Hilbert transform by subjected the signals to a nominal 20 kHz Hp smoothing filter upon which a 50 µs running average was taken and the resulting signal amplitudes were doubled to compensate for the averaging process.

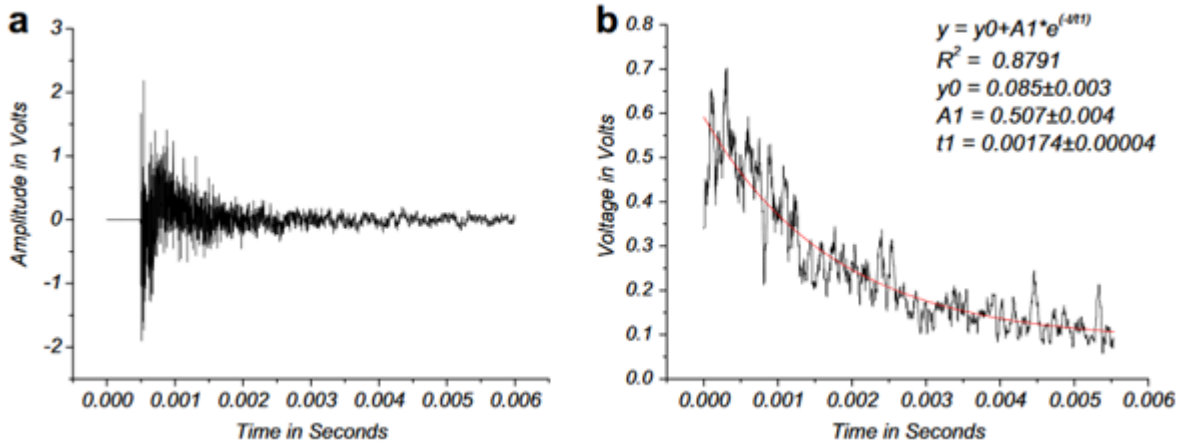

Figure 13: Typical HVI induced acoustic emission signals (a) Raw signal, (b) Processed signal fit by an exponential decay function [5].

Several relationships such as a positive relationships between hole diameter and projectile speed and diameter could be found. These relationships are however dependant on projectile and target material and whether the HVI resulted in a penetration or non-penetration case.

The paper concluded that the peak amplitude of signals produced by HVI 1-1.5 mm projectiles range from 0.1 to a few V and are functions of impact speed, projectile size and angle of incidence. It was suggested that acoustic decay time is not a function of impact velocity but does depend on projectile size, angle of incidence and target material (i.e. decay time one order of magnitude smaller for Duroid compared to Aluminium which is presumed to be caused by the higher mechanical dampening factor of Duroid).

Schäfer et al. [5] evaluated the feasibility and requirements of an impact based sensor network for the detection of hyper velocity impact. In addition to defining a set of primary and secondary requirements for a impact detection sensor network, Schäfer conducted 2

HVI experiments on a 2mm thick aluminium (Al) plate and a aluminium face sheet with an aluminium honeycomb core (Al-H/C SP) . Acoustic signals were captured by a set of 6 ultrasonic transducers attached to the panels. The experiment showed that 2 primary wave forms could be found and thus 2 different arrival times at the sensors were considered. The first of which corresponds to the time when the signal exceeded a noise factor of 2 and the second wave form was defined as the time at which the signal exceeded an arbitrary 2 V threshold.

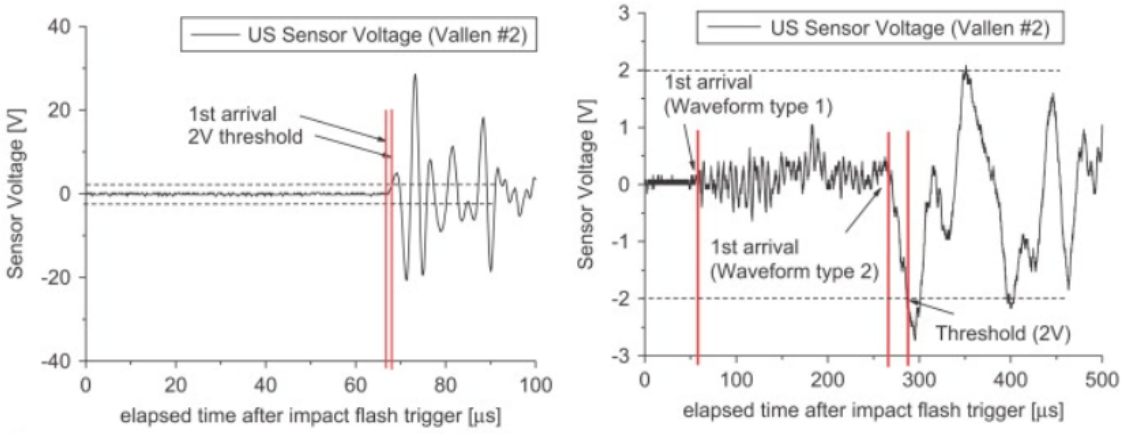

Figure 14: signals recorded by sensor on (left) the 2 mm thick Al-alloy plate, (right) the Al-H/C SP

The paper found that the signals recorded for the Al plate and the Al-H/C SP varied significantly in peak amplitude although the peak amplitudes could be found in roughly the same frequencies. The Al panel exceeding the Al-H/C SP peak amplitude by roughly one order of magnitude and it was also found that the Al-H/C SP acted as a low pass filter, filtering out all frequencies above 40 kHz, while the sensors in the 2 mm Al plate recorded frequencies up to 500 kHz.

A Pythagoras and wave speed based algorithm for HVI localization was developed and applied to the recorded signals. This algorithm was able to successfully predict HVI location. It should be noted that the developed approach for localization appears to perform better and more accurate for the 2mm thick Al panel than the Al-H/C SP likely caused by dampening of the signal through the honeycomb core.

It was concluded that the impact detection system tested was success full in both experiments and that ultrasonic transducers are capable of being used for such a

network. And that while a threshold signal voltage could be used to trigger elapse time measurements needed for localization in both cases, further investigation is needed to evaluate suitability of this method for the Al-H/C SP due to the two different wave forms propagating.

3.2 Analysis of HVI induced Signals

Liu et al. [6] expand on their previously published paper [4] in investigating the HVI induced AE shock waves captured by a piezoelectric sensor network for damage evaluation.

The paper analyzed the HVI induced AE signals captured from HVI experiments in [4] which included HVI at normal and oblique directions as well as penetration and none penetration cases. The paper found that in penetration cases the symmetric wave mode S_0 dominates the asymmetric wave mode A_0 in amplitude while A_0 was observed to exceed the S_0 amplitude in a none penetration case.

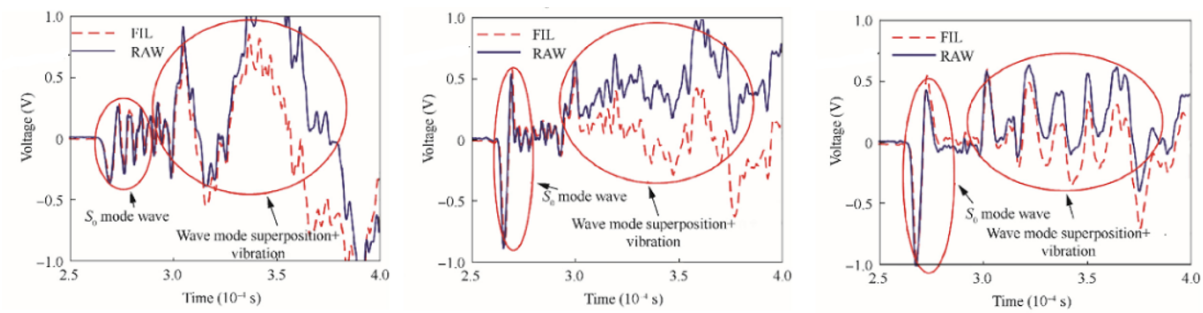

Figure 15: Experimentally acquired AE signals, FIL denotes signals after second order Butterworth filter was applied. Left: Case 1 (no penetration), Middle: Case 2 (penetration) , Right: Case 3 (penetration) [6].

The paper offered an explanation for this phenomenon from the hydrodynamics stress equation for isentropic components

$$\sigma^{\alpha\beta} = -p\chi^{\alpha\beta} + \tau^{\alpha\beta} \tag{6}$$

Where σ represents stress, χ the Kronecker delta , p and τ denoting pressure and deviatoric part shear stress respectively. The pressure p is responsible for the initiation

of the shock wave while the shear stress component τ initiates a shear wave. The energy of the generated shock wave will convert mostly into S_0 mode while the shear wave will convert most of its energy into the A_0 mode.

As HVI occurs, material will be subject to extreme material compression resulting in a much greater pressure value compared to the induced shear stress which is further amplified in penetration cases due to the fluid like behaviour of the impacted material which is thus unable to absorb the shear stress. In non penetration cases however, the shear stress dominates and therefore A_0 is greater than S_0 . It was therefore concluded that the energy ratio and distribution of the S_0 and A_0 modes can be used to evaluate HVI induced damage.

Based on these findings, a frequency domain analysis was performed on the AE signals recorded in case 2 and the energy ratio between the low and high frequency AE signals was calculated giving a relationship between damage severity and average energy ratio.

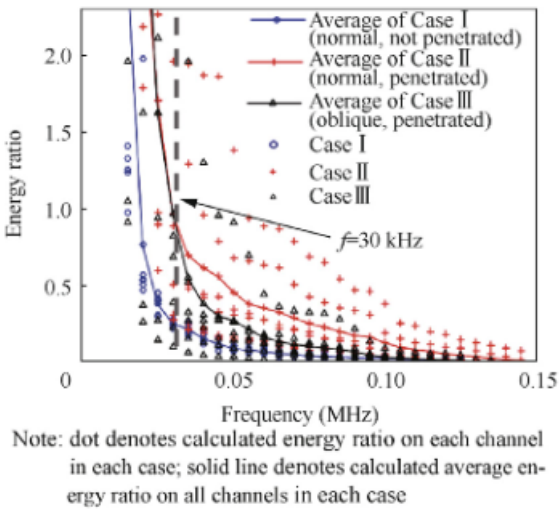

Figure 16: Energy ratio vs Frequency (15 kHz - 145 kHz) from HVI induced AE signals [6].

3.3 HVI induced damage

Clegg et al. [23] produced a two part paper developing a corrected and improved orthotropic material model to predict the thermodynamic responses produced by HVI in composite materials. For the development of the model, a set of experiments was conducted on an aramid-fibre-epoxy specimen to obtain all required material coefficients

required for the model. The developed model was thereafter applied through numerical simulation of an HVI in AUTODYN using a SPH discretisation and was evaluated in its ability to predict damage induced by HVI and HVI produced debris cloud through comparison with experimentally conducted HVI in part II of the paper [7].

The paper concluded that the developed model was successfully able to predict effects of HVI on a wide range of orthotropic materials. Through simulation and experimental comparison, it was found that the simulated HVI using the developed model was able to improve material damage predictions and better describe debris cloud induced damage. The model was suggested to be generally applicable for high-strength composite materials, it was noted, that the model appears to under predict in areas of weaker loading.

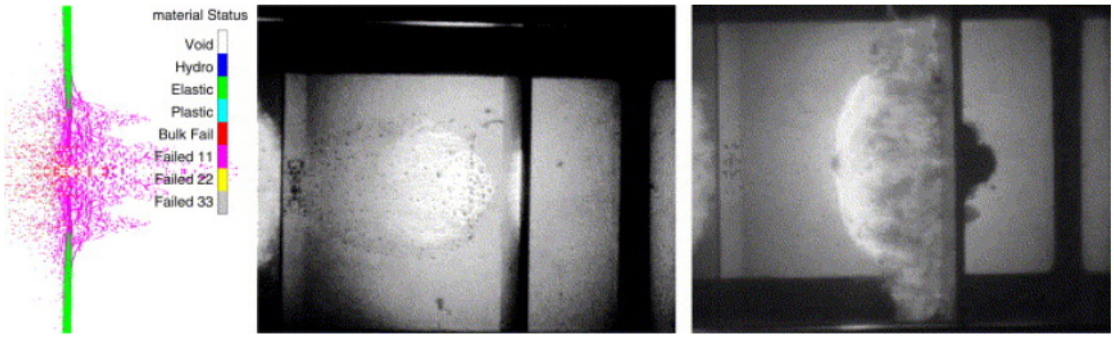

Figure 17: Left: Prediction of HVI induced damage by baseline model, Right: High-speed shadowgraphs (28 s, 55 s; exposure 100 ns) of HVI induced debris cloud impacting a composite plate [7].

Nago et al. [8] performed a series of 27 HVI on Carbon Fiber Reinforced Plastic (CFRP) plates. The tests were carried out altering multiple variables such as projectile diameter, target thickness, and impact velocities, leading to penetration and non penetration cases in the experiment.

It was observed that upon impact, HVI lead to the flipping over of the target surface area close to the impact in both penetration and non penetration cases. This was suggested to be caused by delamination occurring at the front side of the impact, and propagating near the back side causing Mode I fracture.

From the conducted experiments, it could be observed that there is a relationship between damage area and impact energy as well as a relationship between residual strength and impact energy. It is worth noting that while the damage area did not

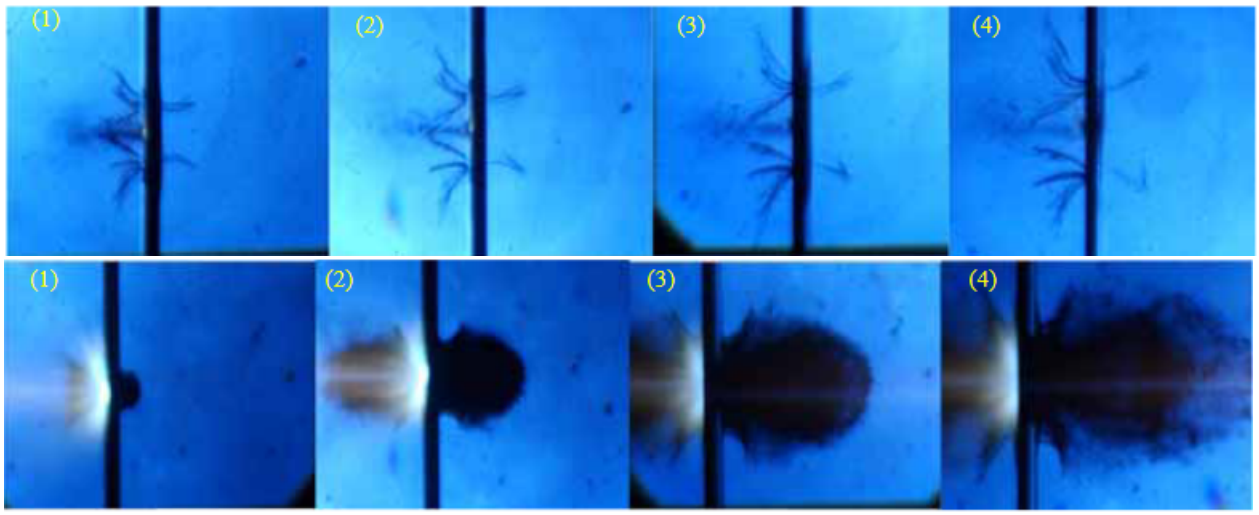

Figure 18: shadow graph of of CFRP plates under HVI. Upper: None penetration case, Lower: Penetration case [8].

vary with thickness for for non penetration cases, the damage area seems to increase with increasing plate thickness for penetration cases. It was suggested that thicker plates were able to absorb more energy than thin plates for the same amount of impact energy. Contradictory it was observed that the residual strength of the CFRP plates depended on thickness for non penetration cases while it can be seen that after penetration cases residual strength converges on a single line regardless of plate thickness.

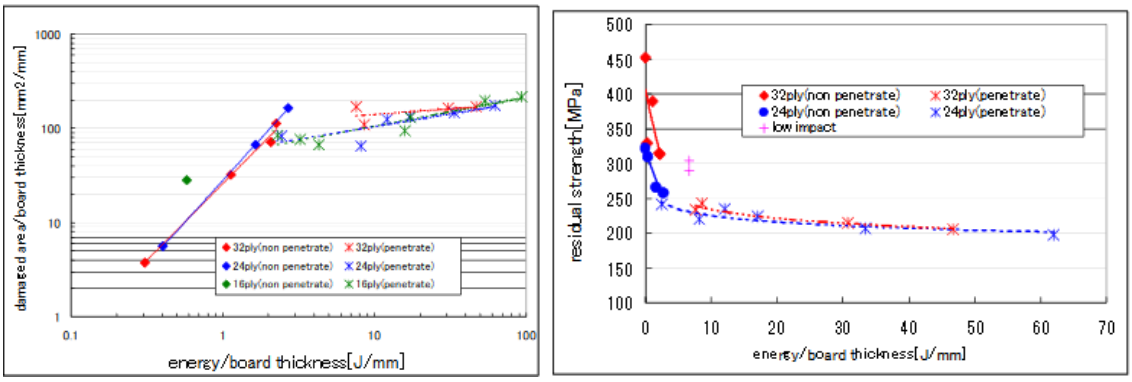

Figure 19: Left: Relationship between damage area vs impact energy and plate thickness (log-log), Right: Relationship vs residual strength vs impact energy and plate thickness [8].

Zhang et al. [9] conducted a series of 92 HVI experiments on 500x500x5mm 5A06 Aluminium alloy plates and investigated common features of the experimentally acquired AE signals. The study found signal characteristic for penetration and crater modes that are in accordance with existing literature. A critical impact velocity of 2.8 km/s, after which the 3.2mm diameter Al projectile would result in penetration, was found. It could

be observed that once the impact velocity increased past the critical velocity, an increase in impact velocity would result in an increase in the S0 mode wave amplitudes and a decrease in A0 mode amplitudes. Zhang noted that the propagation velocity of HVI induced stress waves could be regarded as constant in all directions.

The paper investigated the possibility of a neural network for damage pattern recognition and found that the first through amplitude, the propagation distance, the energy in the high frequency (500kHz +) component corresponding to the S2 mode wave and its ratio could successfully be used as input and training parameters. The trained neural network was able to identify correct damage patterns at a rate of 85% as well as predicting the depth of the crater and hole diameter. The accuracy of the prediction however seemed to be relatively low when the impact was close to the critical velocity of the target.

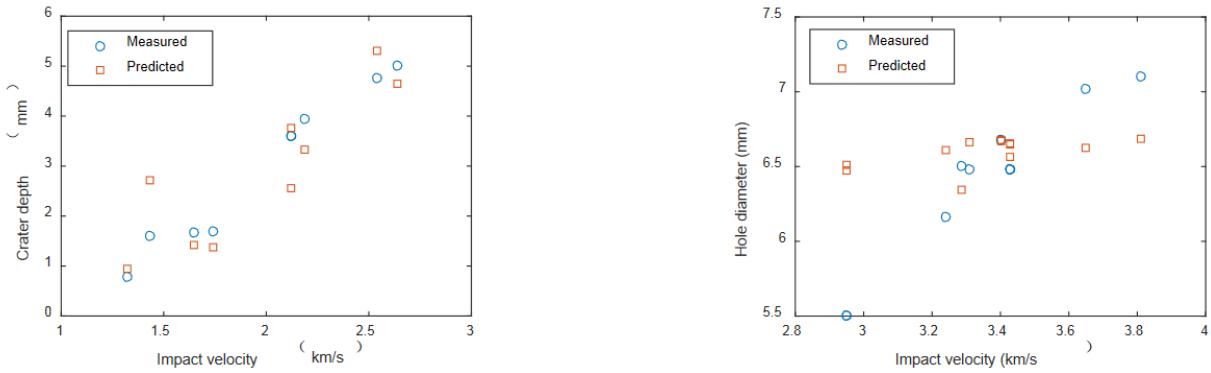

Figure 20: Damage prediction by the neural network. Left: crater mode, right: penetration mode [9]

3.4 Acoustic Emission Signal Analysis

Sohn et al. [10] investigated the application of an enhanced time reversal method of lamb waves for damage detection in composite plates. The study applied the use of the traditional time reversal method, considering only the fundamental asymmetric A0 mode, for signal reconstruction of a numerical Gaussian pulse and 100 kHz tone burst on a thin composite plate. It was found that while the reconstructed signal was of good accordance to the original input signal, the method was more accurate for the 100 kHz tone burst than the Gaussian pulse, which was likely caused by the limited frequency band of the

Gaussian pulse.

The paper subsequently investigated the use of further signal analysis methods such as wavelet transforms and multi resolution analysis to create an enhanced time reversal method for the damage detection in composite plates. The suggested method was observed to recreate experimentally acquired signals to a high level of accuracy when the target plate did not suffer from delamination due to the impact induced damage, while providing poor results when the target plate did suffered internal delimitation.

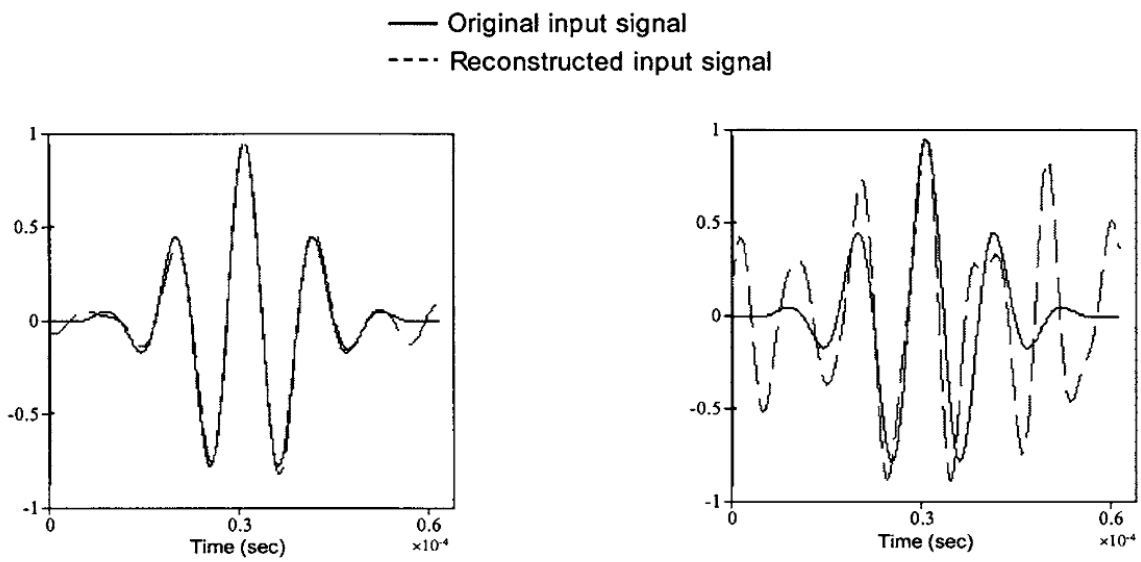

Figure 21: Original vs reconstructed input signal from the enhanced time reversal method. Left: Intact target plate, Right: Target plate with internal delamination[10].

Aggelis and Matikas [11], studied the effect of plate wave dispersion on acoustic emission parameters in metals. The paper described the mode conversion and dispersion that occurs as AE signals propagate through thin metallic plates. It is implied that mode identification based on signal analysis alone, is very complicated as the recorded signal is subject to multiple reflections between the top and bottom surface of the plate. This was visualised through the displacement field of the numerical simulation of stress wave propagation on a 10 mm thick plate subject to a 2 Mhz, one cycle excitation pulse. The only wave form that can easily and clearly identified is the longitudinal wave mode due to its much higher velocity compared to other wave forms.

The parameters of interest in the study were the rise time, RT, and the ratio RA which describes the ratio of the Rise Time/Maximum Amplitude. Signals were recorded at

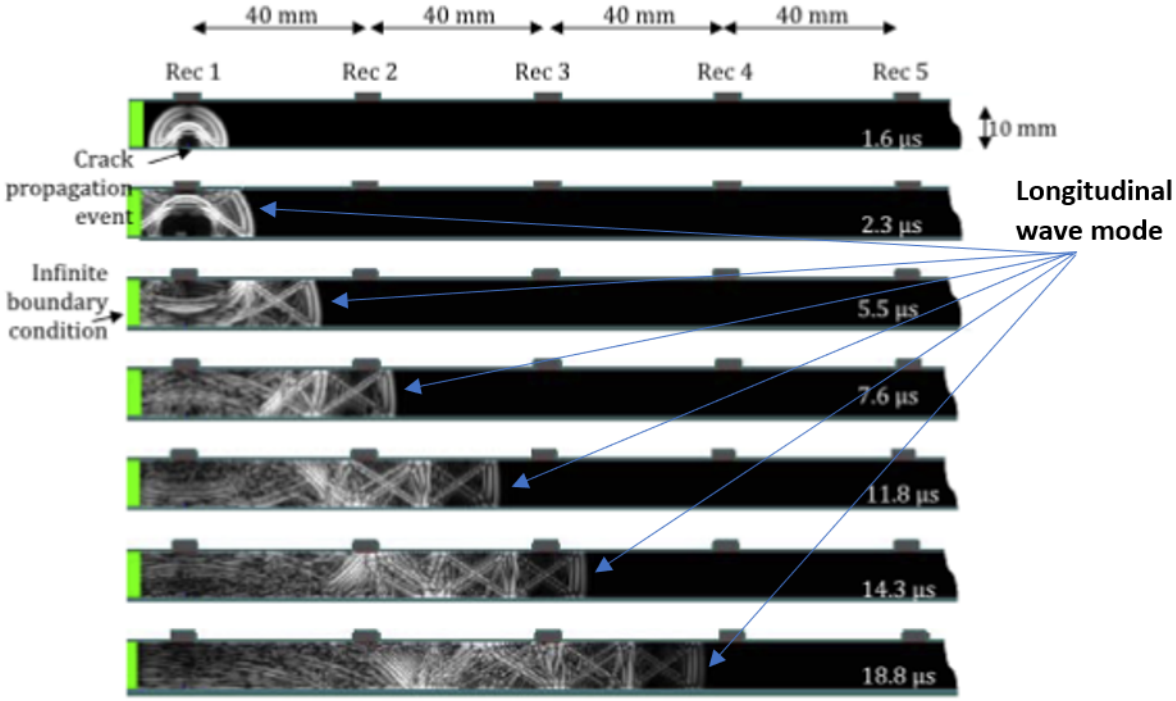

Figure 22: Displacement field snapshots throughout plate due to 2 Mhz excitation pulse [11].

various distances from the source and subsequently normalised with respect to the signal received by the first sensor. It was observed that propagation distance had a significant impact on the waveform and that the recorded waveform resembled the original pulse signal only up to the distance of the 3rd sensor at 80 mm from the signal source.

The study found that the dispersive trends observed were similar for any excitation, however there is a clear increase in the AE parameter shift vs propagation distance once the excitation frequencies are sufficiently large. It was suggested that this could be a result due to the shorter wavelengths relative to the thickness of the plate, as short enough wavelengths could allow Rayleigh waves to form. Regardless of this, the paper states that propagation distance can be used to account for wave dispersion and changes in amplitude.

It was concluded that any criteria concerning AE based characterisation should be accompanied by a procedure that accounts for the effects of wave dispersion based on the distance of the sensor from the signal source.

Gorman [12] investigated pencil lead break AE induced plate waves on aluminium and graphite epoxy composite plates as well as the ability of different transducers at

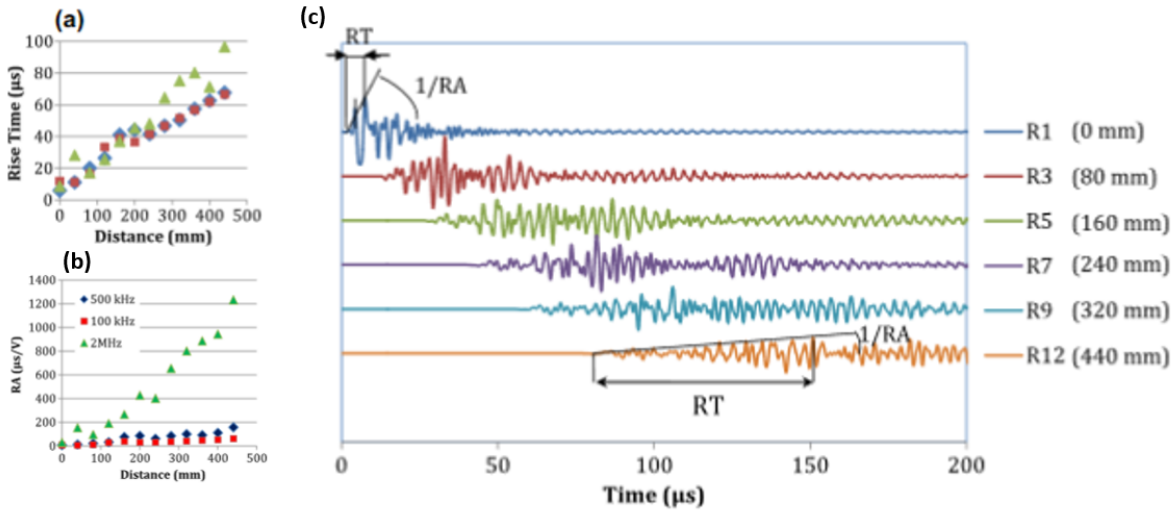

Figure 23: Dispersion trends for pulse excitation of various frequencies. (a): Rise time vs Distance; (b) RA vs Distance; (c) Signals at various sensors due to 2 MHz excitation. pulse [11]

reproducing the characteristic shape of plate waves. The study found that as long as the thickness of the plate is much smaller than the smallest wave length of the induced pulse, either or both of the fundamental plate modes (A0, S0) will be generated. The paper discussed the effect of directionality of the two fundamental plate modes on the captured signal. It was stated while each mode has displacement components in all directions, the biggest displacement components of the extensional S0 mode, is in the in plane direction while the biggest displacement component of the flexural A0 mode is in the out of plane direction. As transducers are usually mounted on the surface of a plate for AE signal acquisition, these systems mainly pick up the out of plane displacement components. When analysing the effect of different transducers for AE signal acquisition, Gorman found the choice of transducer has a significant effect on the received wave forms and the ability of the transducer to replicate the characteristic shapes of plate waves.

The paper concluded that flexural waves should be filtered out for source localisation, as flexural waves are subject to wave dispersion while extensional waves are not subject to this dispersion. The paper made the additional conclusion that the peak amplitude should not be used for source localisation due to the wave dispersion.

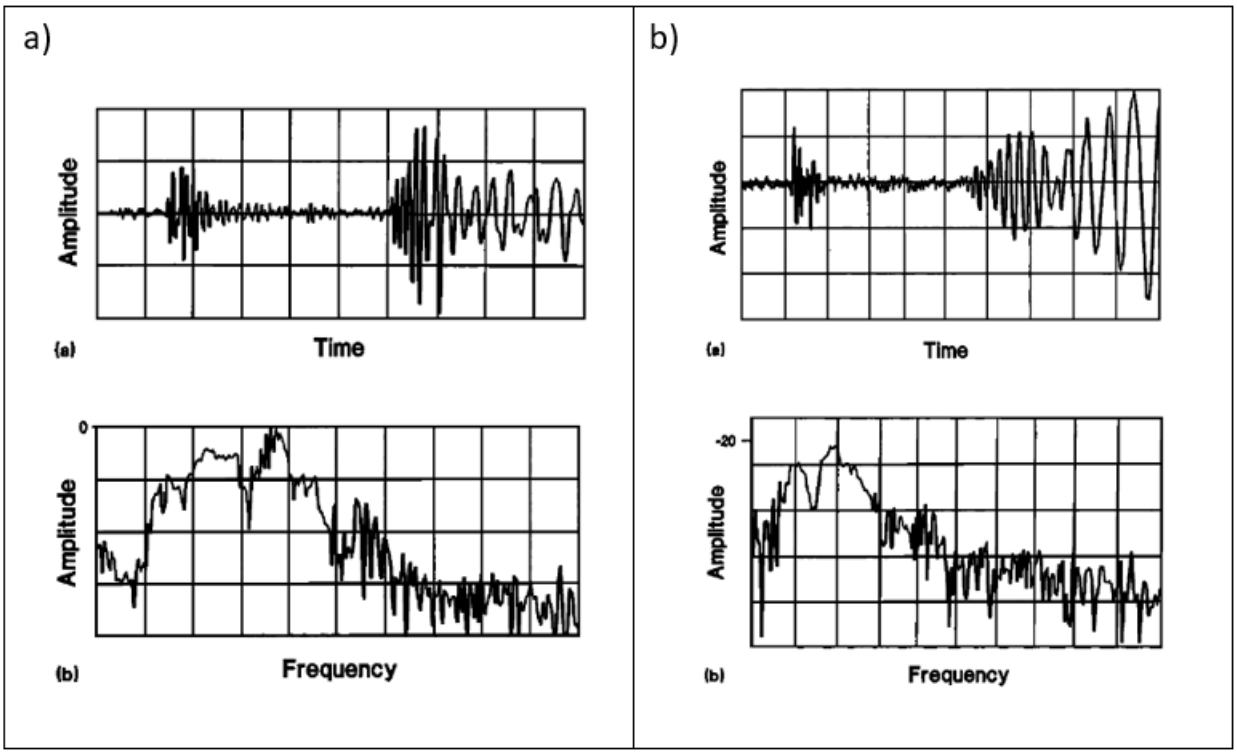

Figure 24: AE signal received and corresponding Fourier Transform, at the same distance from the source for a) Ultrasonic Broadband transducer; b) Point like transducer. [12]

4 Methodology

A flow chart illustrating the main tasks of the project is shown below, the specific stages and tasks are discussed in the subsequent subsections.

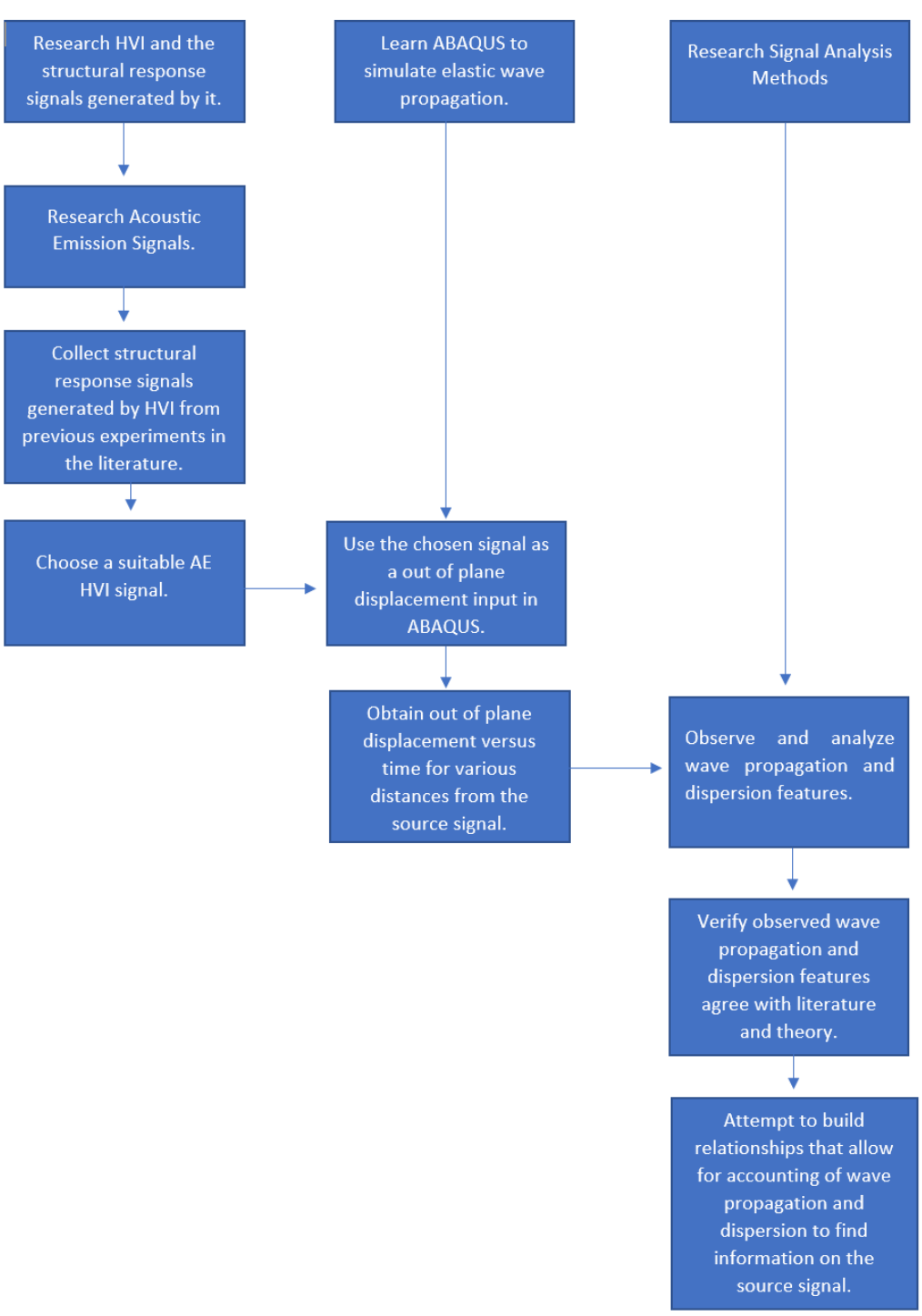

Figure 25: Flow chart of main project activities

4.1 Collection of HVI signals

For the characterisation of the structural response signals generated by HVI, and the latter simulation, a number of HVI induced signals were collected. The collected signals were subsequently compared and evaluated for their suitability as input signal. For this study, only AE signals induced by HVI on thin isotropic aluminium plates were collected due to the simpler analysis than honeycomb sandwich panels.

Schafer and Janovsky [5]

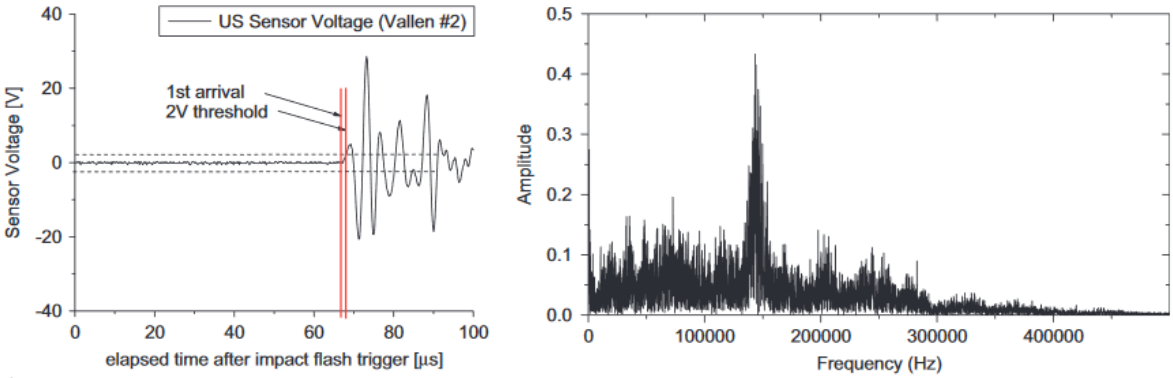

Figure 26: Experimentally acquired AE signal recorded (left) corresponding FFT (right) [5].

Penetration Case			
Target Material & Thickness	Projectile Material & Diameter	Impact Velocity	Penetrated
Al-7975, 2 mm	Al, 2 mm	2.75 km/s	Yes
Impact Direction	Multiple Signals Presented	Information on acquisition distances	Information on sensors used
Normal	No	Yes	Yes

Table 1: Schafer and Janovsky [5], penetration case.

Zhang et al. [9]

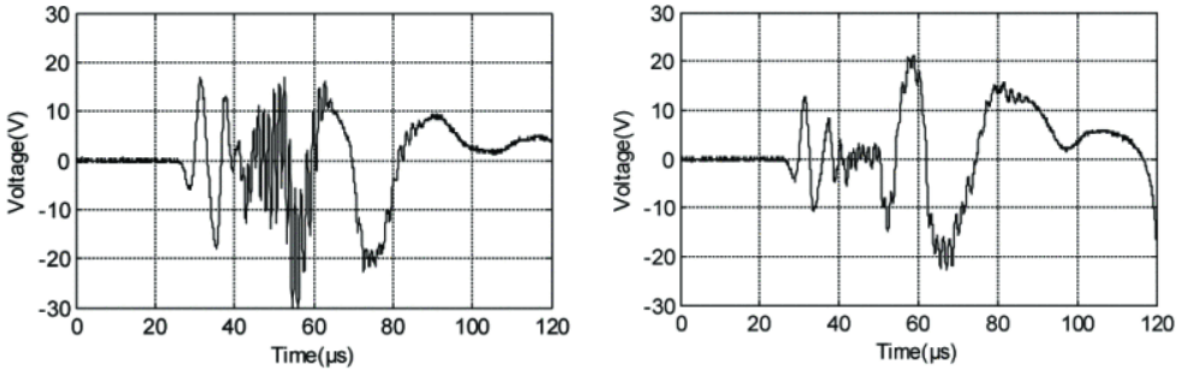

Figure 27: Experimentally acquired AE signals recorded. Penetration Case (left) Non Penetration Case (right) [9]

Penetration Case			
Target Material & Thickness	Projectile Material & Diameter	Impact Velocity	Penetrated
Al-506, 5 mm	Al-2017, 3.2 mm	3.65 km/s	Yes
Impact Direction	Multiple Signals Presented	Information on acquisition distances	Information on sensors used
Normal	No	No	Yes

Table 2: Zhang et al. [9], penetration case

Non Penetration Case			
Target Material & Thickness	Projectile Material & Diameter	Impact Velocity	Penetrated
Al-506, 5 mm	Al-2017, 3.2 mm	1.27 km/s	No
Impact Direction	Multiple Signals Presented	Information on acquisition distances	Information on sensors used
Normal	No	No	Yes

Table 3: Zhang et al. [9], non penetration case

Liu et al. [4, 6]

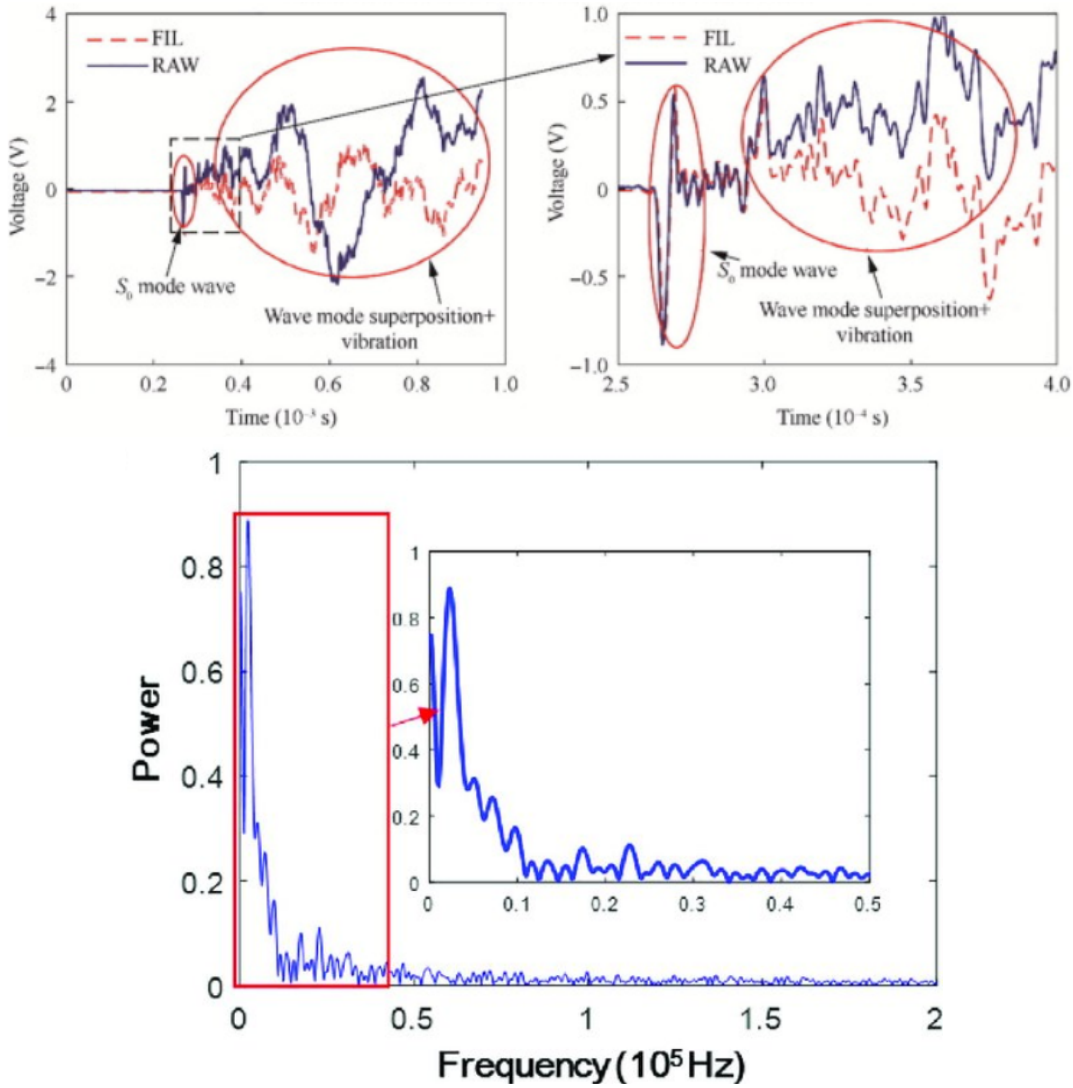

Figure 28: Experimentally acquired AE signals recorded (top left), detailed view of the first arriving waves (top right), FFT of the aquired signal (bottom) [4].

Penetration Case 1			
Target Material & Thickness	Projectile Material & Diameter	Impact Velocity	Penetrated
Al-2024, 2 mm	Al-2024, 3 mm	4.035 km/s	Yes
Impact Direction	Multiple Signals Presented	Information on acquisition distances	Information on sensors used
Normal	Yes	Yes	No

Table 4: Liu et al. [4], normal penetration case.

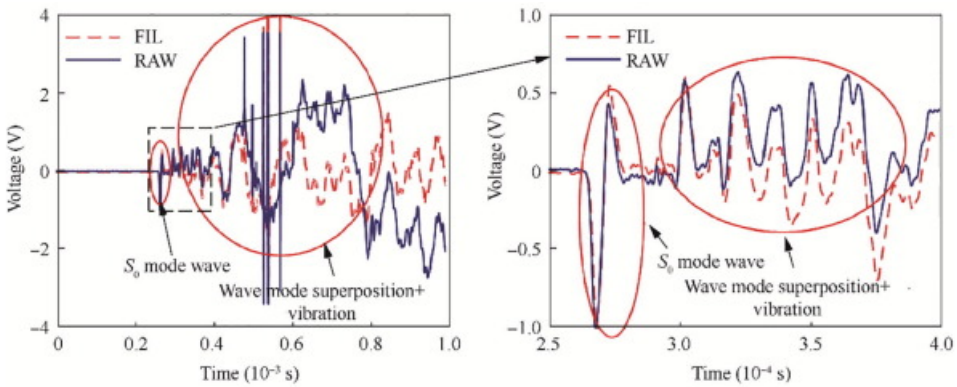

Figure 29: Experimentally acquired AE signals recorded (left), detailed view of the first arriving waves (right) [4].

Penetration Case 2			
Target Material & Thickness	Projectile Material & Diameter	Impact Velocity	Penetrated
Al-2024, 2 mm	Al-2024, 3 mm	4.021 km/s	Yes
Impact Direction	Multiple Signals Presented	Information on acquisition distances	Information on sensors used
Oblique (32°)	Yes	Yes	No

Table 5: Liu et al. [4], oblique penetration case.

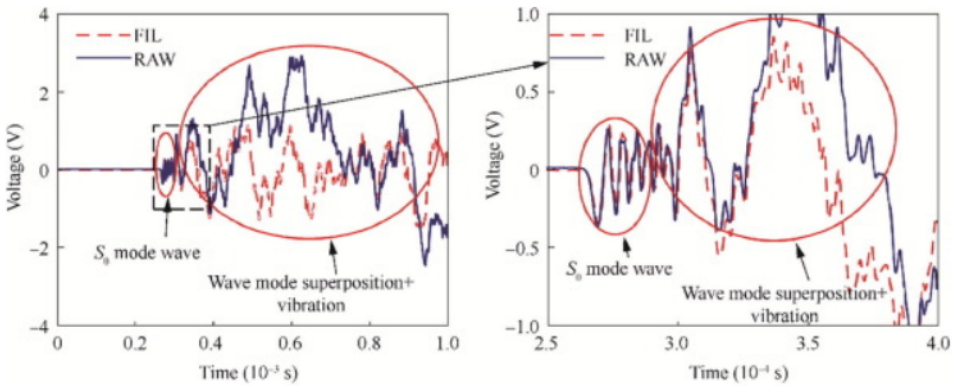

Figure 30: Experimentally acquired AE signals recorded (left), detailed view of the first arriving waves (right) [4].

No Penetration Case			
Target Material & Thickness	Projectile Material & Diameter	Impact Velocity	Penetrated
Al-2024, 8 mm	Al-2024, 3 mm	2.511 km/s	No
Impact Direction	Multiple Signals Presented	Information on acquisition distances	Information on sensors used
Normal	Yes	Yes	No

Table 6: Liu et al. [4], non penetration case.

Iliescu et al. [15]

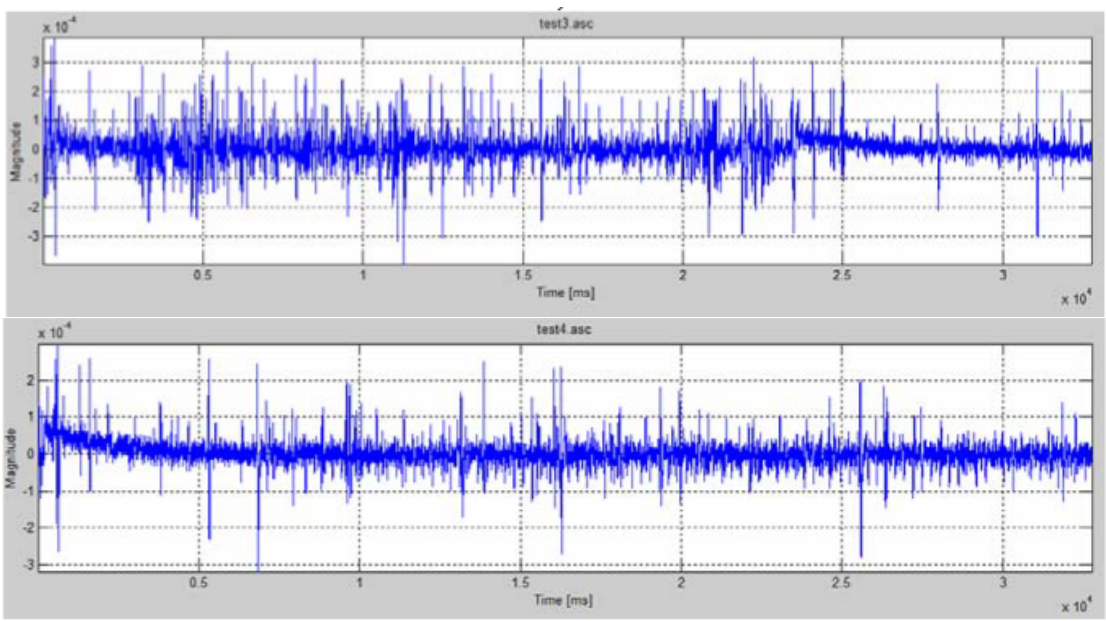

Figure 31: Experimentally acquired AE signal recorded. Penetrated (top), Not Penetrated (bottom) corresponding [5].

Penetration Case			
Target Material & Thickness	Projectile Material & Diameter	Impact Velocity	Penetrated
Al, 2 mm	Al, 3.2 mm	0.57 km/s	Yes
Impact Direction	Multiple Signals Presented	Information on acquisition distances	Information on sensors used
Normal	Yes	Yes	Yes

Table 7: Iliescu et al. [15], penetration case.

None Penetration Case			
Target Material & Thickness	Projectile Material & Diameter	Impact Velocity	Penetrated
Al, 5 mm	Al, 3.2 mm	0.54 km/s	Yes
Impact Direction	Multiple Signals Presented	Information on acquisition distances	Information on sensors used
Normal	Yes	Yes	Yes

Table 8: Iliescu et al. [15], non penetration case.

It is noteworthy that although Iliescu has classified these impacts as Hypervelocity impacts, the velocities presented off 0.57 n0.54 km/s are relatively low and thus not be classified as a hypervelocity impact but as a high velocity impact. It is also noteworthy

that a penetration of the 2mm thick target at a velocity of 0.57 km/s seems unlikely when compared with other literature such as Zhang et al. [9], who found a critical velocity of 2.8 km/s to penetrate a 5mm thick Al target. As such, the signals presented by Iliescu, will be considered obscure and not be considered in further analysis.

Burchell et al. [13]

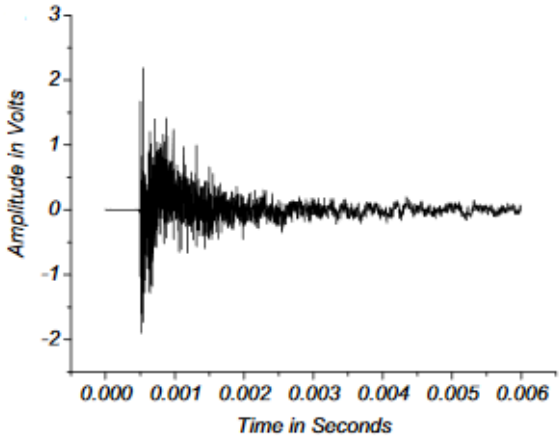

Figure 32: Experimentally acquired AE signal[13]

Penetration Case			
Target Material & Thickness	Projectile Material & Diameter	Impact Velocity	Penetrated
Al, 1.54 mm	Stainless Steel, 1 mm	Unknown	Unknown
Impact Direction	Multiple Signals Presented	Information on acquisition distances	Information on sensors used
Unknown	No	No	Yes

Table 9: Burchell et al. [13] penetration case.

4.2 Selection of Input Signal

For the subsequent simulation of the HVI induced structural response signals an appropriate input signal had to be chosen from the signals presented in section 5.1. It is noteworthy that after lengthy search of relevant literature, section 5.1 represents all the HVI AE singals, on thin isentropic plates, that could be found. While there is a large variety of singals presented for low and high velocity impacts in existing literature, further research and experiments on the AE signals generated by HVI on thin isentropic plates is required to allow for a deeper understanding of the subject. Additionally to this, many of the presented signals could not be chosen as input signal as the papers lack critical information on the experimental set up, such as the paper by Zhang et al. [9] which does not state the propagation distance of the recorded signal.

The final signal chosen as input was the Penetration Case 1 signal by Liu et al. [4] as the paper provided detailed information on the experimental set up as well as providing the AE signals at different distances from the source. The selected signal also offered the additional advantage of having already been characterized by Liu and as such, this study could investigate the propagation and dispersion characteristics of the flexural (A0) and extensional (S0) wave modes independently. From the below presented signal, the signal was extracted up until the S0 mode reflection point as only signals that are unaffected by reflection noise are of interest in this study.

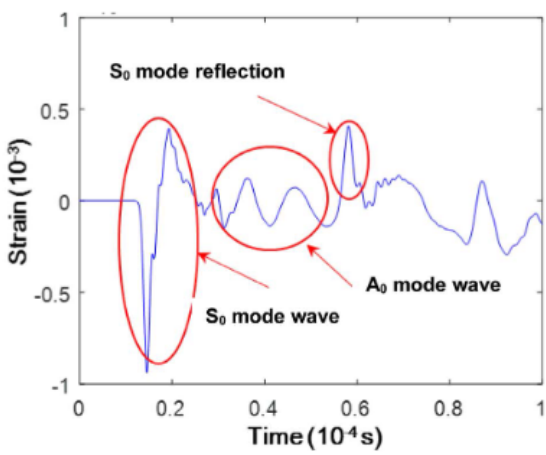

Figure 33: Final chosen input signal [4].

This signal represents a signal captured by a PZT wafer mounted 120 mm from the

impact location on a 2 mm thick Al-2024 plate subject to a 4.035 km/s impact at normal direction to the plate. The projectile consisted of a 3 mm diameter Al-2024 ball and resulted in a through thickness puncture of the target.

4.3 ABAQUS Simulation

For the simulation of the HVI induced structural response signals, a FE model was created in ABAQUS, as this program was recommended by the project supervisor prof. Li. The model characteristics and geometry created were set up in such a way to replicate the original source paper by Liu et al. [4] and the therein conducted FE analysis.

As only the elastic part of the HVI induced signal was simulated however, the model did not include the coupled SPH approach that the source paper described but only on the FE aspect.

An elastic material model was applied with the material characteristics of the aluminum (2024-T4) plate that was used in the original experiments. It is noteworthy that while the experiment stated most material parameters that were used for it's simulation, it did not state the applied elastic modulus. Thus the value used for elastic modulus was obtained from the aluminium manufacturer Gabrian International [24].

The step was chosen as a dynamic, explicit step type with a total step time of 100 μs to ensure that the captured signals did not suffer from noise due to reflection at the model wall boundaries. The incrimination of the step was chosen to be automatic with a global stable increment estimator and a time scaling factor of 1.

The mesh element size chosen for the model was a uniform element length of 0.5 mm. This was done to replicated the original model to the most accurate extend possible as well as based on Lius' criterion allowing for at least 10 elements per wavelength [4]. In addition, a mesh convergence study was undertaken from which it was concluded that the element size of 0.5 mm appeared to have converged towards the grid independent solution, within a reasonable degree of accuracy. While further improvement of the mesh could have resulted in a more accurate solution, this was not possible due to hardware limitations which did not allow for a more refined mesh with reasonable computation

times given the computers provided by the university. The support conditions at the plate boundaries was the symmetric ENCASTRE boundary condition, completely fixing the plate edged.

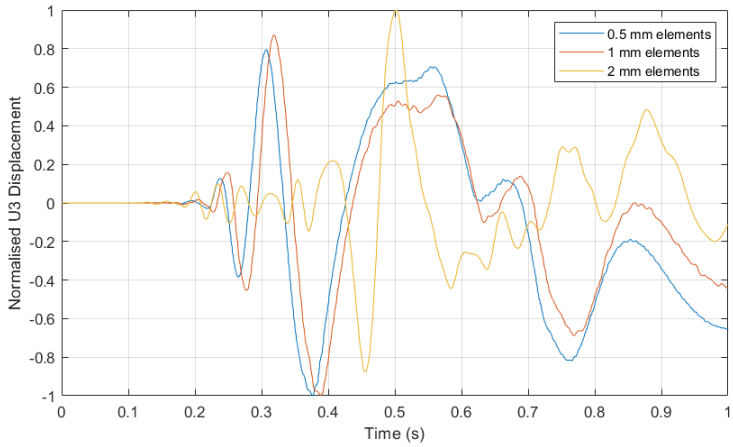

Figure 34: Visualisation of the normalised displacement at a propagation distance of 50 mm for various mesh element sizes.

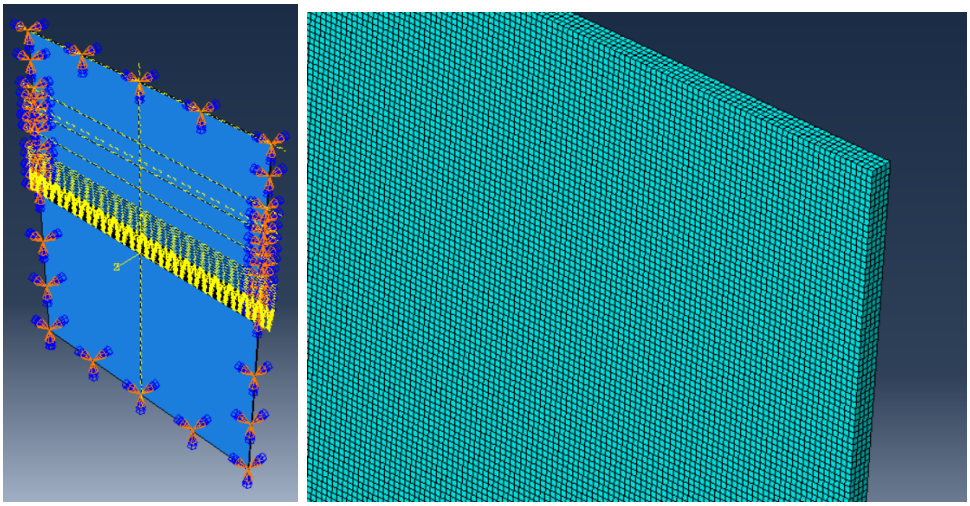

Figure 35: Left: Visualisation of the simulated plate and it's support condition as well the partitions used at the points of interest; Right: Visualisation of the uniform 0.5 mm element mesh grid.

Material Properties		
Material Density	Poisson's Ratio	Elastic Modulus
$\rho = 2785$ kg/m^3	$v = 0.33$	$E = 73$ GPa
Model Properties		
Length	Width	Thickness
$l = 0.6$ m	$w = 0.5$ m	$t = 0.002$ mm

Table 10: Material and model properties used for ABAQUS simulation.

4.3.1 Simulation Inputs

PZT wafers convert the stress signals in the structure into a corresponding voltage. This voltage however is affected by both in plane and out of plane displacement and thus cannot be directly converted into an equivalent force in the in or out of plane directions. This study proposes that inputting the signals as a pure U3 displacements, as this should be the dominant displacement in a thin isentropic plate subject to a normal HVI. Thus, these signals should result in signals reflecting the characteristics of the original signal. This is suggester as the newly applied signals would still contain the frequency and amplitude characteristics of the original signal, as well as due to the fact that the original signal should be dominated by the out of plane displacement.

The chosen signal was characterised by Liu et al. into three distinct stages, firstly the arrival of the dominant S0 wave mode, the arrival of the A0 wave mode and the subsequent arrival of signals that have reflected off the plate boundaries. As this study was concerned only with the investigation of pure and non-corrupted signals, only the first two stages were of concern, i.e. the S0 wave mode, the A0 wave mode and a complete signal, containing the entire wave mode up until the reflection. These inputs were subsequently normalised and subsequently inputted as a out of plane (U3) displacement with an arbitrary scaling factor of 0.0001.

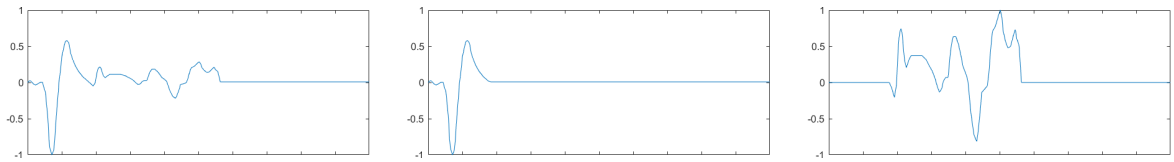

Figure 36: Visualisation the three inputs investigated in this study. Left: Complete wave mode input; Middle: S0 wave mode input; Right: A0 wave mode input.

From this, the resulting U3 displacement signals were collected at 50 points on a straight line at the surface of the plate as Zhang et al. noted that the velocity of HVI induced stress waves can be regarded as constant in all directions [9].

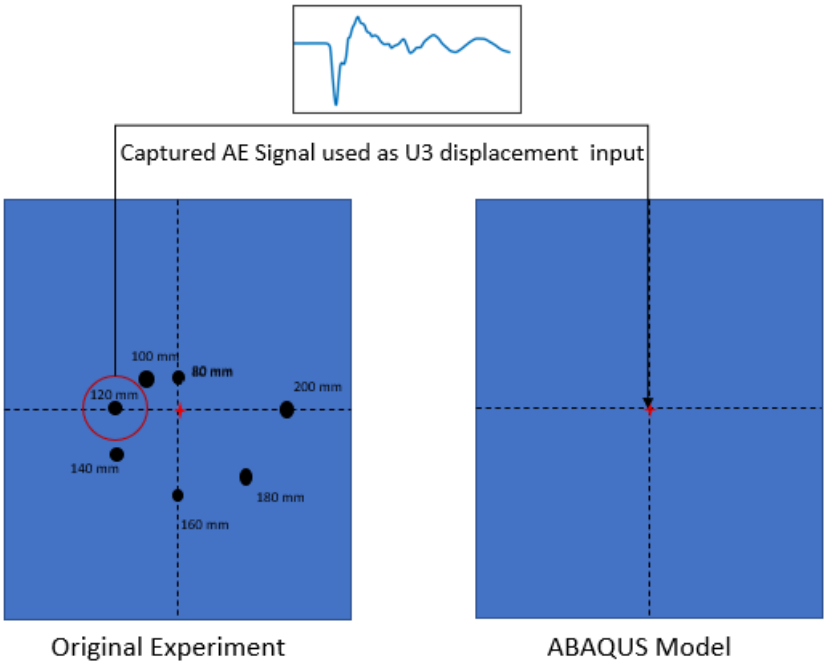

Figure 37: Visualisation of the application of the original experimental sensor reading as input in the ABAQUS model.

Sensor (X, Y) Coordinates			
S0 = (0, 0)	S1 = (0.00, 0.001)	S2 = (0.00, 0.002)	S3 = (0.00, 0.003)
S4 = (0.00, 0.004)	S5 = (0.00, 0.005)	S6 = (0.00, 0.006)	S7 = (0.00, 0.007)
S8 = (0.00, 0.008)	S9 = (0.00, 0.009)	S6 = (0.00, 0.010)	S7 = (0.00, 0.011)
S12 = (0.00, 0.012)	S13 = (0.00, 0.013)	S14 = (0.00, 0.014)	S15 = (0.00, 0.015)
S16 = (0.00, 0.016)	S16 = (0.00, 0.017)	S18 = (0.00, 0.018)	S19 = (0.00, 0.019)
S20 = (0.00, 0.020)	S21 = (0.00, 0.021)	S22 = (0.00, 0.022)	S23 = (0.00, 0.023)
S24 = (0.00, 0.024)	S25 = (0.00, 0.025)	S26 = (0.00, 0.026)	S27 = (0.00, 0.027)
S28 = (0.00, 0.028)	S29 = (0.00, 0.029)	S30 = (0.00, 0.030)	S31 = (0.00, 0.031)
S32 = (0.00, 0.032)	S33 = (0.00, 0.033)	S34 = (0.00, 0.034)	S35 = (0.00, 0.035)
S36 = (0.00, 0.036)	S37 = (0.00, 0.037)	S38 = (0.00, 0.038)	S39 = (0.00, 0.039)
S40 = (0.00, 0.040)	S41 = (0.00, 0.045)	S42 = (0.00, 0.050)	S43 = (0.00, 0.055)
S44 = (0.00, 0.060)	S45 = (0.00, 0.065)	S46 = (0.00, 0.075)	S47 = (0.00, 0.080)
S48 = (0.00, 0.085)	S49 = (0.00, 0.090)		

Table 11: Locations of sensors on the surface of the model.

4.4 Calculation of Arrival Times

One method that allows for the characterisation of the structural response signals generated under HVI, is the comparison of the signal arrival times versus their theoretical arrival times. This can provide valuable information as different wave modes propagate at different velocities and as such they should be identifiable in the recorded signals. As aforementioned in section 2, stress signals usually propagate throughout a thin isentropic structure in longitudinal or transverse wave modes or in the distinct flexural and extensional plate wave modes. The theoretical propagation velocity can subsequently be calculated for each of the wave modes

The theoretical propagation velocities are a factor of the target structure and its material properties and were subsequently calculated for the target that was used in the experiment conducted by Liu et al. [4] and replicated in this project.

Longitudinal Wave Velocity	Transverse Wave Velocity	Extensional Wave Velocity
$C_L = 5119$ m/s	$C_T = 3139$ m/s	$C_E = 5424$ m/s

Table 12: Theoretical mode velocities.

The flexural wave velocity C_F however, is dependent on the angular frequency of the signal, i.e $C_f = [Et^2/12\rho(1-v)^2]^{1/4}\sqrt{\omega}$ [2], and as such was calculated for each of the recorded signals. The angular frequencies were obtained through a fast Fourier transform of which the dominant frequency component was chosen. The theoretical arrival times $t_{Theoretical}$ were thus be calculated using the theoretical propagation velocities of each wave mode.

$$t_{Theoretical} = t_{Max,Input} + d_{Sensor}/C_{Mode} \tag{7}$$

Where $t_{Max,Input}$, denotes the time at the maximum amplitude of the respective input signal, d_{Sensor} the distance of the sensor from the input source and C_{Mode} denotes the theoretical propagation velocity of the mode.

4.5 Source Localisation

An important aspect of the characterisation of the structural response signals generated by HVI, is the localisation of the impact, i.e. the signal source. This project investigated the accuracy of source localisation through triangulation through a time of arrival (TOA) method developed by Nivesrangsan et al. [14].

4.5.1 TOA Triangulation

Through the derivations made by Nivesrangsan et al. [14], it is possible to locate the AE signal source location through a triangular sensor system. This is done, through the application of a velocity and energy based time of arrival difference method.

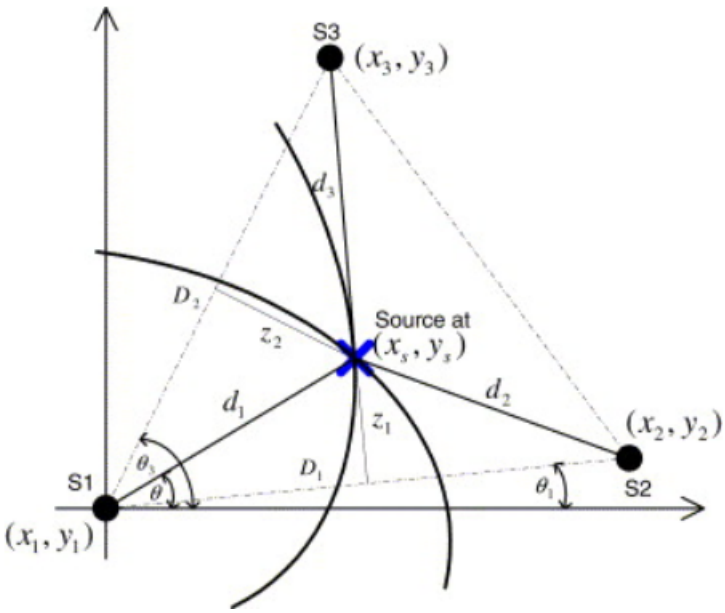

Figure 38: Schematic diagram of the energy based triangulation method developed for source localisation by Nivesrangsan et al. [14].

The method describes the distance d_1 between sensor 1, S1 (x_1, y_1), and the source (x_s, y_s) where

$$d_1 = \frac{D_1^2 - c^2 \Delta t_1^2}{2(c\Delta t_1 + D_1 \cos(\theta - \theta_1))} \tag{8}$$

and

$$d_1 = \frac{D_2^2 - c^2 \Delta t_2^2}{2(c\Delta t_2 + D_2 \cos(\theta_3 - \theta))} \tag{9}$$

where

$$\Delta t_1 = t_2 - t_1 \tag{10}$$

and

$$\Delta t_2 = t_3 - t_1 \tag{11}$$

thus

$$x_s = x_1 + d_1 \cos\theta \tag{12}$$

and

$$y_s = y_1 + d_1 \sin\theta \tag{13}$$

Here c denotes the velocity of the propagating wave, D_1 and D_2 the distance between the respective sensors and θ, θ_1 and θ_3 describe the angles as defined in the above figure. Δt_1 and Δt_2 describe the time difference between the arrival of the signal at the sensors S2 to S1 as and S3 to S1 respectively.

The original paper suggested the use of a suitable iteration scheme to find the value of θ that would result in the lowest error between the two calculated values of d_1. However, as in this project all the sensors used were aligned along a straight line, this triangulation based algorithm lead to a sometimes large error, which will be discussed in further detail in the subsequent section. Therefore the convergence approach was substituted for a more computationally expensive method lowest error method, as it was not possible to find a convergence criteria suitable to all wave inputs. In this method the angle was chosen corresponding to the lowest resulting error from a linearly spaced grid of angles between 0 and 2π with a angle spacing of 0.000001 rad.

As this method requires knowledge of the arrival times and the velocity of the propagating wave, an additional attempt at the characterisation of the recorded signals was made by comparing the accuracy of the predicted source location based on the use of the extensional, longitudinal or transverse wave velocities. The flexural wave velocity could not be investigated by this method as it is a factor of the angular velocity of the signal which was unknown. Additionally, the accuracy was compared for each of the

velocities using the time of arrival of the signal or the time of the maximum amplitude of the signal. This was done due to the latter findings showing that the using the time of maximum amplitude resulted in a accurate prediction of the arrival time for the S0 and combined wave mode inputs.

5 Results and Discussion

5.1 Wave Propagation Characteristics

5.1.1 S0 Wave Input

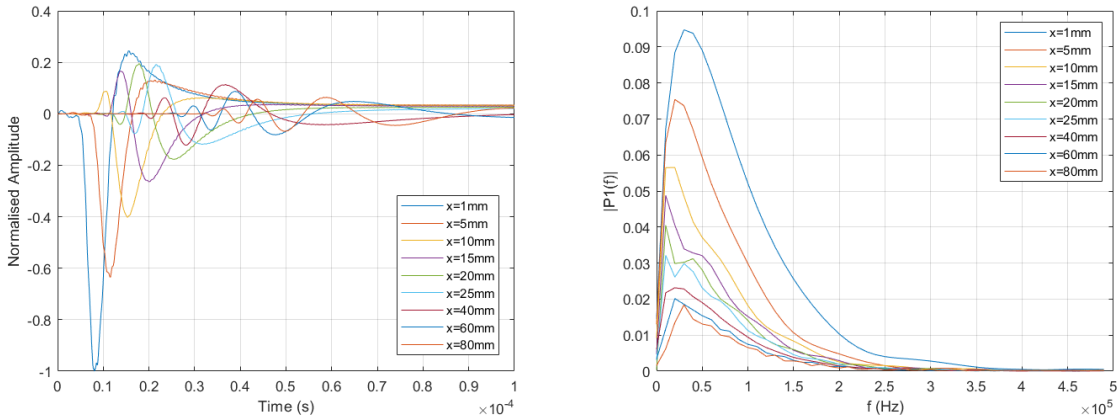

Figure 39: Left: Normalised out of plane displacement signals due to S0 Wave mode input; Right: FFT spectra due to the S0 wave mode input.

Figure (??????) shows the normalised out of plane displacement due to the S0 wave mode input. It is visible that the signals seem to be decaying exponentially as the distance from the signal source increases. Below, the individual wave forms, normalised with respect to themselves aswell as with respect to the signal captured at 1 mm propagation distance form the source. From this, it can be seen that the recorded wave forms quickly disperse and the original input is longer recognisable after just 5 mm of wave propagation. However, while the waveform is no longer recognisable after 5 mm of propagation, it was notable that when applying a fast Fourier transform to the captured signals, the frequency spectra seemed to be in good accordance of the original spectrum regardless of the propagation distance. A noticeable exception to this, were the spectra captured at 20 and 25 mm propagation distance as these indicated to be composed of two separate distinct signal components while all other spectra indicated a single dominant frequency component.

The wave propagation was subsequently compared to the theoretical wave arrival times of the longitudinal and transverse wave modes as well as the extensional and flexural lamb wave modes. It was noticeable that except for the transverse wave mode, which

consistently and accurately predicts the arrival of the signal, the longitudinal as well as the extensional wave modes predict the arrival of the wave too early. Notably, the flexural wave mode velocity appears to lead to the highest inaccuracy when used to predict the signal arrival times.

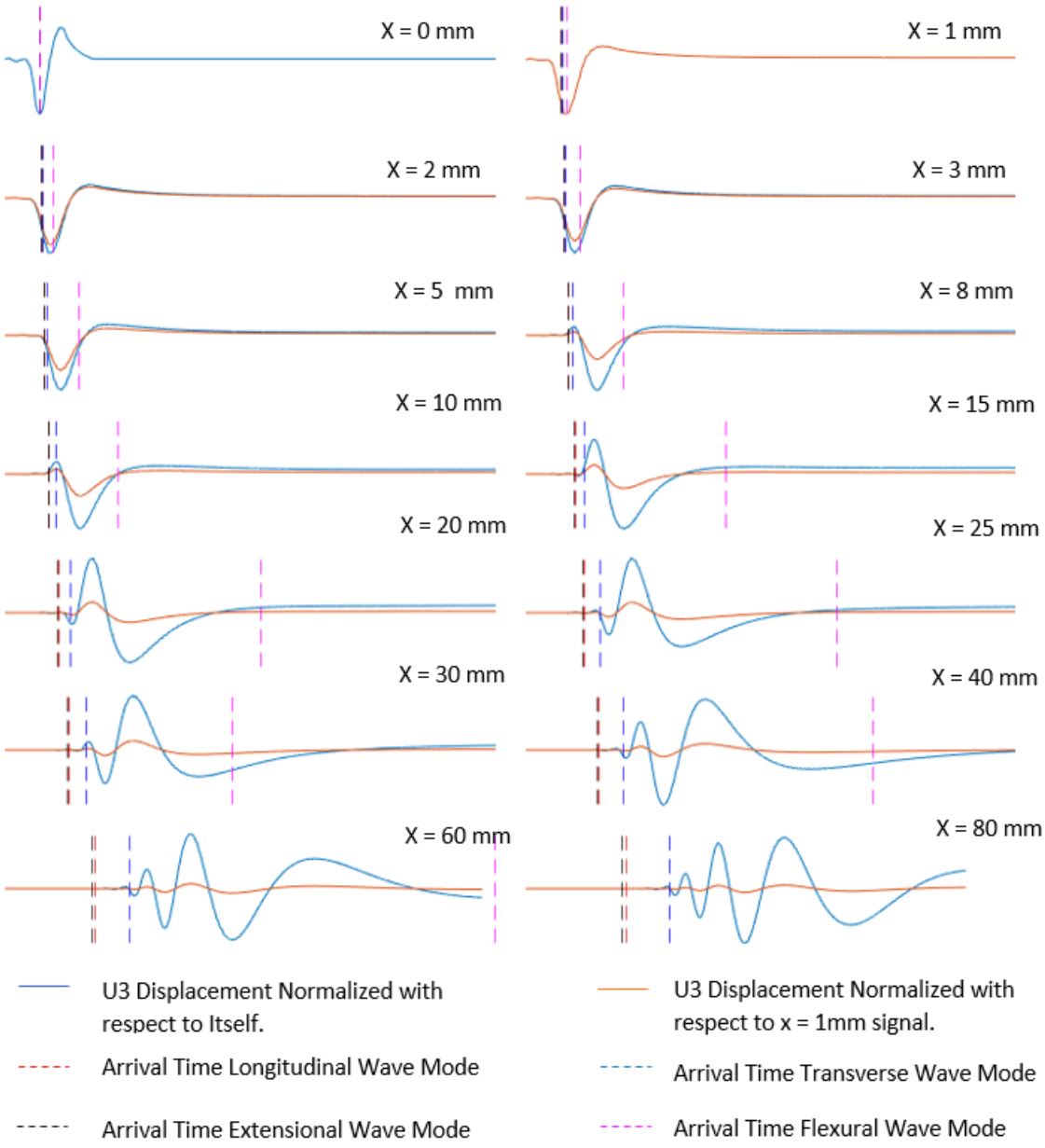

Figure 40: S0 input induced wave forms at various distances from the signal source.

5.1.2 A0 Wave Input

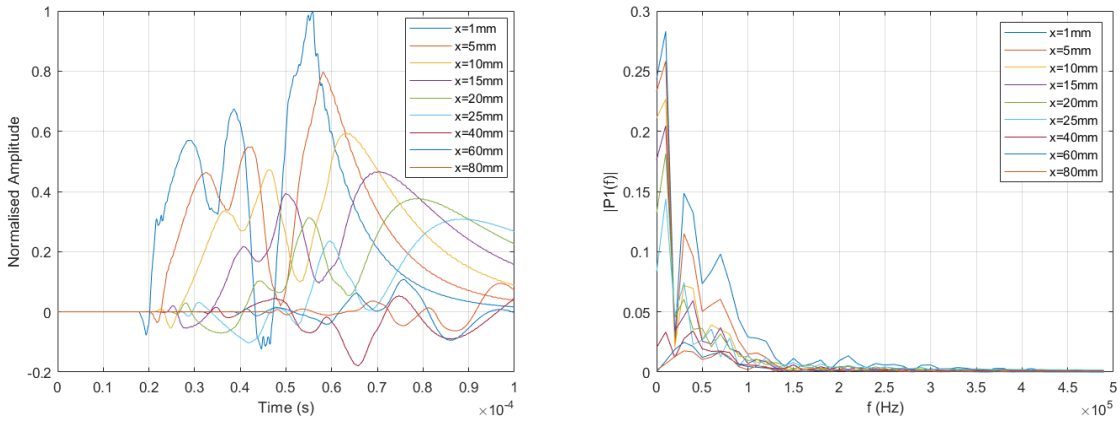

Figure 41: Left: Normalised out of plane displacement signals due to A0 wave mode input; Right: FFT spectra due to the A0 wave mode input.

Figure (????) shows the normalised out of plane displacement due to the A0 wave mode input. Like the displacement due to the S0 wave mode input, the amplitudes of the recorded displacement signals seem to follow an exponential decay function. The signals recorded due to A0 wave mode input however appear to resemble the original input signal up to 15 mm of propagation distance. The captured frequency spectra showed like the S0 wave mode input, nearly all captured frequencies somewhat reflecting the spectra of the original signal. Unlike the frequency spectra recorded for the S0 wave mode input, these however seem to resemble the original spectrum significantly less, especially propagation distances larger than 15 mm. This was expected as Gorman [12] stated that flexural waves unlike extensional waves do suffer from signal dispersion.

When comparing the displacement signals with the theoretical wave mode velocities, the theoretical arrival time did not seem to indicate a common signal trend. This is unlike predicted times for the S0 wave mode input, which appeared, to accurately predict the arrival of the first wave peak. However, it appears that the theoretical flexural wave mode velocity was able to predict the arrival time of the induced peak amplitude with fairly good accuracy, up until a propagation distance of 5 mm.

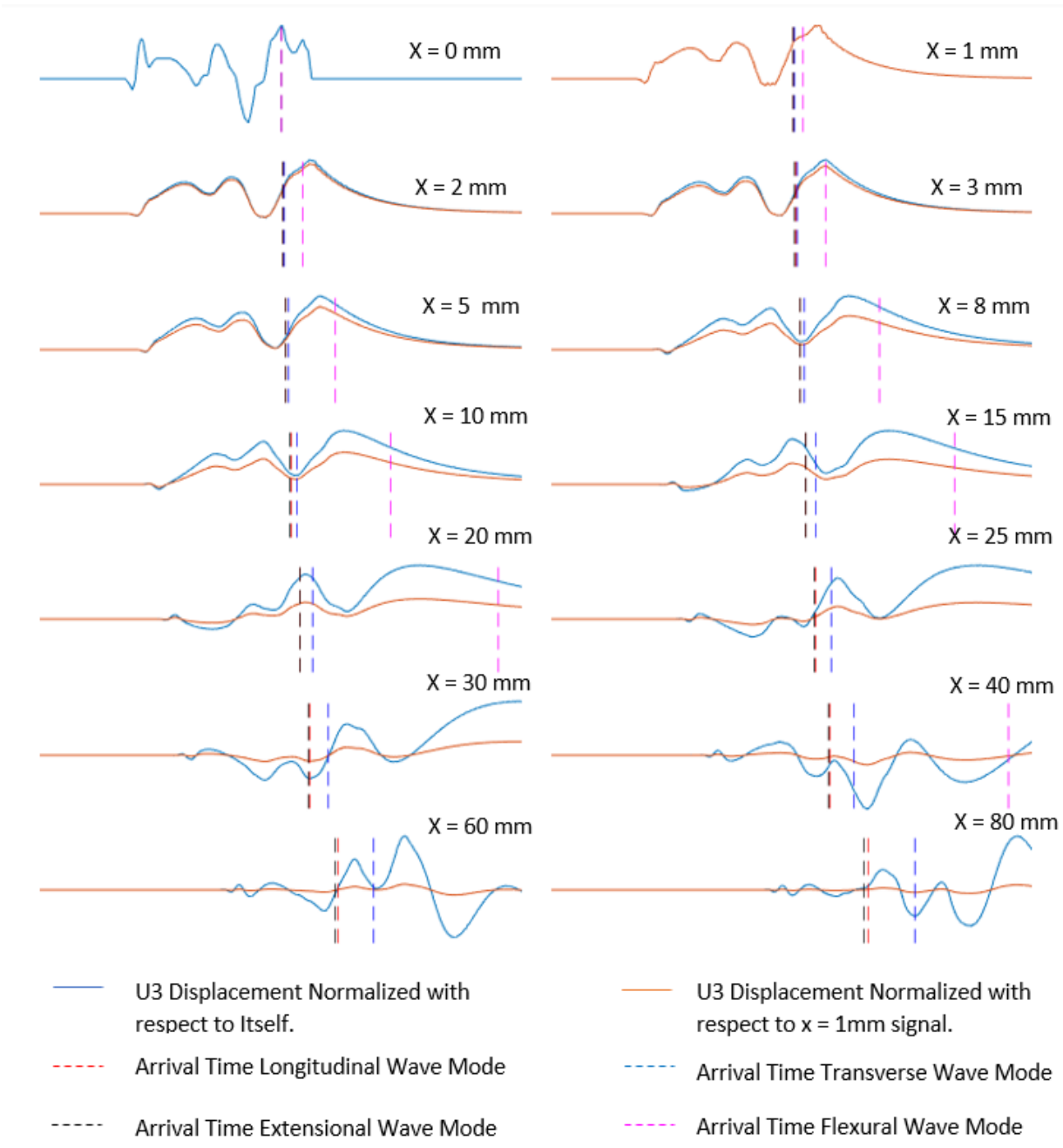

Figure 42: A0 input induced wave forms at various distances from the signal source.

5.1.3 Combined Input

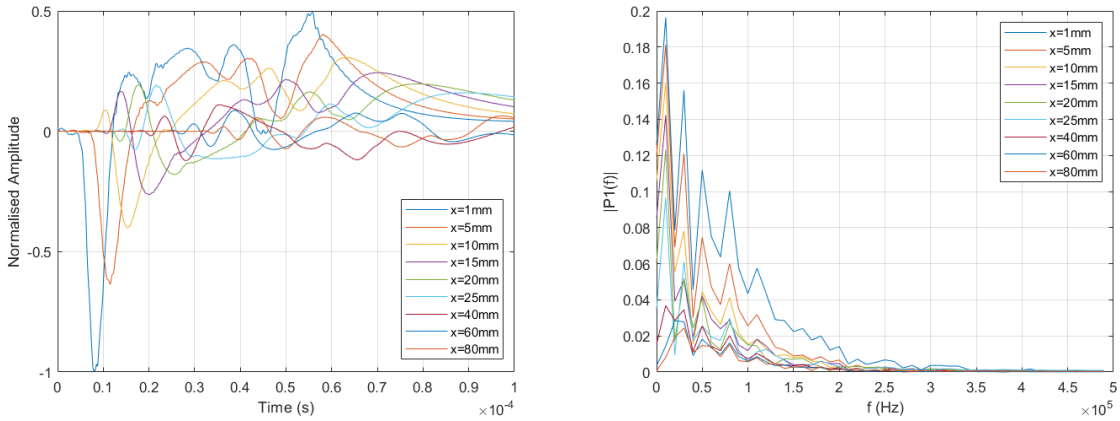

Figure 43: Left: Normalised out of plane displacement signals due to complete wave input; Right: FFT spectra due to the complete wave input.

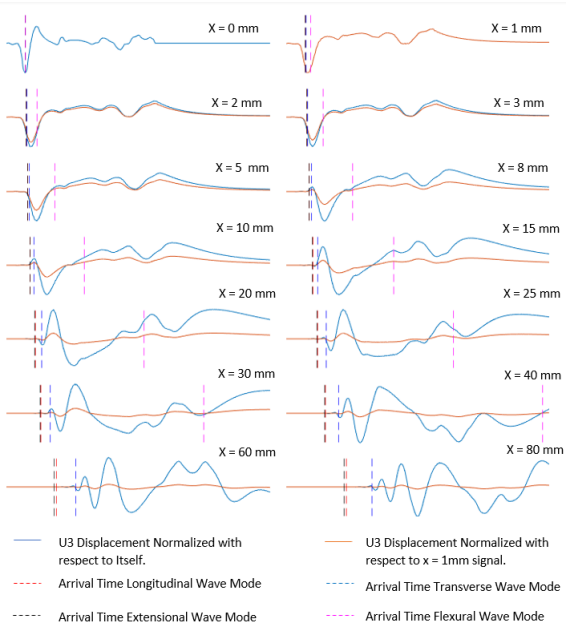

Figure 44: Complete wave input induced wave forms at various distances from the signal source.

Figure (???) shows the normalised out of plane displacement due to the combined wave mode input. As expected from the results due to the individual wave modes, the captured signal amplitude once again appears to follow an exponential decay function. It is noteworthy that the captured frequency spectra for the combined wave mode input seemed to resemble the originally captured spectrum more closely than the spectra captured due to either of the original wave mode inputs at any propagation distance.

5.1.4 HVI induced amplitude characteristics

As the recorded signals measured the out of plane displacement due to an out of plane input, the out of plane displacement amplitude characteristics of the induced signals were studied for each of the inputs. The first parameter of interest was the maximum recorded displacement at the various propagation distances. These displacements, shown below, were normalised with respect to the first sensor at a propagation distance of x = 1 mm. The values were normalised with respect to this sensor rather than the maximum displacement at the input source, as this value would not usually be known in experimental circumstances.

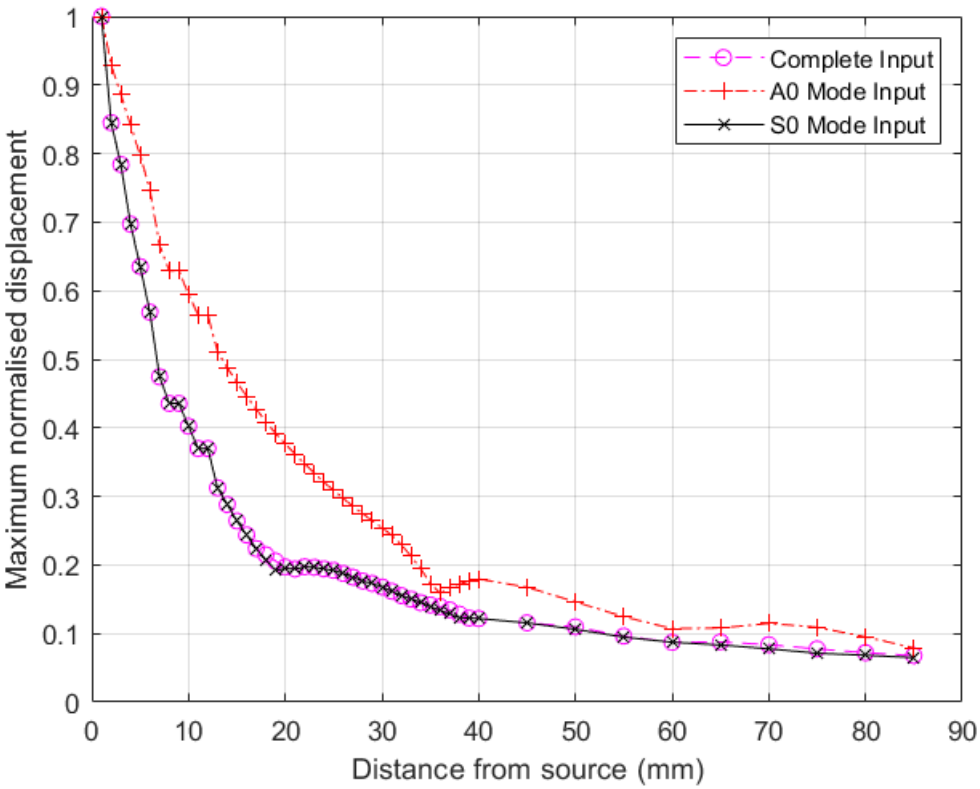

Figure 45: Maximum displacement at various distances from source input

This shows that the resultant displacements due to the A0 wave mode and S0 wave mode inputs, both seem to follow an exponential decay function. It can however be observed that the displacement due to a normalised A0 mode displacement input was consistently larger than the displacements recorded by the normalised S0 mode input. It can also be observed, that even when the entire signal was considered for the combined

input, the resultant normalised maximum displacement fitted almost perfectly to the resultant normalised maximum displacement due to the S0 wave mode input. This suggests that it might be possible to obtain significant information on the severity of the induced damage by only considering the initial part of the HVI induced signal. This would be in accordance with the source paper [4] which found that HVI induced AE signals are dominated by the S0 mode.

The maximum displacements, as a function of the distance from the signal source, were plotted and fitted with a double exponential decay function for each of the 3 cases. In each case, the fitted decay functions, closely resemble the recorded data which indicated that the expected maximum displacement at any point could be predicted if the location of the source signal is known in addition to the maximum displacement at any point on the plate. It is noteworthy that the double exponential functions for the S0 mode and the combined input are almost identical, once again indicating that the S0 mode alone could be used to predict certain characteristics of the induced waves on the plate.

These fitted functions also show that in each of the 3 cases, it is possible to fairly accurately predict the normalised maximum displacement at the input source through the application of the double exponential decay functions. This suggests that this method could be used to obtain important information regarding the extent of damage at the impact location and could potentially be used to characterise the depth of crater formation in a non-penetration case. Further research and investigation of this method through the application of a signal obtained from a non-penetration case, is however required to validate this.

Additionally to the maximum displacement, the rise time (time from signal onset to the maximum value of the signal) and the ratio RA (Maximum Amplitude/Rise Time), as suggested by Gorman [12], were investigated for the different inputs.

The results obtained for the recorded rise time due to the various inputs showed that these have significantly different characteristics. The S0 wave mode input results in an almost linear function that experience a step decrease of roughly 25 % every 19 mm. The A0 wave mode input however resulted in a much less predictable outcome in which

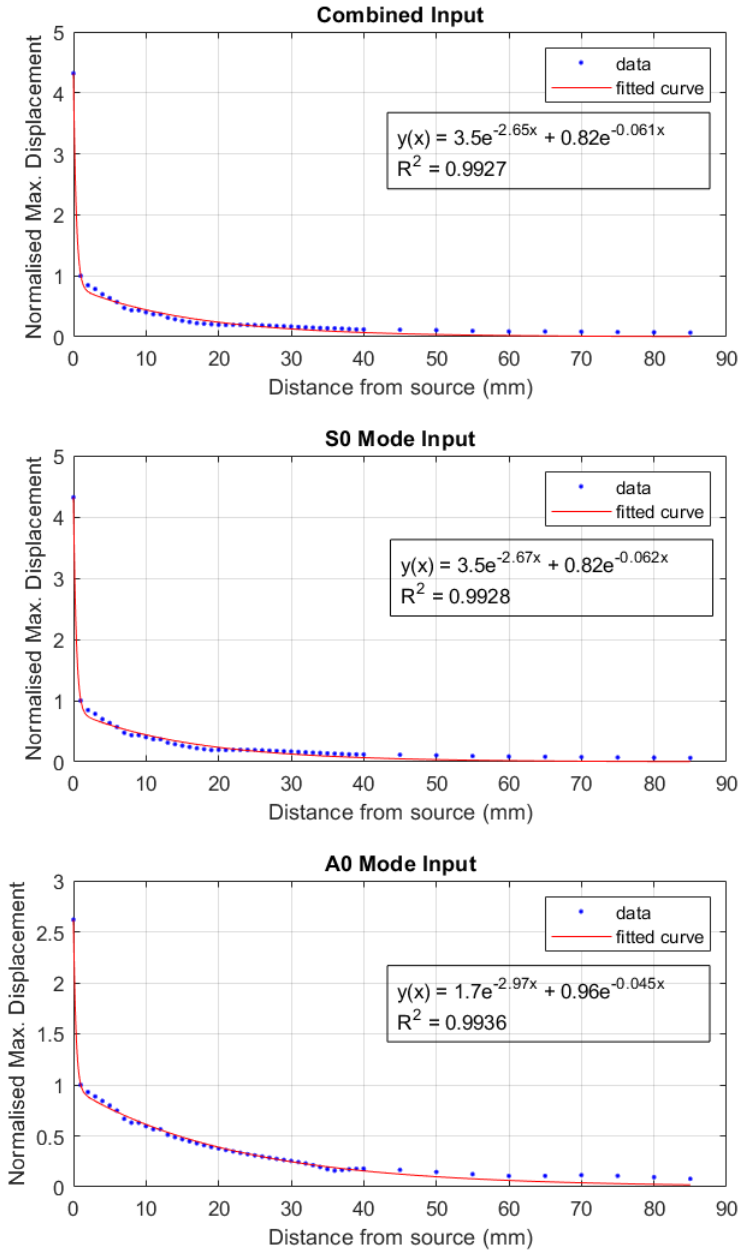

Figure 46: Maximum displacement at various distances from source input, fitted with a double exponential decay function for the S0 mode, A0 mode and combined input.

the rise time follows an exponential increase for the first 35 mm of propagation, after which it adopts the same linear increase with repeated step decreases, as could be seen for the S0 mode input. Further research into this phenomenon is required as this suggests a significant difference in the near and medium field propagation characteristics of the A0 wave mode induced displacement. The observed rise time for the combined input,

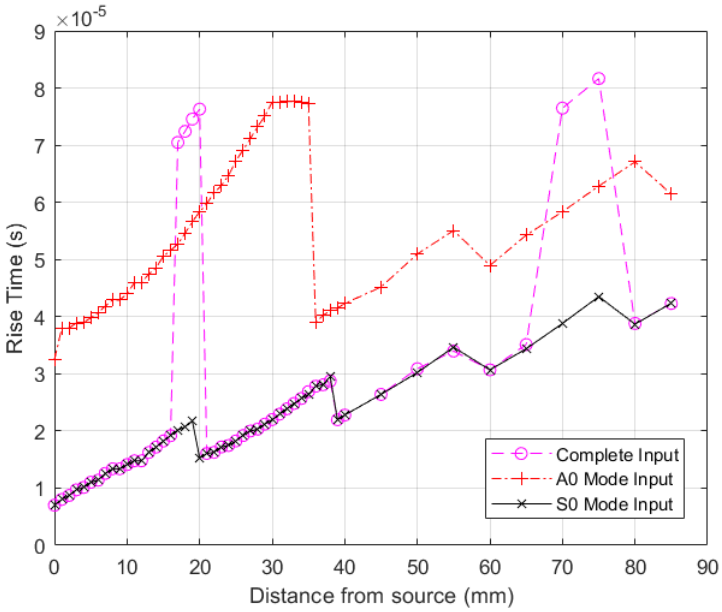

Figure 47: Rise Time of the three inputs as a function versus the distance from the signal source.

once again closely followed the observed results of the rise time due to the S0 mode input except for significant jumps in rise time between 16-21 mm and 65-80 mm. It is suggested that a possible explanation of this could be constructive interference between the S0 and A0 modes.

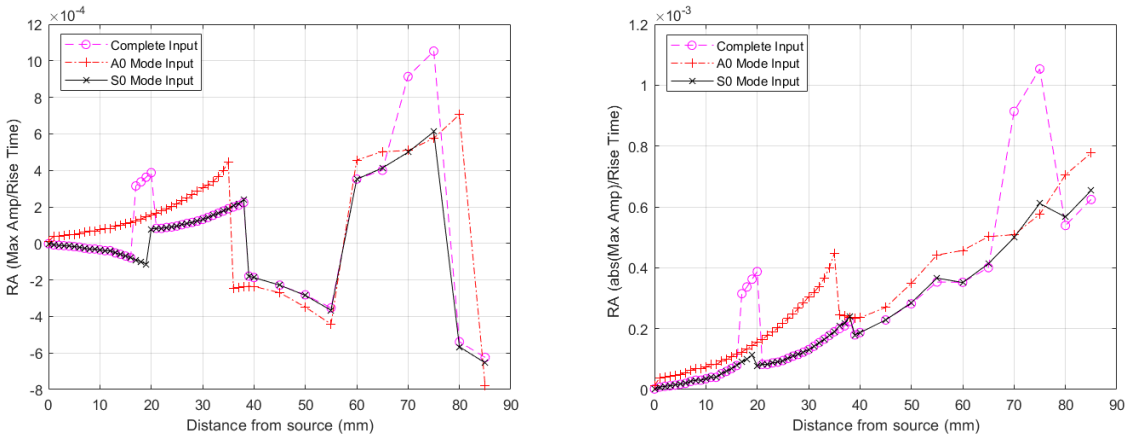

Figure 48: RA ratio versus propagation distance from the input source. Left: Max. displacement/rise time., Right: Absolute max. displacement/rise time

Like the rise time, the ratio RA, was also observed to follow predictable behaviour for the S0 mode input and a much less so predictable behaviour for the A0 mode input. It was also noted that the S0 mode input, once again almost perfectly matched the results due to the complete input except for the two discrepancies that at 16-21 mm and 65-80

mm propagation distance. Interestingly, it was observed that the noted step decreases that were observed for the rise time, correspond with a sign change in the maximum recorded displacement. It is suggested that this is likely correlated to the wavelength of the propagating signals.

This could explain why the A0 wave seems to be less predictable as it could be seen from the FFT in section 5.1.2, that the A0 wave input consists out of various distinct frequency components while section 5.1.1 showed that the S0 mode input resulted in a single dominant frequency. As such the A0 wave mode input would consist of various wavelengths which would explain the much less predictable behaviour compared to the S0 mode input as this would cause wave dispersion. This would be in good accordance with the findings of Gorman [12] who stated that flexural AE waves are subject to wave dispersion while extensional AE waves are not and as such the flexural waveform is less predictable. The combined input however seemed to be fairly reliably predictable with only a few notable exceptions. This could suggest that the extensional S0 wave mode should be used to characterisation and prediction of HVI induced AE signals.

Another characteristic of interest was the signal energy envelope as described by Kaphle [2] which effectively describes the total area below a voltage-time graph. As this simulation had the output in terms of displacement rather than voltage, the displacement was used to calculate a proportionally equivalent energy content, normalised with respect to the energy content of the signal captured at x = 1 mm, to evaluate any obvious trends in this.

Interestingly, this showed a very different effect than expected from the previous graphs, with the correlations between the three inputs differing strongly from the previously discovered correlation characteristics. For the energy envelope, it appears that the decay due to the A0 mode input resembled the energy decay due to the complete input more closely than the decay due to the S0 mode input, which resulted in the lowest energy drop out of the three inputs. Another considerable difference to the relationships identified for the maximum normalised displacement along the propagation path is that in terms of the maximum displacement, the S0 and complete inputs both experienced a

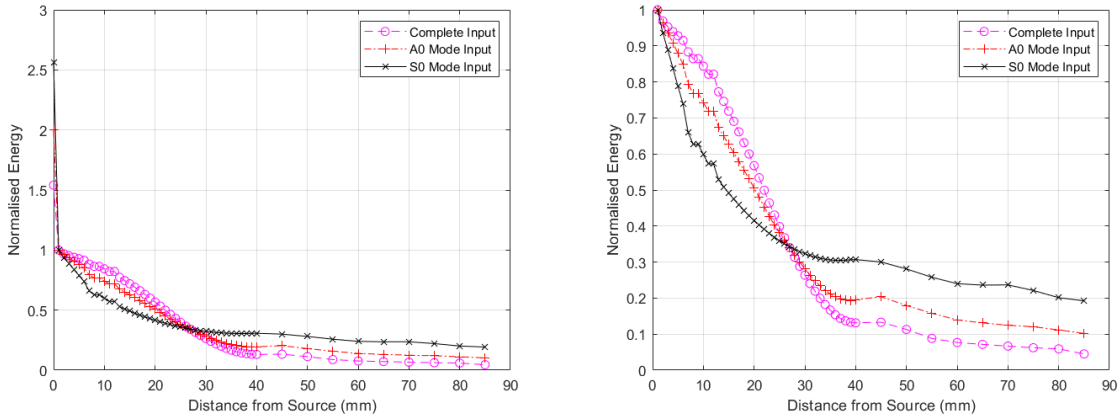

Figure 49: Signal total proportionally equivalent energy content versus propagation distance. Left: Including the energy of the source input, Right: Excluding the energy if the source input.

drop of roughly 75 % while the A0 mode resulted in a 62 % drop in the first millimetres of propagation. It can be seen on the energy envelope graph that the complete input resulted in the lowest drop of 35 %, while the A0 and S0 inputs resulted in drops of 50 % and 61 % respectively.

Another notable observation made, were the gradient characteristics of the energy envelope graph. In all inputs, there seemed to be a distinct difference in the gradient of the energy envelope between the propagation distance of 0 to 40 mm versus the gradient from 35 to 85 mm. The gradient of the A0 and complete input seemed to follow a similar and almost linear decay until 35 mm propagation distance while the energy gradient of the S0 mode seemed to resemble an exponential decay function. After the 35 mm propagation distance, however, all three energy envelopes, while differing in magnitude appeared to exhibit the same linear gradient. This suggests that the different modes experience different near field energy propagation characteristics but similar propagation characteristics in the medium field region.

5.1.5 HVI induced frequency characteristics

For the analysis of the HVI induced frequency characteristics, the first two characteristics of interest were the dominant frequency of the FFT spectrum and the mean frequency, obtained from the power spectrum of the individual FFT spectra, versus propagation distance.

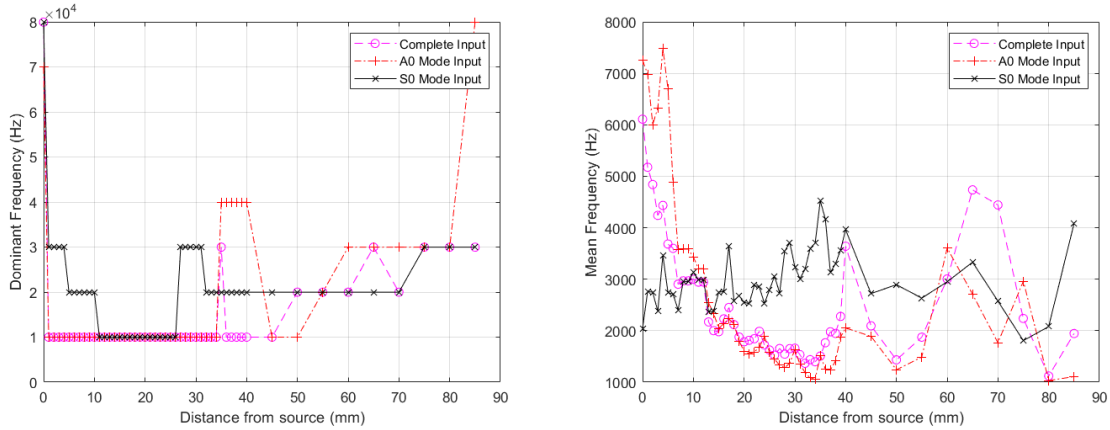

Figure 50: Left: Dominant frequency versus propagation distance; Right: Mean frequency versus propagation distance.

The dominant frequency versus propagation distance graph showed the dominant frequencies due to all three inputs seemed to follow a sort of step-function pattern. All three of the inputs resulted in a steep drop from the recorded dominant frequency at the input source, it was however notable that this dominant frequency was the same for the combined and the A0 mode input. Additionally to this, all three inputs resulted in the same dominant frequencies at certain proportion distances e.g. 10 - 20 mm. However, no direct pattern could be identified from the obtained data and thus further research into the dominant frequency characteristics versus propagation distance is suggested.

The mean frequency versus propagation distance graph however revealed a much less step-like behaviour and showed a clear difference between the mean frequencies due to the S0 mode input versus the mean frequencies due to the A0 mode and complete inputs. The A0 mode and complete input appear to induce similar relationships causing a steep decay during the first few millimetres of propagation after which they seemingly stabilise and increase while the mean frequencies due to the S0 mode input experience a much smaller variation and no steep drop from the original inputs' mean frequency.

It is noted that when evaluating the frequencies at the longer propagation distances, the recorded dominant and mean frequency accuracies, likely suffer due to the short simulation time. As the recorded signals likely miss certain frequency components which have not yet reached the latter sensors, a non-complete frequency spectrum is recorded, possibly affecting the result. This could explain anomalies such as the large dominant frequency jump recorded at the 85 mm propagation distance due to the A0 mode input.

The recorded results, however, were concluded to be potentially unreliable as each of the inputs resulted in a dominant frequency in the same order of magnitude as the originally recorded signal but neither of them were able to replicated the originally recorded dominant frequency of 2.4 KHz [4] at any propagation distance.

To investigate these frequency phenomena, the short time Fourier transforms (STFTs') were gathered at various propagation distances for signals obtained due to the 3 inputs. All STFTs' were obtained from the out of plane displacement signals normalised with respect to the values obtained at 1 mm propagation distance.

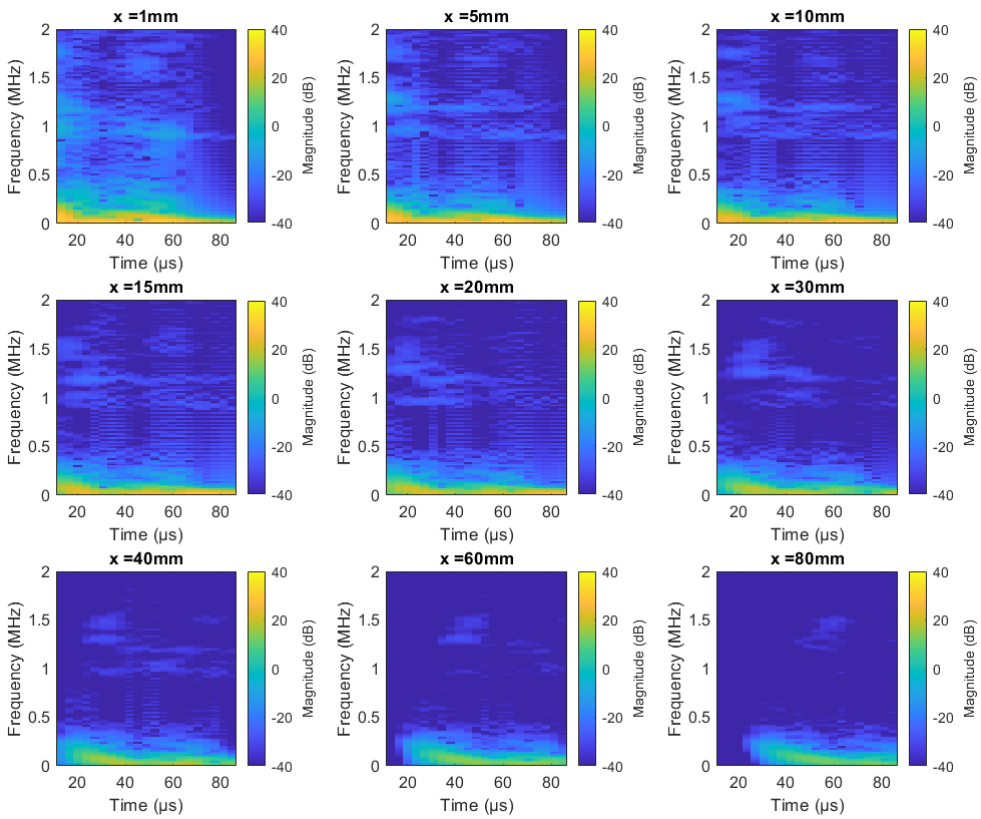

Figure 51: STFT of signals received due to combined input at various distances from the source.

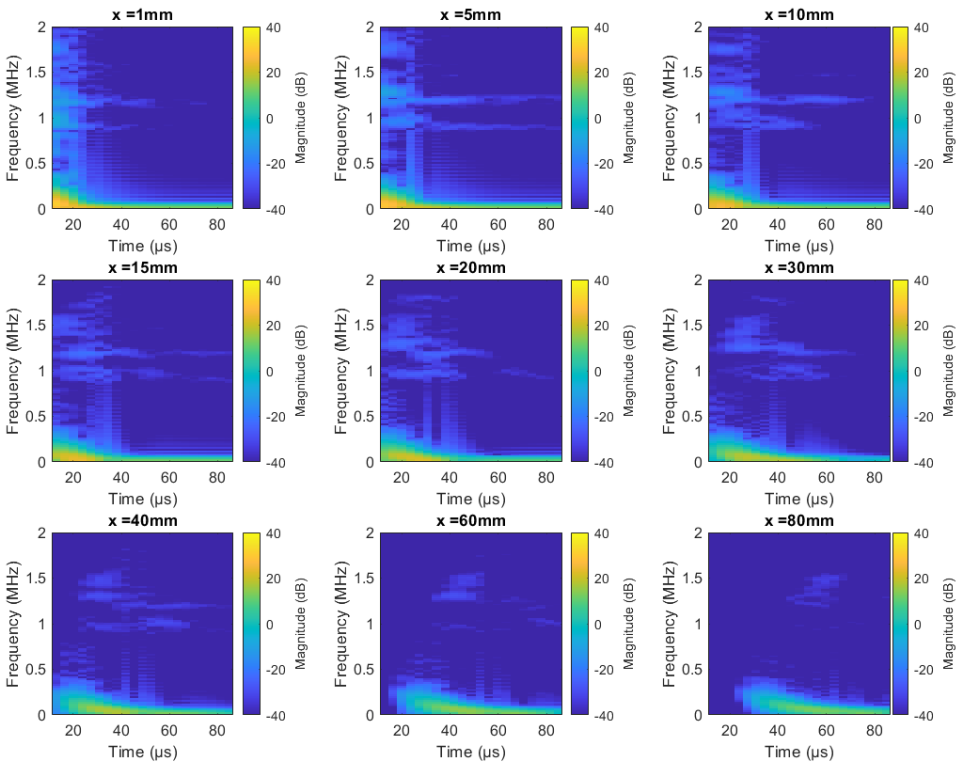

Figure 52: STFT of signals received due to S0 input at various distances from the source.

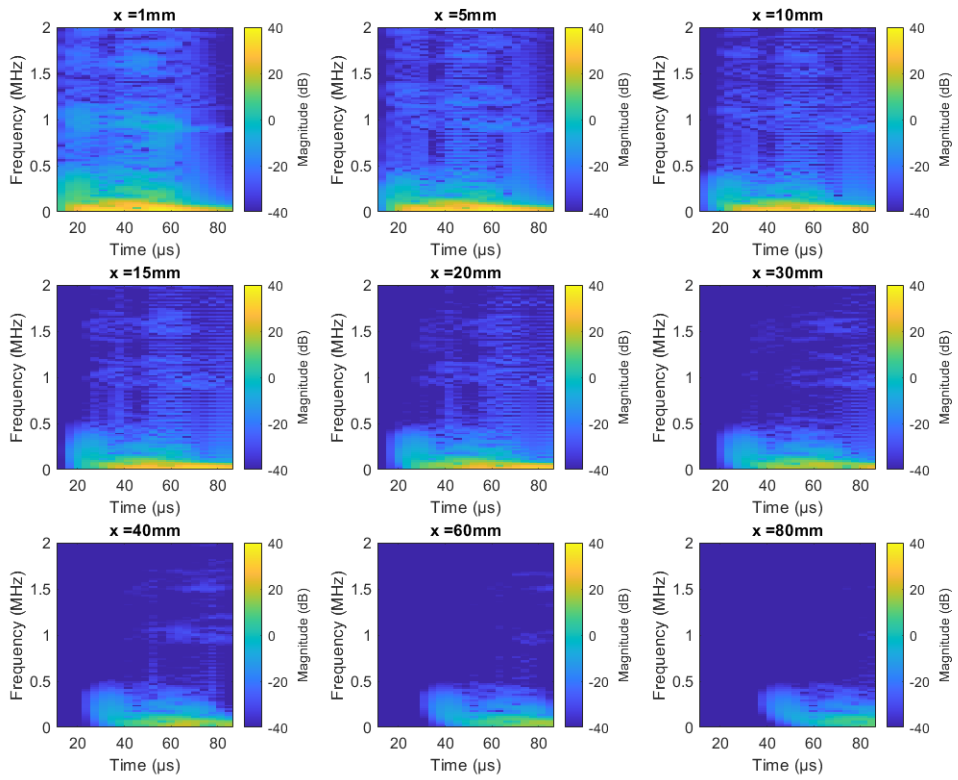

Figure 53: STFT of signals received due to A0 input at various distances from the source.

From the STFSs', it can be seen that the combined and A0 input resultant signals appear to be composed of more dominant higher frequency components than the signals obtained from the S0 mode input. These high-frequency components appear to attenuate much faster than the low-frequency components of the signals explaining the large and quick drop in mean frequency that was recorded from the A0 and complete wave mode input.

A noticeable feature of the induced signals due to each of the inputs was that clear signal dispersion was observable. With all inputs, it could be observed that as the propagation distance was small, the weaker high-frequency components arrived alongside the dominant low-frequency components. However, as the propagation distance increased, it can be seen that the low-frequency components arrive before the high-frequency components of the induced signal. Additionally to this, it can be seen that as the propagation distance increases, in each of the three cases, the dominant low-frequency components ($f < 0.5$ MHz) seem to disperse such that its higher frequency components (0.2 MHz $< f <$ 0.5 MHz) arrive before its lowest-frequency components (0 MHz $< f <$ 0.2 MHz). These findings show that the low-frequency components (below 0.5 MHz) of the HVI induced structural response signals appear to generally propagate at higher velocities than the high-frequency components at frequencies. Below 0.5 MHz however, there appear to be distinct velocities, with the higher frequency components seemingly propagating at a higher velocity than the lower frequency components.

Overall, it is noted that out of the three inputs, the signals recorded due to the S0 mode input, appear to show the least dispersion which is in good accordance with the findings of Gorman [12] who found that the extensional wave, unlike the flexural wave, did not suffer from dispersion with propagation distance.

5.2 Source Localisation

The accuracy of signal source localisation method developed by Nivesrangsan et al. [14], was investigated for all the the studied wave mode inputs. All the inputs resulted in a fairly accurate prediction of the source location with a maximum error of approximately 30mm. However, as this method resulted in a large range of errors, no appropriate common convergence criteria, such as the one chosen by Nivesrangsan, could be found for the signals. This meant that a more computationally expensive approach, which did not rely on convergence but rather the choice of the lowest error value from a set covering a large range of angles, had to be used .

5.2.1 S0 Wave input

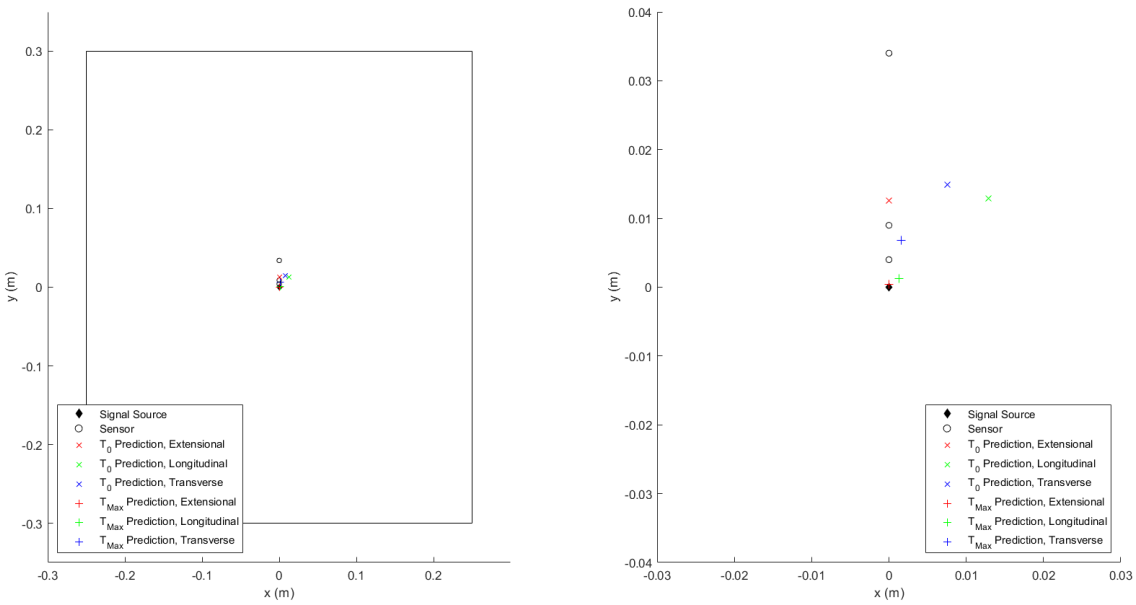

Figure 54: Visualisation of the source predictions made by the TOA triangulation algorithm, based on the S0 wave input. Left: Source prediction visualised on the entire target plate; Right: Close up of the source prediction.

As can be seen above, through the application of the S0 wave mode input, the location of the source could be predicted with a reasonable accuracy for almost all velocities and and signal times. However, it can be seen that in all cases, the source location prediction was significantly more accurate through the use of the time of maximum amplitude, T_{Max} rather than the absolute signal arrival time T_0. Additionally, it can be seen that in both

cases the extensional and longitudinal velocities were able to predict the source location at a significantly higher accuracy than the transverse wave velocity. It is notable that the prediction made through the use of the maximum amplitude time and the extensional wave velocity was able to almost perfectly identify the source location with a minimum error of 0.38 mm. This would suggest that the S0 mode was correctly characterised as the S0 mode itself corresponds to the extensional wave mode and as such should be best described by the extensional wave mode velocity.

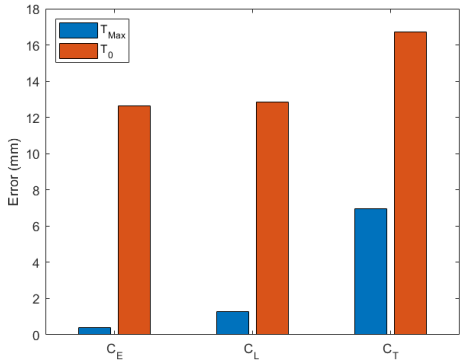

Figure 55: Comparison of the errors through the use of the extensional wave velocity C_E, the longitudinal wave velocity C_L and the transverse wave velocity C_T.

5.2.2 A0 Wave input

In comparison with the S0 mode input, the A0 wave mode input, resulted in a less accurate source prediction. It can also be seen that unlike the S0 mode input, in which the predictions made through the use of T_{Max}, were always significantly more accurate, this is not the case for the A0 mode input. The lowest recorded error for the A0 mode input, was through the T_{Max} transverse wave velocity, which resulted in an error of 9.91 mm.

This reduction in accuracy compared to the predictions made for the S0 mode input, were however expected as the A0 mode corresponds to the flexural wave velocity C_F, which was not used for source localisation as the angular velocities, and thus the flexural wave velocity was unknown.

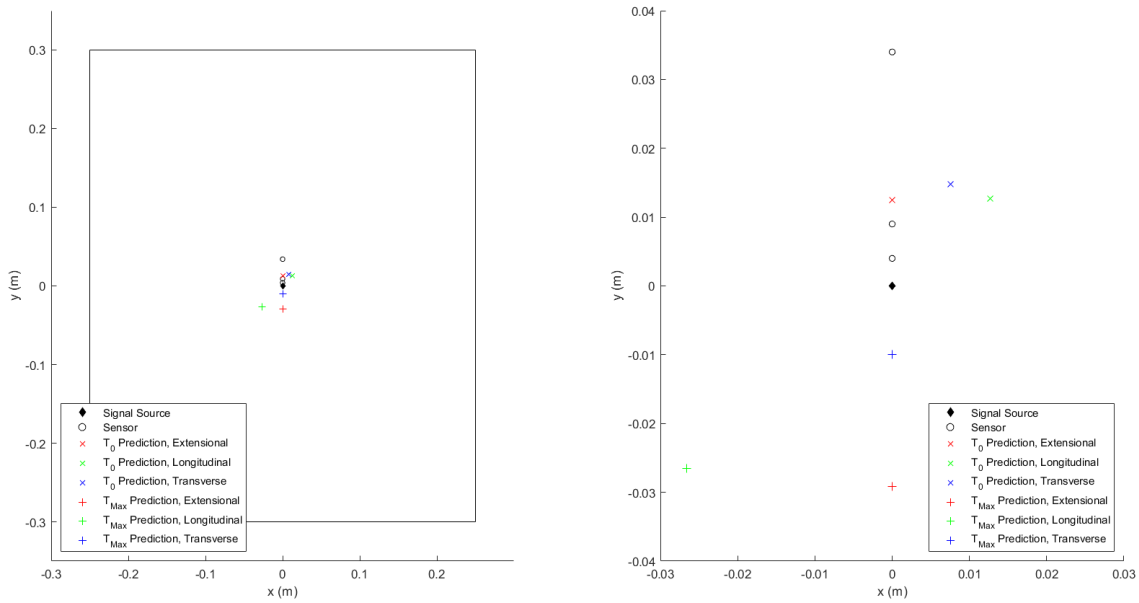

Figure 56: Visualisation of the source predictions made by the TOA triangulation algorithm, based on the A0 wave input. Left: Source prediction visualised on the entire target plate; Right: Close up of the source prediction.

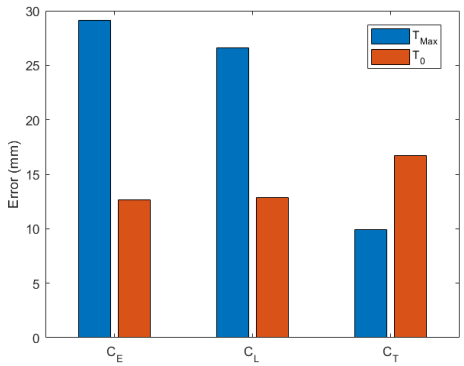

Figure 57: Comparison of the errors through the use of the extensional wave velocity C_E, the Longitudinal wave velocity C_L and the Transverse wave velocity C_T.

5.2.3 Complete Wave input

As expected from the previous findings in section 5.1, the source localisation due to the complete wave mode input, completely resembled the results due to the S0 mode input, once again suggesting that the S0 mode alone carries the required information for the characterisation of an HVI induced event. This was expected as the source localisation used parameters such as the arrival time of the wave, which as previously shown in section 5.1.4, are almost perfectly resembling of one another for the S0 mode and the complete input.

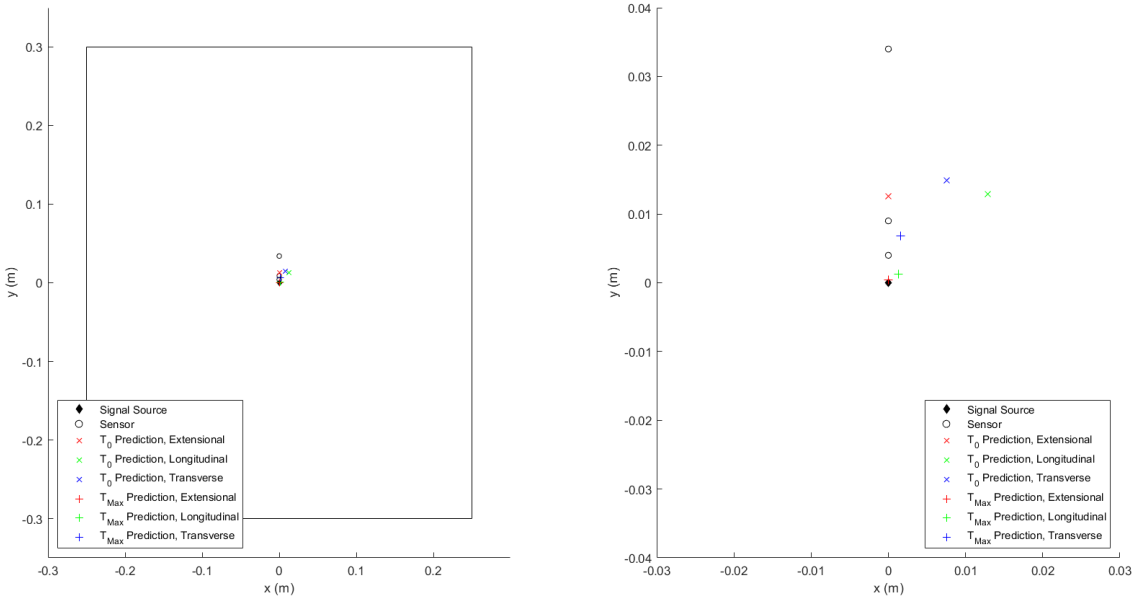

Figure 58: Visualisation of the source predictions made by the TOA triangulation algorithm, based on the complete wave input. Left: Source prediction visualised on the entire target plate; Right: Close up of the source prediction.

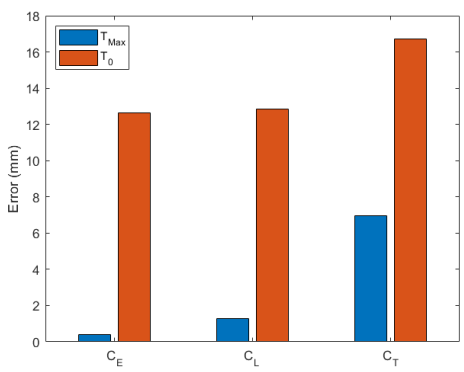

Figure 59: Comparison of the errors through the use of the extensional wave velocity C_E, the Longitudinal wave velocity C_L and the Transverse wave velocity C_T.

6 Conclusion & Future Work

6.1 Common Features of HVI induced AE signals

From the review and collection of previous literature a few common factors that are present in the structural response signals induced by HVI on thin isentropic plates could be found. It is concluded that the structural response signals produced in thin plates under HVI are strongly dependant on the impact condition, i.e. whether the target was perforated or not. Generally speaking, it was noted that a perforation case results in the signal being dominated by the lower frequency extensional wave component while in non perforation cases the signal is dominated by the higher frequency flexural wave component.

As existing literature regarding AE signals generated by HVI on thin isentropic plates, is quite limited, these findings can not be described with complete confidence due to a lack of sufficient data. This lack of access to experimental HVI data proved to be one of the major challenges of the project and severely limited the scope of the project.

It is suggested that future research studying the Acoustic Emission signals generated by HVI on thin isentropic plates is conducted. More data needs to be available on the wave forms of HVI induced AE signals. It is suggested that research is undertaken in such a way to release data sets containing the wave forms of HVI induced AE signals at various propagation distances for a variety of plate thicknesses for both perforation and non perforation cases.

6.2 A novel method to study HVI induced AE signal features

For the study of the HVI induced structural response signals, a novel method replicating the structural response signal features induced by HVI was developed as a complete simulation of a HVI event was unfeasible in the given time frame of the project. This method takes an HVI induced AE signal from previous literature as an out of plane displacement input in the numerical simulation software ABAQUS.

This method developed to model and study HVI induced signal propagation and

dispersion features, was considered successful. It was able to successfully reproduce important signal features induced through HVI evens, such as lamb wave dispersion and the expected S0 mode dominance of the propagating signals. This method could allow for the fairly simple study of HVI induced signal features reducing the need for complex experimental procedures or the much more complex coupled SPH & FE approach used by Liu et al. [4].

However, due to a lack of data and access to experimental facilities, this method could not be validated in terms of its ability to replicate the signals produced by the actual HVI impact. Thus while it may provide important information on the general signal dispersion and propagation features that are present due to HVI, further research is required to investigate the ability of this method in replicating the original HVI event.

It is consequently suggested that future research is undertaken with a specific focus on this method and it's ability to replicate the waveform of HVI induced signals at various propagation distances.

6.3 HVI induced signal propagation characteristics

6.3.1 Amplitude Characteristics

It was concluded that the HVI induced amplitude characteristics follow a double decay function, allowing for a fairly accurate prediction of the maximum amplitude of the signal at any point on the impacted target. This could allow for the quick characterisation of a HVI induced event regarding the extend of damage as well as whether the impact resulted in penetration of the shielding structure. It was also concluded that almost all signal amplitude features induced by HVI could be predicted by the analysis of the S0 mode. This meant that the results were in good accordance with the source paper and literature provided by Liu et al. [4, 6], which found that the HVI induced signals are dominated by the S0 mode in a penetration case such as the one investigated.

The ability to predict the induced signal characteristics of a HVI based purely on the analysis of the S0 mode could be of great significance as, in nearly all investigated literature it is the first arriving wave mode, due to it usually higher velocity compare to

the A0 mode. This suggests that data acquisition equipment used to obtain waveform data on HVI induced signal features would require a much smaller storage capacity than if they needed to record the entire signal. Thus, it could reduce the cost and complexity of the equipment needed for the study and characterisation of HVI induced signals.

It would also allow for a faster response time for an automated in situ detection network as it could process the expected HVI induced damage at a faster rate. This faster response time could be of great significance in the case of a HVI event on a crewed spacecraft, as it could provide the crew with the time required to ensure the safety of the spacecraft and on board personal.

It is suggested that further research regarding these amplitude characteristics is conducted for various other HVI impact conditions such as various plate thicknesses and projectile impact velocities. Additionally, further study investigating the HVI induced amplitude characteristics for non perforation cases is recommended. This is due to the fact that non perforation cases tend to induce structural response signals which are dominated by the A0 mode rather than the S0 mode.

6.3.2 Frequency Characteristics

The author suggests further research and validation into the recorded HVI induced frequency characteristics, as the applied method seemingly was not able to replicate the exact dominant frequency found by the source paper, but rather just dominant frequencies that were within the same order of magnitude as the original.

From the obtained findings it could be seen that the resultant dominant frequency due to all three inputs, did not appear to follow a predictable pattern, but were observed to follow a step function like behaviour for which no explanation could be found. Notably, the dominant frequencies due to all inputs appeared to often display the same dominant frequencies which would suggest common frequency components between the S0 and A0 mode.

The mean frequency versus propagation characteristics revealed two findings of interest. Firstly, it appeared to confirm previous literature such as the one by Gorman [12]

who stated that the extensional wave does not suffer from signal dispersion while the flexural wave does. Additionally, it showed that in contrast to the amplitude characteristics of the complete HVI induced signal, which could be described well solely through the extensional, S0, wave mode. The opposite appears to be the case for the HVI induced frequency characteristics, where the flexural, A0, wave mode seemed to closely resemble the characteristics of the complete wave, while the frequency characteristics due to the S0 wave mode, did not appear to have any correlation with the complete input.

The frequency-time domain highlighted the presence of mode dispersion for each of the signal inputs accenting the various propagation frequencies of the different modes. Three main velocities could be observed, the slowest of these were the velocities at frequencies above 0.5 MHz. Below 0.5 MHz, however, it could be observed that frequencies above 0.2 MHz, seemingly propagated at a higher velocity compared to the frequencies below 0.2 MHz. This suggested that each of the inputs resulted in the creation of the two fundamental modes and potentially a third higher-order mode, such as the A1 mode. While the characterisation of the velocity belonging to the third mode requires further research, the author concluded that from the obtained signals, it appears that the faster propagating S0 mode, contains its dominant frequencies between 0.2 MHz and 0.5 MHz.

6.4 Source Localisation

A successful application of the time of arrival triangulation algorithm developed by Nivesrangsan et al. [14] was studied for each of the inputs. This algorithm, however had to be modified with regards to the wave velocity used for calculations, as this was not previously known. The use of the transverse, longitudinal and extensional wave velocities, to predict the source location was thus additionally used as a method to characterise the various resultant signals. The algorithm was additionally compared and evaluated on it's accuracy when using the time of the maximum amplitude of the signal rather than the time of arrival.

For all inputs, the algorithm was able to predict the source location for all velocities to a reasonable accuracy, with a maximum error of 30 mm. It could be observed that like

the previously investigated amplitude characteristics, the results due to complete input matched perfectly with the results due to the S0 input. This is however likely caused by the method of normalisation of the signal rather than another factor and as such was expected.

The source localisation method using the time of maximum amplitude however, was able to successfully characterise the S0 mode and complete input, as these were dominated by their maximum amplitude which corresponded to the arrival of the S0 mode shock wave. Thus, through the use of the extensional wave velocity and time time of maximum amplitude a source localisation factor to an error of only 0.38 mm was achieved.

7 Appendix 1

7.1 Project Plan Management

Initial project plan

Task ID	Task	Progress	Start	End
	Research and Learning			
1.1.1	Research HVI	0%	05-Oct	11-Oct
1.1.2	Research HVI experiments done	0%	07-Oct	22-Nov
1.1.3	Research HVI signals obtained from experiments	0%	02-Nov	22-Nov
1.1.4	Research HVI damage	0%	09-Nov	06-Dec
1.1.5	Research HVI damage localisation methods	0%	17-Nov	13-Dec
1.1.6	Research wave propogation induced by HVI	0%	09-Nov	03-Jan
1.1.7	Research Numerical Solutions to HVI	0%	04-Jan	07-Feb
1.2.1	Research signal analysis methods	0%	23-Nov	27-Dec
1.3.1	Research Structural Health Monitoring on Spacecraft	0%	14-Dec	10-Jan
1.4.1	Learn Abaqus	0%	16-Nov	20-Dec
1.4.2	Learn how to simulate wave propogation in solids	0%	30-Nov	04-Jan
	Simulation			
2.1.1	Obtain signals from previous HVI experiments	0%	09-Nov	29-Nov
2.1.2	Analyse signals to reproduce a HVI resembeling signal	0%	23-Nov	27-Dec
2.2.1	Simulate the HVI in Abaqus	0%	07-Dec	27-Dec
2.2.2	Compare results with original source to verify	0%	14-Dec	03-Jan
2.3.2	Simulate similar HVI on Cylindrical Shape	0%	04-Jan	01-Feb
	Analysis			
3.1.1	Analyse Results Obtained	0%	04-Jan	07-Mar
3.1.2	Attempt Characterisation of Signals	0%	11-Jan	14-Mar
3.2.1	Locate damgage location	0%	25-Jan	21-Mar
3.2.2	Locate damage size	0%	09-Feb	28-Mar
3.2.3	Locate damage severity	0%	08-Mar	04-Apr
	Project Work			
4.1	Create Project Proposal	0%	05-Oct	17-Oct
4.2	Literature Review	0%	14-Oct	04-Jan
4.3	Create Project Plan	0%	26-Oct	22-Nov
4.4	Write Disertation	0%	01-Feb	06-May
4.5	Create poster Ideas	0%	08-Feb	21-Feb
4.6	Finalise Poster	0%	15-Feb	08-Mar
	University Work			
5.1	Coursework	/	/	/
5.2	Assesments	/	/	/
5.3	Exam Period	/	/	/
5.4	Holiday	/	/	/
5.5	Internship applications	0%	26-Oct	15-Feb
	Other			
6.1	Personal Commitments	/	/	/
6.2	Free Time	/	/	/

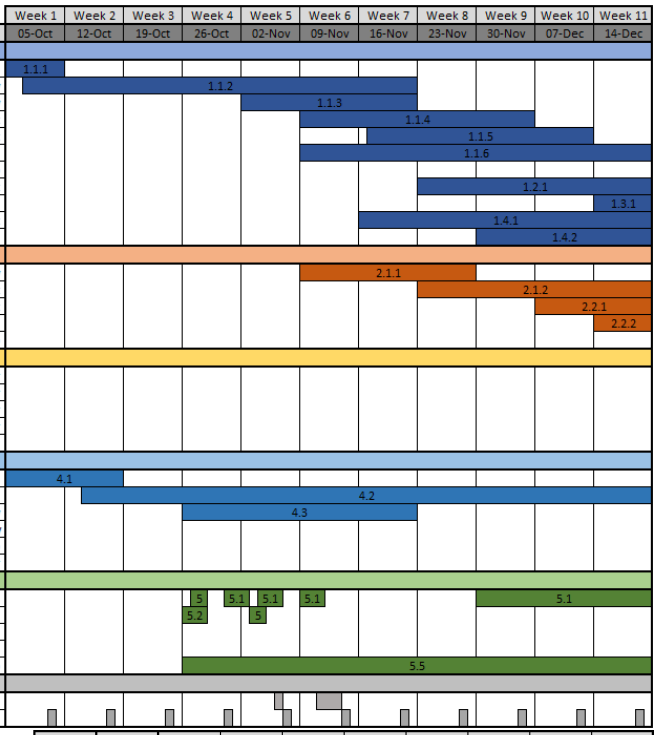

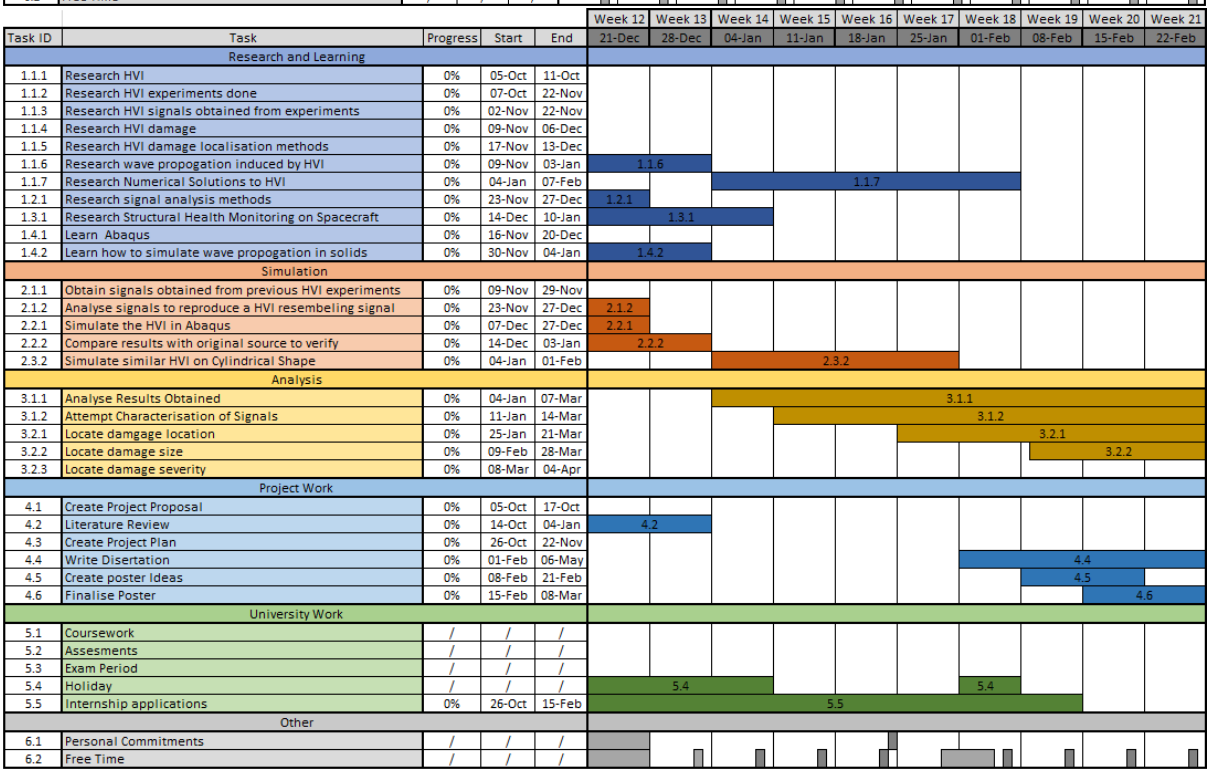

Task ID	Task	Progress	Start	End
	Research and Learning			
1.1.1	Research HVI	0%	05-Oct	11-Oct
1.1.2	Research HVI experiments done	0%	07-Oct	22-Nov
1.1.3	Research HVI signals obtained from experiments	0%	02-Nov	22-Nov
1.1.4	Research HVI damage	0%	09-Nov	06-Dec
1.1.5	Research HVI damage localisation methods	0%	17-Nov	13-Dec
1.1.6	Research wave propogation induced by HVI	0%	09-Nov	03-Jan
1.1.7	Research Numerical Solutions to HVI	0%	04-Jan	07-Feb
1.2.1	Research signal analysis methods	0%	23-Nov	27-Dec
1.3.1	Research Structural Health Monitoring on Spacecraft	0%	14-Dec	10-Jan
1.4.1	Learn Abaqus	0%	16-Nov	20-Dec
1.4.2	Learn how to simulate wave propogation in solids	0%	30-Nov	04-Jan
	Simulation			
2.1.1	Obtain signals obtained from previous HVI experiments	0%	09-Nov	29-Nov
2.1.2	Analyse signals to reproduce a HVI resembeling signal	0%	23-Nov	27-Dec
2.2.1	Simulate the HVI in Abaqus	0%	07-Dec	27-Dec
2.2.2	Compare results with original source to verify	0%	14-Dec	03-Jan
2.3.2	Simulate similar HVI on Cylindrical Shape	0%	04-Jan	01-Feb
	Analysis			
3.1.1	Analyse Results Obtained	0%	04-Jan	07-Mar
3.1.2	Attempt Characterisation of Signals	0%	11-Jan	14-Mar
3.2.1	Locate damgage location	0%	25-Jan	21-Mar
3.2.2	Locate damage size	0%	09-Feb	28-Mar
3.2.3	Locate damage severity	0%	08-Mar	04-Apr
	Project Work			
4.1	Create Project Proposal	0%	05-Oct	17-Oct
4.2	Literature Review	0%	14-Oct	04-Jan
4.3	Create Project Plan	0%	26-Oct	22-Nov
4.4	Write Disertation	0%	01-Feb	06-May
4.5	Create poster Ideas	0%	08-Feb	21-Feb
4.6	Finalise Poster	0%	15-Feb	08-Mar
	University Work			
5.1	Coursework	/	/	/
5.2	Assesments	/	/	/
5.3	Exam Period	/	/	/
5.4	Holiday	/	/	/
5.5	Internship applications	0%	26-Oct	15-Feb
	Other			
6.1	Personal Commitments	/	/	/
6.2	Free Time	/	/	/

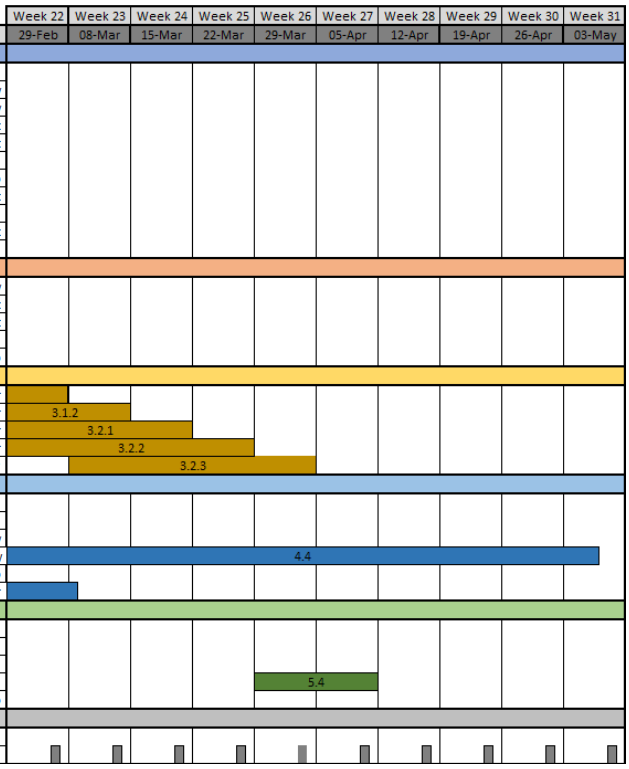

The initial project plan presented, ultimately proved too optimistic, as it underestimated the time required to obtain a good understanding of the theory of structural response signals and hypervelocity impact. The plan especially did not account for the limited amount of literature available regarding the topic of the structural response signals generated by HVI on thin isentropic plates.

Significant delays to the project were caused by the first semester Conceptual Aerospace Systems Design course module. This design course module proved to be an highly time-intensive and complex assessment due to limited guidance on behalf of the university and unclear requirements. It was subsequently concluded that less time should have been spent on this module, and instead, further literature research should have been undertaken.

Regardless of the optimistic timeline, this plan proved to provide outstandingly valuable guidance concerning initial research topics and the order of the undertaken research. This allowed for a clear and logical progression into the field, which was of significant importance as the undertaken research was within a topic the researcher had no previous experience with.

Updated re-plan

Task ID	Task	Progress	Start	End
	Research and Learning			
1.1.1	Research HVI	100%	05-Oct	15-Oct
1.1.2	Research HVI experiments done	60%	07-Oct	29-Nov
1.1.3	Research HVI signals obtained from experiments	20%	02-Nov	01-Dec
1.1.4	Research HVI damage	10%	09-Nov	06-Dec
1.1.5	Research HVI damage localisation methods	0%	17-Nov	13-Dec
1.1.6	Research wave propogation induced by HVI	0%	09-Nov	03-Jan
1.1.7	Research Numerical Solutions to HVI	0%	04-Jan	07-Feb
1.2.1	Research signal analysis methods	5%	23-Nov	03-Jan
1.3.1	Research Structural Health Monitoring on Spacecraft	0%	14-Dec	10-Jan
1.4.1	Learn Abaqus	0%	16-Nov	27-Dec
1.4.2	Learn how to simulate wave propogation in solids	0%	30-Nov	17-Jan
	Simulation			
2.1.1	Obtain signals from previous HVI experiments	0%	16-Nov	06-Dec
2.1.2	Analyse signals to reproduce a HVI resembeling signal	0%	29-Nov	03-Jan
2.2.1	Simulate the HVI in Abaqus	0%	07-Dec	27-Dec
2.2.2	Compare results with original source to verify	0%	14-Dec	03-Jan
2.3.2	Simulate similar HVI on Cylindrical Shape	0%	04-Jan	01-Feb
	Analysis			
3.1.1	Analyse Results Obtained	0%	04-Jan	07-Mar
3.1.2	Attempt Characterisation of Signals	0%	11-Jan	14-Mar
3.2.1	Locate damgage location	0%	25-Jan	21-Mar
3.2.2	Locate damage size	0%	09-Feb	28-Mar
3.2.3	Locate damage severity	0%	08-Mar	04-Apr
	Project Work			
4.1	Create Project Proposal	100%	05-Oct	17-Oct
4.2	Literature Review	10%	14-Oct	04-Jan
4.3	Create Project Plan	40%	26-Oct	22-Nov
4.4	Write Disertation	0%	01-Feb	06-May
4.5	Create poster Ideas	0%	08-Feb	21-Feb
4.6	Finalise Poster	0%	15-Feb	08-Mar
	University Work			
5.1	Coursework	/	/	/
5.2	Assesments	/	/	/
5.3	Exam Period	/	/	/
5.4	Holiday	/	/	/
5.5	Internship applications	10%	26-Oct	15-Feb
	Other			
6.1	Personal Commitments	/	/	/
6.2	Free Time	/	/	/

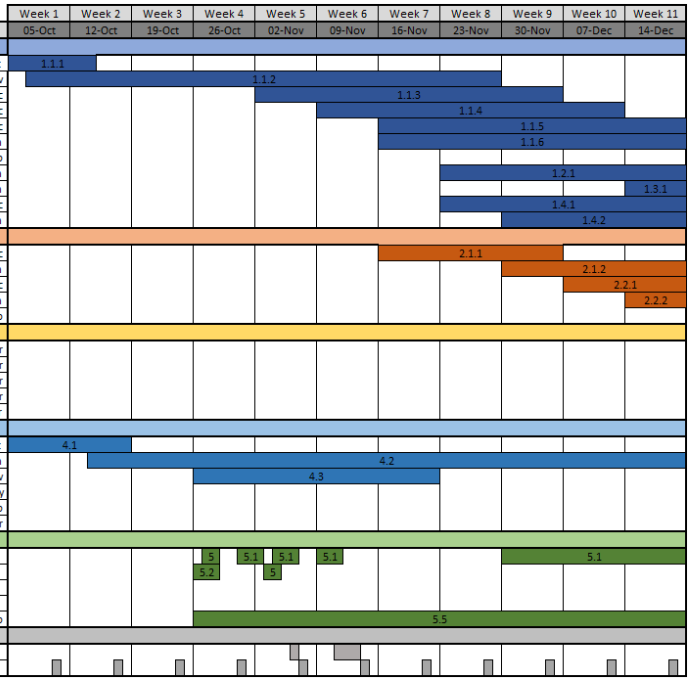

Task ID	Task	Progress	Start	End
	Research and Learning			
1.1.1	Research HVI	100%	05-Oct	15-Oct
1.1.2	Research HVI experiments done	60%	07-Oct	29-Nov
1.1.3	Research HVI signals obtained from experiments	10%	02-Nov	01-Dec
1.1.4	Research HVI damage	0%	09-Nov	06-Dec
1.1.5	Research HVI damage localisation methods	0%	17-Nov	13-Dec
1.1.6	Research wave propogation induced by HVI	0%	09-Nov	03-Jan
1.1.7	Research Numerical Solutions to HVI	0%	04-Jan	07-Feb
1.2.1	Research signal analysis methods	0%	23-Nov	03-Jan
1.3.1	Research Structural Health Monitoring on Spacecraft	0%	14-Dec	10-Jan
1.4.1	Learn Abaqus	0%	16-Nov	27-Dec
1.4.2	Learn how to simulate wave propogation in solids	0%	30-Nov	17-Jan
	Simulation			
2.1.1	Obtain signals obtained from previous HVI experiments	0%	16-Nov	06-Dec
2.1.2	Analyse signals to reproduce a HVI resembeling signal	0%	29-Nov	03-Jan
2.2.1	Simulate the HVI in Abaqus	0%	07-Dec	27-Dec
2.2.2	Compare results with original source to verify	0%	14-Dec	03-Jan
2.3.2	Simulate similar HVI on Cylindrical Shape	0%	04-Jan	01-Feb
	Analysis			
3.1.1	Analyse Results Obtained	0%	04-Jan	07-Mar
3.1.2	Attempt Characterisation of Signals	0%	11-Jan	14-Mar
3.2.1	Locate damgage location	0%	25-Jan	21-Mar
3.2.2	Locate damage size	0%	09-Feb	28-Mar
3.2.3	Locate damage severity	0%	08-Mar	04-Apr
	Project Work			
4.1	Create Project Proposal	100%	05-Oct	17-Oct
4.2	Literature Review	5%	14-Oct	04-Jan
4.3	Create Project Plan	40%	26-Oct	22-Nov
4.4	Write Disertation	0%	01-Feb	06-May
4.5	Create poster Ideas	0%	08-Feb	21-Feb
4.6	Finalise Poster	0%	15-Feb	08-Mar
	University Work			
5.1	Coursework	/	/	/
5.2	Assesments	/	/	/
5.3	Exam Period	/	/	/
5.4	Holiday	/	/	/
5.5	Internship applications	10%	26-Oct	15-Feb
	Other			
6.1	Personal Commitments	/	/	/
6.2	Free Time	/	/	/

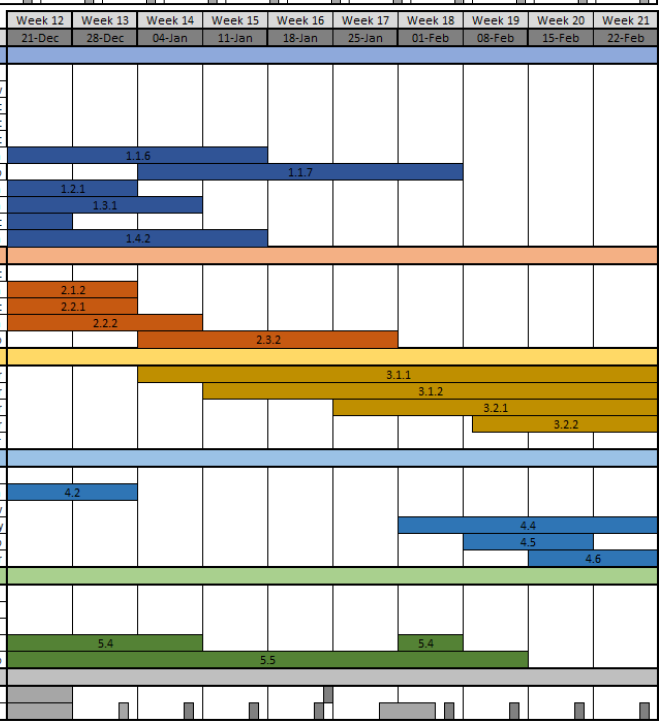

Task ID	Task	Progress	Start	End
	Research and Learning			
1.1.1	Research HVI	100%	05-Oct	15-Oct
1.1.2	Research HVI experiments done	60%	07-Oct	29-Nov
1.1.3	Research HVI signals obtained from experiments	10%	02-Nov	01-Dec
1.1.4	Research HVI damage	0%	09-Nov	06-Dec
1.1.5	Research HVI damage localisation methods	0%	17-Nov	13-Dec
1.1.6	Research wave propogation induced by HVI	0%	09-Nov	03-Jan
1.1.7	Research Numerical Solutions to HVI	0%	04-Jan	07-Feb
1.2.1	Research signal analysis methods	0%	23-Nov	03-Jan
1.3.1	Research Structural Health Monitoring on Spacecraft	0%	14-Dec	10-Jan
1.4.1	Learn Abaqus	0%	16-Nov	27-Dec
1.4.2	Learn how to simulate wave propogation in solids	0%	30-Nov	17-Jan
	Simulation			
2.1.1	Obtain signals obtained from previous HVI experiments	0%	16-Nov	06-Dec
2.1.2	Analyse signals to reproduce a HVI resembeling signal	0%	29-Nov	03-Jan
2.2.1	Simulate the HVI in Abaqus	0%	07-Dec	27-Dec
2.2.2	Compare results with original source to verify	0%	14-Dec	03-Jan
2.3.2	Simulate similar HVI on Cylindrical Shape	0%	04-Jan	01-Feb
	Analysis			
3.1.1	Analyse Results Obtained	0%	04-Jan	07-Mar
3.1.2	Attempt Characterisation of Signals	0%	11-Jan	14-Mar
3.2.1	Locate damgage location	0%	25-Jan	21-Mar
3.2.2	Locate damage size	0%	09-Feb	28-Mar
3.2.3	Locate damage severity	0%	08-Mar	04-Apr
	Project Work			
4.1	Create Project Proposal	100%	05-Oct	17-Oct
4.2	Literature Review	5%	14-Oct	04-Jan
4.3	Create Project Plan	40%	26-Oct	22-Nov
4.4	Write Disertation	0%	01-Feb	06-May
4.5	Create poster Ideas	0%	08-Feb	21-Feb
4.6	Finalise Poster	0%	15-Feb	08-Mar
	University Work			
5.1	Coursework	/	/	/
5.2	Assesments	/	/	/
5.3	Exam Period	/	/	/
5.4	Holiday	/	/	/
5.5	Internship applications	10%	26-Oct	15-Feb
	Other			
6.1	Personal Commitments	/	/	/
6.2	Free Time	/	/	/

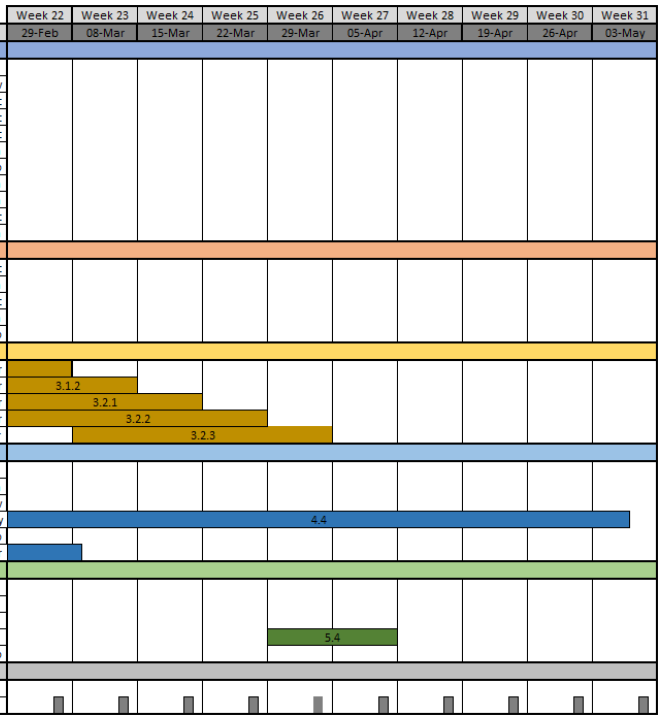

The updated re-plan reflects the plan of the project timeline at the project proposal stage. At this time, a significant amount of literature concerning HVI induced AE signals had been covered and a clearer understanding of the research topic had been developed.

It is noteworthy, however, that at this stage, there was confusion on the exact scope of the project, specifically with regards to the method used to replicate the structural response features induced by HVI. Roughly one month of the project time was spent on the attempt to develop a method allowing for the conversion of the HVI induced, PZT wafer captured voltage-time data of previous literature into an equivalent out of plane force-time or displacement-time history. This was based on a misunderstanding from the suggestion of the PhD advisor Xianglin Huang. The aforementioned method proved to be infeasible in the scope and time frame of the project and as such a more simplified model and input had to be developed.

In this stage of the project, the first attempts of simulating the HVI induced AE signals in ABAQUS were conducted. This resulted in two additional factors which resulted in significant delays in the project timeline.

Firstly, after the development of the model, an model validation study was attempted. This, however, proved impossible as existing literature in this field is lacking the missing

data for model validation. Specifically, no research or literature could be found, which published the data sets of the HVI induced AE signals, that would allow for validation of the developed model at various propagation distances. After lengthy research into the relevant literature, this was discussed with the PhD advisor Xianglin Huang, who suggested that no further validation of the model should be attempted and that the remaining time should instead be used to study the induced signal dispersion and propagation features.

Secondly, the use of Citrix Workspace and the universities remote desktop system caused severe delays in the project. This remote desktop tool had to be used as the universities COVID-19 policy did not allow the direct use of on-campus computational resources, while not providing the ABAQUS licenses required to execute the software at the required mesh quality on the personal computer of the author. This impacted the timeline due to the limited hardware capabilities of the available university remote desktops, resulting in exceedingly high computation times. Additionally, it impacted the project due to persistent software and IT issues by the university. This caused the remote desktops to recurrently encounter system errors making the software unavailable at times, as well as frequently crashing during simulations.

Irrespective of these delays, the updated re-plan provided a well structured and clear timeline of activities to be conducted, greatly aiding in the management of the project. Although the specifics of the project activities and their respective timelines were still hard to estimate, the section covering the planned time frames for the poster proved to be highly accurate.

Final plan at project completion

Task ID	Task	Progress	Start	End
	Research and Learning			
1.1.1	Research HVI	100%	05-Oct	15-Oct
1.1.2	Research HVI experiments done	100%	07-Oct	18-Jan
1.1.3	Research HVI signals obtained from experiments	100%	02-Nov	27-Dec
1.1.4	Research HVI damage	100%	09-Nov	13-Dec
1.1.5	Research HVI damage localisation methods	100%	17-Nov	13-Dec
1.1.6	Research wave propogation induced by HVI	100%	09-Nov	03-Jan
1.1.7	Research Numerical Solutions to HVI	100%	04-Jan	07-Feb
1.2.1	Research signal analysis methods	100%	23-Nov	03-Jan
1.3.1	Research Structural Health Monitoring on Spacecraft	100%	14-Dec	10-Jan
1.4.1	Learn Abaqus	100%	22-Nov	27-Dec
1.4.2	Learn how to simulate wave propogation in solids	100%	30-Nov	17-Jan
	Simulation			
2.1.1	Obtain signals from previous HVI experiments	100%	16-Nov	24-Jan
2.1.2	Analyse signals to reproduce a HVI resembeling signal	100%	29-Nov	31-Jan
2.2.1	Simulate the HVI in Abaqus	100%	07-Dec	22-Feb
2.2.2	Compare results with original source to verify	100%	01-Feb	28-Feb
	Analysis			
3.1.1	Analyse Results Obtained	100%	04-Jan	14-Mar
3.1.2	Attempt Characterisation of Signals	100%	11-Jan	14-Mar
3.2.1	Locate damgage location	100%	29-Feb	02-May
	Project Work			
4.1	Create Project Proposal	100%	05-Oct	17-Oct
4.2	Literature Review	100%	14-Oct	28-Feb
4.3	Create Project Plan	100%	26-Oct	22-Nov
4.4	Write Disertation	100%	01-Feb	17-May
4.5	Create poster Ideas	100%	08-Feb	21-Feb
4.6	Finalise Poster	100%	15-Feb	08-Mar
	University Work			
5.1	Coursework	/	/	/
5.2	Assesments	/	/	/
5.3	Exam Period	/	/	/
5.4	Holiday	/	/	/
5.5	Internship applications	100%	26-Oct	15-Feb
	Other			
6.1	Personal Commitments	/	/	/
6.2	Free Time	/	/	/

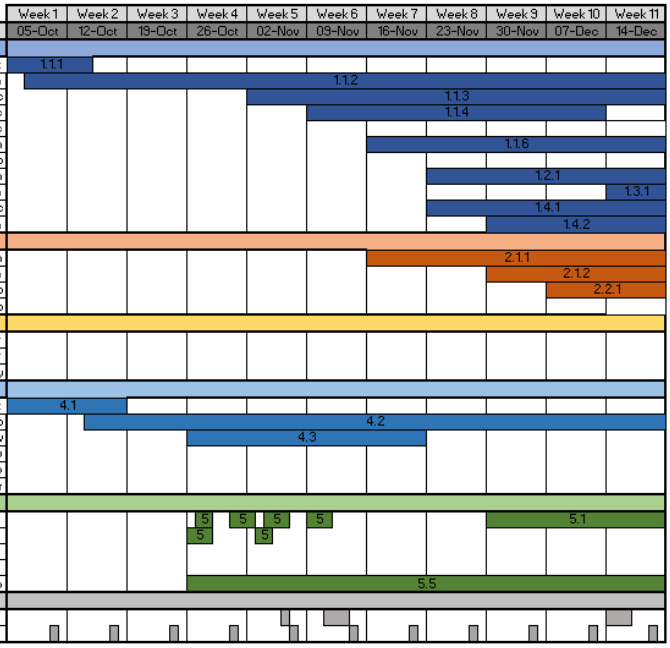

Task ID	Task	Progress	Start	End
	Research and Learning			
1.1.1	Research HVI	100%	05-Oct	15-Oct
1.1.2	Research HVI experiments done	100%	07-Oct	18-Jan
1.1.3	Research HVI signals obtained from experiments	100%	02-Nov	27-Dec
1.1.4	Research HVI damage	100%	09-Nov	13-Dec
1.1.5	Research HVI damage localisation methods	100%	17-Nov	13-Dec
1.1.6	Research wave propogation induced by HVI	100%	09-Nov	03-Jan
1.1.7	Research Numerical Solutions to HVI	100%	04-Jan	07-Feb
1.2.1	Research signal analysis methods	100%	23-Nov	03-Jan
1.3.1	Research Structural Health Monitoring on Spacecraft	100%	14-Dec	10-Jan
1.4.1	Learn Abaqus	100%	22-Nov	27-Dec
1.4.2	Learn how to simulate wave propogation in solids	100%	30-Nov	17-Jan
	Simulation			
2.1.1	Obtain signals obtained from previous HVI experiments	100%	16-Nov	24-Jan
2.1.2	Analyse signals to reproduce a HVI resembeling signal	100%	29-Nov	31-Jan
2.2.1	Simulate the HVI in Abaqus	100%	07-Dec	22-Feb
2.2.2	Compare results with original source to verify	100%	01-Feb	28-Feb
	Analysis			
3.1.1	Analyse Results Obtained	100%	04-Jan	14-Mar
3.1.2	Attempt Characterisation of Signals	100%	11-Jan	14-Mar
3.2.1	Locate damgage location	100%	29-Feb	02-May
	Project Work			
4.1	Create Project Proposal	100%	05-Oct	17-Oct
4.2	Literature Review	100%	14-Oct	28-Feb
4.3	Create Project Plan	100%	26-Oct	22-Nov
4.4	Write Disertation	100%	01-Feb	17-May
4.5	Create poster Ideas	100%	08-Feb	21-Feb
4.6	Finalise Poster	100%	15-Feb	08-Mar
	University Work			
5.1	Coursework	/	/	/
5.2	Assesments	/	/	/
5.3	Exam Period	/	/	/
5.4	Holiday	/	/	/
5.5	Internship applications	100%	26-Oct	15-Feb
	Other			
6.1	Personal Commitments	/	/	/
6.2	Free Time	/	/	/

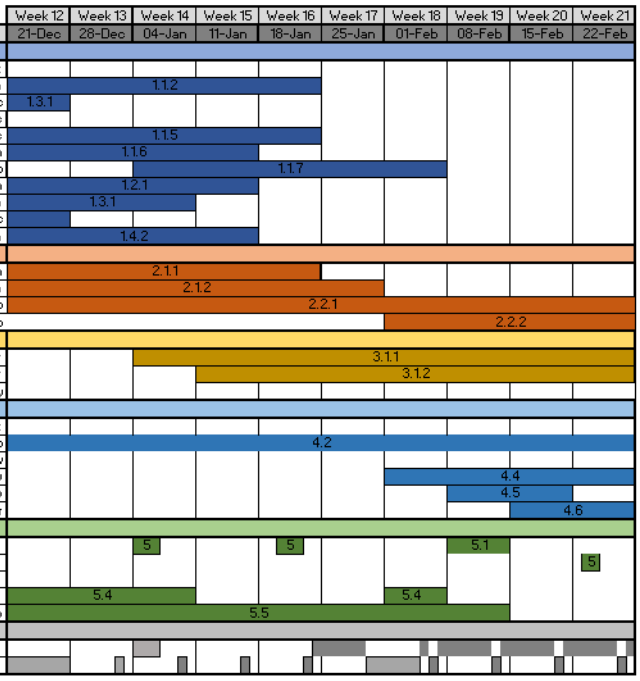

Task ID	Task	Progress	Start	End
	Research and Learning			
1.1.1	Research HVI	100%	05-Oct	15-Oct
1.1.2	Research HVI experiments done	100%	07-Oct	18-Jan
1.1.3	Research HVI signals obtained from experiments	100%	02-Nov	27-Dec
1.1.4	Research HVI damage	100%	09-Nov	13-Dec
1.1.5	Research HVI damage localisation methods	100%	17-Nov	13-Dec
1.1.6	Research wave propogation induced by HVI	100%	09-Nov	03-Jan
1.1.7	Research Numerical Solutions to HVI	100%	04-Jan	07-Feb
1.2.1	Research signal analysis methods	100%	23-Nov	03-Jan
1.3.1	Research Structural Health Monitoring on Spacecraft	100%	14-Dec	10-Jan
1.4.1	Learn Abaqus	100%	22-Nov	27-Dec
1.4.2	Learn how to simulate wave propogation in solids	100%	30-Nov	17-Jan
	Simulation			
2.1.1	Obtain signals obtained from previous HVI experiments	100%	16-Nov	24-Jan
2.1.2	Analyse signals to reproduce a HVI resembeling signal	100%	29-Nov	31-Jan
2.2.1	Simulate the HVI in Abaqus	100%	07-Dec	22-Feb
2.2.2	Compare results with original source to verify	100%	01-Feb	28-Feb
	Analysis			
3.1.1	Analyse Results Obtained	100%	04-Jan	14-Mar
3.1.2	Attempt Characterisation of Signals	100%	11-Jan	14-Mar
3.2.1	Locate damgage location	100%	29-Feb	02-May
	Project Work			
4.1	Create Project Proposal	100%	05-Oct	17-Oct
4.2	Literature Review	100%	14-Oct	28-Feb
4.3	Create Project Plan	100%	26-Oct	22-Nov
4.4	Write Disertation	100%	01-Feb	17-May
4.5	Create poster Ideas	100%	08-Feb	21-Feb
4.6	Finalise Poster	100%	15-Feb	08-Mar
	University Work			
5.1	Coursework	/	/	/
5.2	Assesments	/	/	/
5.3	Exam Period	/	/	/
5.4	Holiday	/	/	/
5.5	Internship applications	100%	26-Oct	15-Feb
	Other			
6.1	Personal Commitments	/	/	/
6.2	Free Time	/	/	/

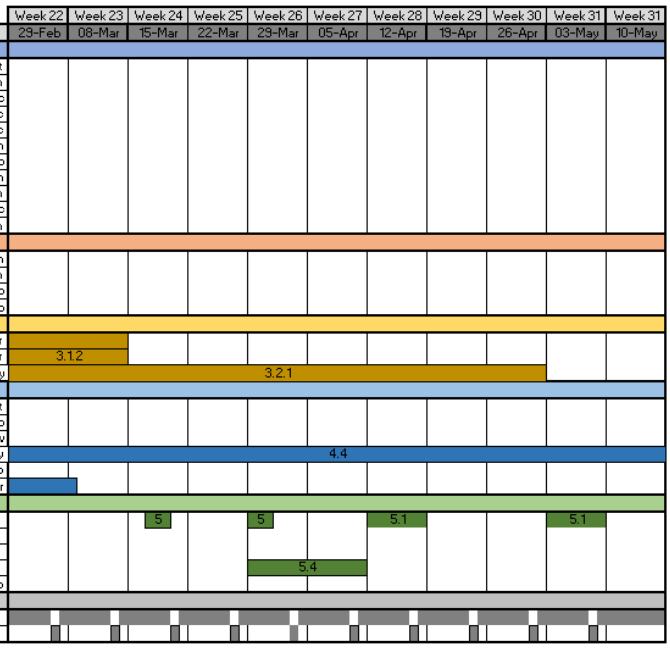

The above-shown figures represent the timeline of the project after its completion. It was noted that overall, the project had deviated from the original timeline by a significant amount as well as undergoing a re-scoping to make it more feasible within the given time frame.

The project no longer attempted tasks such as damage size estimation or the simulation of the HVI on a cylindrical surface. These research topics were of interest, but the author was not able to investigate them in sufficient detail due to time constraints. Nonetheless, the author is confident that the conducted research is of significance, as it provided some findings of interest regarding the wave propagation and dispersion characteristics of HVI induced AE signals. If the discovered trends can be confirmed through future research, it could allow for a potentially significantly reduced in-situ response time for future AE based characterisation of HVI events.

The reduced scope of the project was due to three main factors which significantly affected the authors' availability to work on the project. The first and most prominent of these factors was the acceptance of the author into the UK's leading student start-up accelerator programme, Accelerate Me, in December of 2020. Alongside S. Strat, the author founded a start-up, aiming to deliver satellite companies with decoration that would allow them a tangible and elegant connection to their space-borne assets.

This business required a significant time investment by the author as in addition to the development of a prototype and website, a marketing intern had to be recruited and managed in the months of February to May.

Secondly, the authors time was additionally constrained due to his servicing and hosting of the website Steam-Tables.com . This website provided an interpolation tool for the thermodynamic transport properties of gasses and vapours as well as simple thermodynamic question solvers for simple flow and non-flow thermodynamic problems. The website experienced an unexpected surge of over 1000 users from 50 countries during the project, which resulted in the unplanned required time to ensure that the website would stay functional and updated for all of its' users.

The third significant time constraint to the project resulted due to the authors' commitments as University of Manchester Aerospace Peer Assisted Study Session(PASS) scheme leader and scheme coordinator. These commitments required more time than initially anticipated as they involved the mentoring of new first-year students at the university, whose mental health and educational experience was significantly impacted by COVID-19 and the universities response to it. As such, an average of 4 hours per week had to be committed to PASS which adversely affected the authors' ability to conduct work on the individual project. This time commitment was notably increased during the months between February and March, as the recruitment of PASS leaders for the subsequent academic year required the authors' involvement in over 30 interviews and two assessment centre days.

Although these factors resulted in a reduced scope of the project, the author is confident that the quality of the delivered work did not suffer. It is thus the authors' opinion that all of the external factors and the individual lessons that could be learned from them, merited the reduction in scope with regards to the personal and professional development of the author.

References

[1] K. Endsley. [Online]. Available: http://www.geo.mtu.edu/UPSeis/waves.html

[2] M. R. Kaphle, "Analysis of acoustic emission data for accurate damage assessment for structural health monitoring applications," Ph.D. dissertation, Queensland University of Technology, 2012.

[3] M. G. Lozev *et al.*, "Acoustic emission monitoring of steel bridge members," Virginia Transportation Research Council, Tech. Rep., 1997.

[4] M. Liu, Q. Wang, Q. Zhang, R. Long, and Z. Su, "Characterizing hypervelocity (> 2.5 km/s)-impact-engendered damage in shielding structures using in-situ acoustic emission: Simulation and experiment," *International Journal of Impact Engineering*, vol. 111, pp. 273–284, 2018.

[5] F. Schäfer and R. Janovsky, "Impact sensor network for detection of hypervelocity impacts on spacecraft," *Acta Astronautica*, vol. 61, no. 10, pp. 901–911, 2007.

[6] L. Menglong, W. Qiang, Q. Zhang, L. Renrong, C. Fangsen, and S. Zhongqing, "Hypervelocity impact induced shock acoustic emission waves for quantitative damage evaluation using in situ miniaturized piezoelectric sensor network," *Chinese journal of aeronautics*, vol. 32, no. 5, pp. 1059–1070, 2019.

[7] W. Riedel, H. Nahme, D. M. White, and R. A. Clegg, "Hypervelocity impact damage prediction in composites: Part ii—experimental investigations and simulations," *International Journal of Impact Engineering*, vol. 33, no. 1-12, pp. 670–680, 2006.

[8] Y. Nagao, S. Kibe, K. Daigo, A. Francesconi, and D. Pavarin, "Hypervelocity impact studies simulating debris collision on composites material," in *Proceedings of the 4th European Conference on Space Debris (ESA SP-587)*, 2005, p. 413.

[9] K. Zhang, B. Pang, R. Chi, and H. Jiao, "Hypervelocity damage pattern recognition on aluminum alloy based on acoustic emission," in *2019 6th International Conference on Information Science and Control Engineering (ICISCE)*. IEEE, 2019, pp. 329–332.

[10] H. Sohn, H. W. Park, K. H. Law, and C. R. Farrar, "Damage detection in composite plates by using an enhanced time reversal method," *Journal of Aerospace Engineering*, vol. 20, no. 3, pp. 141–151, 2007.

[11] D. Aggelis and T. Matikas, "Effect of plate wave dispersion on the acoustic emission parameters in metals," *Computers & structures*, vol. 98, pp. 17–22, 2012.

[12] M. R. Gorman, "Plate wave acoustic emission," *The Journal of the Acoustical Society of America*, vol. 90, no. 1, pp. 358–364, 1991.

[13] S. Mark Burchell, C. Cole, L. Giovance, S. Pisacane, and Stansbery, "Acoustic response of aluminium and duroid plates to hypervelocity impacts," *International Journal of Impact Engineering*, vol. 38, pp. 426–433, 2010.

[14] P. Nivesrangsan, J. Steel, and R. Reuben, "Source location of acoustic emission in diesel engines," *Mechanical systems and signal processing*, vol. 21, no. 2, pp. 1103–1114, 2007.

[15] L. Iliescu, A. Lakis, and A. Abou-Antoun, "Hypervelocity impact (hvi) tests & signal recordings," *Universal Journal of Aeronautical & Aerospace Sciences*, vol. 2, pp. 80–113, 2014.

[16] "What are hypervelocity impacts?" [Online]. Available: https://www.esa.int/Enabling_Support/Operations/What_are_hypervelocity_impacts

[17] "About space debris." [Online]. Available: https://www.esa.int/Safety_Security/Space_Debris/About_space_debris

[18] "Two stage light gas guns," Sep 2015. [Online]. Available: https://www.nasa.gov/centers/wstf/site_tour/remote_hypervelocity_test_laboratory/two_stage_light_gas_guns.html

[19] W. H. Prosser, M. R. Gorman, and D. H. Humes, "Acoustic emission signals in thin plates produced by impact damage," 1999.

[20] M. Kaphle, A. Tan, and D. Thambiratnam, "Structural health monitoring of bridges using acoustic emission technology and signal processing techniques," in *Proceedings of the 13th Asia Pacific Vibration Conference*. University of Canterbury, 2009, pp. 1–10.

[21] C. Scruby, "An introduction to acoustic emission," *Journal of Physics E: Scientific Instruments*, vol. 20, no. 8, p. 946, 1987.

[22] P. Bevelacqua. [Online]. Available: https://www.thefouriertransform.com/transform/fourier.php

[23] R. Clegg, D. White, W. Riedel, and W. Harwick, "Hypervelocity impact damage prediction in composites: Part i—material model and characterisation," *International Journal of Impact Engineering*, vol. 33, no. 1-12, pp. 190–200, 2006.

[24] "2024 aluminum: Get to know its properties and uses," Jun 2020. [Online]. Available: https://www.gabrian.com/2024-aluminum-properties/

8 Appendix 2

[framed,numbered,autolinebreaks,useliterate]mcode

function [power,freq] = powerSpectrum(Signal,Fs)

N = length(Signal); xdft = fft(Signal); xdft = xdft(1:N/2+1); psdx = (1/(Fs*N)) * abs(xdft).^{2}; $psdx(2:end-1) = 2*psdx(2:end-1); freq = 0:Fs/length(Signal):Fs/2;$

power = 10*log10(psdx); end